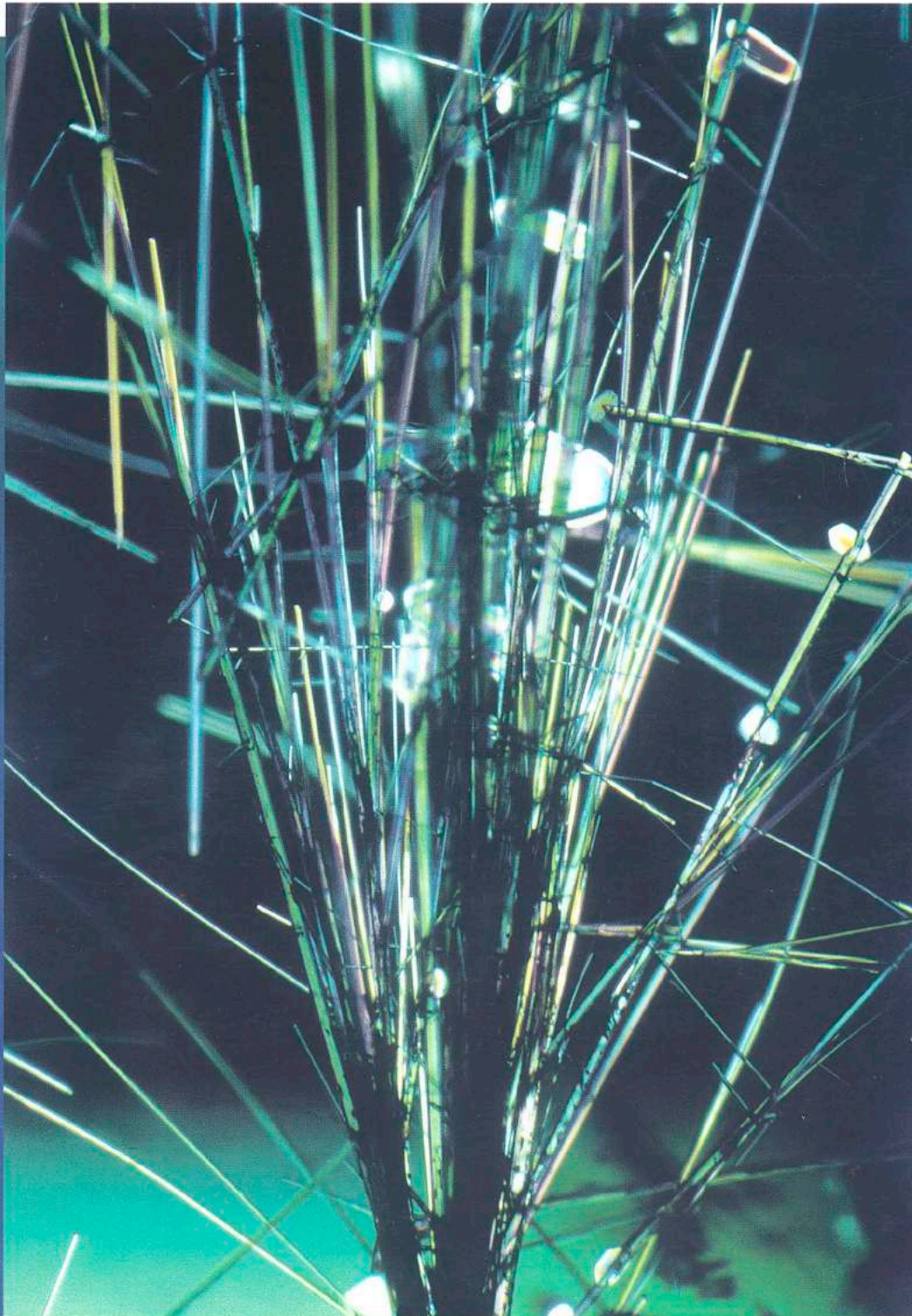




The Journal of
Gemmology

Volume 29 No. 5/6
January/April 2005



Gemmological Association and Gem Testing Laboratory of Great Britain

27 Greville Street, London EC1N 8TN

Tel: +44 (0)20 7404 3334 • **Fax:** +44 (0)20 7404 8843

e-mail: information@gem-a.info • **Website:** www.gem-a.info

President: E A Jobbins

Vice-Presidents: N W Deeks, R A Howie, D G Kent, R K Mitchell

Honorary Fellows: Chen Zhonghui, R A Howie, K Nassau

Honorary Life Members: H Bank, D J Callaghan, E A Jobbins, J I Koivula, I Thomson, H Tillander

Council: A T Collins – Chairman, S Burgoyne, T M J Davidson, S A Everitt, L Hudson, E A Jobbins, J Monnickendam, M J O'Donoghue, E Stern, P J Wates, V P Watson

Members' Audit Committee: A J Allnut, P Dwyer-Hickey, J Greatwood, B Jackson, L Music, J B Nelson, C H Winter

Branch Chairmen: **Midlands** – G M Green, **North East** – N R Rose, **North West** – D M Brady, **Scottish** – B Jackson, **South East** – C H Winter, **South West** – R M Slater

Examiners: A J Allnut MSc PhD FGA, L Bartlett BSc MPhil FGA DGA, Chen Meihua BSc PhD FGA DGA, S Coelho BSc FGA DGA, Prof A T Collins BSc PhD, A G Good FGA DGA, D Gravier FGA, J Greatwood FGA, S Greatwood FGA DGA, G M Green FGA DGA, He Ok Chang FGA DGA, G M Howe FGA DGA, B Jackson FGA DGA, B Jensen BSc (Geol), T A Johne FGA, L Joyner PhD FGA, H Kitawaki FGA CGJ, Li Li Ping FGA DGA, M A Medniuk FGA DGA, T Miyata MSc PhD FGA, M Newton BSc DPhil, C J E Oldershaw BSc (Hons) FGA DGA, H L Plumb BSc FGA DGA, N R Rose FGA DGA, R D Ross BSc FGA DGA, J-C Ruffli FGA, E Stern FGA DGA, S M Stocklmayer BSc (Hons) FGA, Prof I Sunagawa DSc, M Tilley CG FGA, R K Vartiainen FGA, P Vuillet à Ciles FGA, C M Woodward BSc FGA DGA, Yang Ming Xing FGA DGA

The Journal of Gemmology

Editor: Dr R R Harding

Assistant Editors: M J O'Donoghue, P G Read

Associate Editors: Dr C E S Arps (Leiden), G Bosshart (Horgen), Prof A T Collins (London), J Finlayson (Stoke-on-Trent), Dr J W Harris (Glasgow), Prof R A Howie (Derbyshire), Dr J M Ogden (London), Prof A H Rankin (Kingston upon Thames), Dr J E Shigley (Carlsbad), Prof D C Smith (Paris), E Stern (London), Prof I Sunagawa (Tokyo), Dr M Superchi (Milan)

Production Editor: M A Burland

Tribute



Professor Dr Edward Joseph Gübelin

A tribute by E. Alan Jobbins

It is with great sadness that we report the passing of Edward Gübelin on the 15 March 2005, only a day before his 92nd birthday. With his death the worldwide gemmological fraternity has lost a most remarkable and inspirational scientific leader. He was a very early proponent of the use of inclusions in the identification of gem materials and their treatments. He was widely respected internationally and

became a mentor to generations of gemmologists (including this writer) through his enthusiastic writings and beautiful inclusion photomicrographs and topographical photographs.

Edward Joseph Gübelin was born in Lucerne, Switzerland, on the 16 March 1913 into a family of *grands joailliers* where he was given great encouragement

by his father, even to the extent of being treated to a new winter overcoat when he made a particularly successful jewellery sale. Following his father's establishment of a private gemmological laboratory in the early '30s, he continued its development with constant updating with the latest instrumentation. He initially studied mineralogy and the history of art at Zürich. In 1936/37 in Vienna he worked under Professor H. Michel (who had introduced 'microgemmology' some years earlier) where his fascination for inclusions in gemstones was nurtured. Later in 1937 he was working with Professor K. Schlossmacher in Idar Oberstein – a major lapidary centre. He also worked, and began a firm friendship, with Basil Anderson at the London Gem Testing Laboratory. They shared a passion for Burmese gems and many fine specimens from A.C.D. Pain in Burma were then available and being marketed by Charles Mathews in Hatton Garden in the 1940s and '50s.

Edward gained his doctorate in 1938 and his formal gemmological qualification (GG) in residence at the Gemological Institute of America in California in 1939, and was the first recipient of their Research Diploma. He was awarded his FGA in 1946 with Distinction and the GA Research Diploma followed in 1957 for his work on 'Inclusions that occur in gemstones'.

Edward was the founder member of a small group of early laboratory specialists, including B. W. Anderson (UK), O. Dragsted (Denmark), G. Gobel (France), K. Schlossmacher (Germany) and H. Tillander (Finland), who met in various European countries to discuss ongoing problems facing the gemstone industry, such as synthetic corundums and spinels. These annual meetings widened in scope and developed in the early 1950s into the International Gemmological Conference. Edward was an active participant from its

inception and was made an Honorary Member in 1985. His seminal paper 'Differences between Burma and Siam rubies' using their distinctive inclusions appeared in *Gems & Gemology* as early as 1940. In 1953 his classic book *Inclusions as a Means of Gemstone Identification* was published in monochrome, and he introduced a systematic classification of inclusions based on their age relative to the host gemstone mineral. This was followed in 1974 by his inspirational book *Internal of World of Gemstones* with colour plates. Over the decades he wrote over two hundred papers – many of groundbreaking research importance – and published in many international journals with fine colour illustrations.

In 1978 he met John Koivula at the Gemological Institute of America in California; both had visions of a profusely illustrated work on gemstone inclusions, and the *Photoatlas of Inclusions in Gemstones* was the outcome, published in 1986 – a significant work of science and art. By 1989 gemmological research had moved on and planning for a second volume of the *Photoatlas* was initiated on an excursion of the International Gemmological Conference from the Alps to Vesuvius in Italy. The work involved in producing such a volume inevitably meant a long gestation period. The final text and photographs for this volume, which will contain a cornucopia of over 2000 plates of gemmological 'works of inclusion art' by the two gifted authors, was completed in late 2004, but tragically Edward did not live to see their *opus magnum*, now expected to be published in late 2005. His interest and comprehension of art history continued throughout his life, and he was eager to take opportunities to visit art galleries on his journeys around the world. In 1999 his popular book *Gemstones: Symbols of Beauty and Power*, co-authored with Franz-Xavier Erni, appeared in German, followed by an English edition in 2000. Aimed at a

wider readership, it was graced by a stunning series of colour plates by the gifted photographers Harold and Erica Van Pelt and others.

Edward was an intrepid traveller and visited gem deposits in many inhospitable lands. In the early 1960s, before the military government was in power, he was able to visit Mogok in Upper Burma with his eldest daughter, Marie-Helen, and made an excellent and timely film of the traditional gemstone workings, which he subsequently took great pleasure in showing to many audiences – Mogok then being difficult of access until the early '90s. He was also a great collector, and I remember an occasion in his home in Lucerne discussing with him the rare colourless chrysoberyls and pale bluish-green alexandrites from Mogok, whereupon he produced several fine specimens from his Burma (locality) collection only to follow them with other beauties from his equally comprehensive species collection.

He was a prolific correspondent, always ready to provide helpful advice and information, invariably written in his own inimitable and flowing English, and I treasure my file of letters from him going back nearly forty years.

His lovely wife Idda died in 1991, but he is survived by his five daughters, 12 grandchildren and 11 great-grandchildren.

He was a kind and generous man, a gemmological polymath and visionary. Throughout the world many gemmologists and mineralogists will share with me the thought that our distinguished friend Edward will be as in the words of Homer "Forever honour'd, forever mourn'd" (*Iliad*).



In honour of Professor Dr Edward J. Gübelin

Contributed by John I. Koivula

Reflecting an adventurous life, this 10 mm spray of acicular tourmaline crystals protogenetically embellished with microcrystals of quartz rests for eternity encased in rock crystal, a true symbol of beauty in nature. Sample personally collected in 1987 by Edward J Gübelin and John I. Koivula at the Golconda Mine in Minas Gerais, Brazil, during a field excursion at the XXI International Gemmological Conference. Polarized light with compensator. Photomicrograph by John I. Koivula, courtesy of microWorld of Gems.

If you think
it's child's play
to spot synthetic and
treated gems, grade
diamonds
and identify
antique jewellery,
you can buy
loupes in some
pretty
colours



For the rest of you we supply the building blocks

Gem♦A

The Gemmological Association and Gem Testing Laboratory of Great Britain
27 Greville St., London EC1N 8TN

T: +44 (0)20 7404 3334 - F: +44 (0)20 7404 8843 - E: info@gem-a.info - W: www.gem-a.info

Worldwide Gemmological Training - Seminars
Instruments - Books - Laboratory Services

HPHT treatment of different classes of type I brown diamonds

Thomas Hainschwang¹, Andrey Katrusha²
and Heiner Vollstaedt³

1. GEMLAB Gemological Laboratory, Landstrasse 193, FL-9491 Ruggell, Liechtenstein
2. Institute for SuperHard Materials, Kiev, Ukraine
3. AphroDiamante GmbH – R&D Center, Pappelallee 29, D-14555 Seddiner See, Germany

Abstract: As part of a study of the classification and origin of colour of brown diamonds by one of the authors (Hainschwang, 2003), seven stones belonging to defined classes were selected and treated by the HPHT process. Each diamond was tested extensively before and after the treatment using standard and advanced gemmological methods, including FTIR spectroscopy, low temperature Vis/NIR and photoluminescence spectroscopy. On treatment, all diamonds except the CO₂ and 'Pseudo CO₂' diamonds lost their brown coloration and exhibited various shades of yellow. It was found that the spectra of all diamonds except CO₂ and 'Pseudo CO₂' diamonds showed very apparent changes of which the elimination of the amber centre with its primary peak between 4070 and 4165 cm⁻¹ in the FTIR spectra is of particular interest. The results of the treatment are discussed in detail and correlated with the proposed classification, of which a summary is presented. One of the major results of this research is the identification of several origins of the brown colour in diamonds, including plastic deformation with associated defects and impurities such as CO₂.

Introduction

Diamonds have been artificially coloured for a very long time. Until the late 1990s this was done either by superficial coating, by painting or by the creation of lattice defects by irradiation, sometimes followed by annealing. The primary treatment since the early 20th century was irradiation / annealing, by which the colours of mainly type Ia and Ib yellow to pale brown diamonds can be changed. In this treatment, the high energy particles in the radiation displace some carbon atoms and thus create vacancies and

interstitials (Bienemann-Kuespert *et al.*, 1967); annealing causes these defects to diffuse through the lattice where the vacancies will be mostly trapped by nitrogen to form various nitrogen-vacancy defects, such as the NV⁻centre with absorption (zero phonon line(ZPL)) at 637 nm (Bienemann-Kuespert *et al.*, 1967). The primary radiation treatment results in green to greenish-blue to blue coloration, which can be changed to yellow, greenish-yellow or orange in type Ia pale yellow diamonds and to pink or purple in

type Ib diamonds by annealing at 600°–800°C (Bienemann-Kuespert *et al.*, 1967). The majority of brown type Ia diamonds, particularly the darker colours, are unsuitable for irradiation/annealing and are still mainly brown after such treatment. In the late 1990s, relatively large numbers of intensely coloured yellow to yellow-green diamonds with very strong green luminescence – also visible as transmission – appeared in the gemstone market. Such stones, which are frequently termed ‘green transmitters’, were very rarely seen before and are considered to be extremely scarce in nature. Buerki *et al.* were the first group to postulate in 1999 that these stones were produced by a new treatment: they proposed that the diamonds were treated by irradiation followed by very high temperature annealing at stabilizing pressure. However, Collins *et al.* (2000) doubted that irradiation was involved and thought that these diamonds were treated by high temperature annealing at stabilizing pressure only; the treatment was called the high pressure high temperature (HPHT) treatment and conditions of 1700°–2500°C at about 6.5 GPa were reported. Since then, several publications have covered the subject of the HPHT treatment; these include papers about the decoloration of type IIa brown diamonds (e.g. Smith *et al.*, 2000) and the production of green transmitters from type Ia brown diamonds (Reinitz *et al.*, 2000; Katrusha *et al.*, 2003) by HPHT. It was postulated that the reduction of the brown coloration is caused by the realignment of distortions in the crystal lattice; such distortion was (and by some still is) believed to be the sole cause the brown coloration of diamonds. According to this theory, vacancies are released during the realignment. The vacancies are trapped by nitrogen in type Ia diamonds but are mostly annihilated in type IIa diamonds since there is not enough nitrogen present; therefore type Ia diamonds will change colour while type IIa diamonds change to (near-) colourless after HPHT treatment. More recently, it has been suggested, that the brown colour of diamonds is due to graphitic (Ewels *et al.*, 2001) or amorphous carbon (E. Fritsch, pers.

comm. 2002), i.e. sp² bonded carbon; this may be recrystallized by the HPHT process causing release of vacancies and changes of colour like those described above.

Experiment

A classification of brown diamonds has been established by Hainschwang (2003) based on standard and advanced gemmological analysis of 63 samples selected from 900 brown diamonds using FTIR spectroscopy. Research on the possible formation of brown coloration and a detailed study of certain defects, notably the ‘amber centre’(see Box A) were also carried out. To investigate some of the theories and ideas, it was decided to take one or several samples from most of the proposed classes and treat a total of seven stones by HPHT at 2000°C and 6.5 GPa. The total HPHT cycle or process lasted 30 minutes and consisted of an increase of temperature to the maximum value of 2000°C, holding this for ten minutes and then switching off the power with rapid cooling. For the run, the stones were placed in a graphite capsule.

Materials and methods

The seven brown diamonds were analyzed using standard and advanced gemmological techniques before and after the HPHT treatment. The diamonds included one brown diamond each of type IaA, IaB, IaA/B, Ib, Ia containing solid CO₂ (Schrauder and Navon, 1993), Ia ‘Pseudo-CO₂’ (Hainschwang, 2003) and one olive-brown stone of type IaA. The colour of the stones was observed using 6200 K daylight illumination; and colour distribution was observed with the stones immersed in methylene iodide using diffuse transmitted light. The diamonds were examined with a binocular microscope fitted with crossed polarizing filters to see any strain and extinction patterns. Luminescence to long-wave and short-wave ultraviolet radiation was observed, including any observable phosphorescence after the UV source was shut off. Advanced analysis included FTIR spectroscopy and Vis/NIR as well as

photoluminescence (PL) spectroscopy. The IR spectra were recorded with a Perkin Elmer Spectrum BXII FTIR spectrometer using a DIGS detector, at resolutions of 4 cm^{-1} and 2 cm^{-1} . The Vis/NIR spectra covering the range of 400-1000 nm were recorded on an SAS2000 system equipped with an Ocean Optics SD 2000 dual channel spectrometer with a resolution of 1.5 nm. A 2048-element linear silicon CCD detector was employed. The samples were analysed in an integration sphere; all spectra were recorded at 77K. The direct measurement in the integration sphere causes a particular phenomenon when the spectra of strongly luminescent diamonds are recorded: in such stones emission bands can be apparent on the lower energy side of the ZPL of a luminescent centre such as H3; thus for the H3 centre with its ZPL at 503 nm, a vibronic structure as seen in luminescence can be found with three emission bands at 511, 520 and 528 nm (see Figure 6). The photoluminescence spectra were also measured with the stones immersed in liquid nitrogen using an SAS2000 Raman system equipped with a 532 nm semiconductor laser and having a resolution of 1.5 nm. This system employed the same spectrometer and detector as mentioned above.

Table 1: The colours of seven diamonds before and after HPHT treatment.

Sample number, type based on FTIR and features	Colour before HPHT	Colour after HPHT
DUG 7 Ib		
DUG 10 IaA, double amber centre 4070 cm^{-1} $/4165\text{ cm}^{-1}$		
DUG 18 IaA/B, very strong absorption due to platelets		
DUG 22 IaB (very little A), high hydrogen		
DUG 46 IaA		
DUG 3 Ia, solid CO ₂		
DUG 30 Ia, 'Pseudo CO ₂ '		

Results

Visual appearance

Before: The seven samples included six 'regular' brown diamonds and one olive-brown stone. Their tones varied from medium to dark.

After: In five stones, the brown colour was practically eliminated; the treatment did not change the colour of the CO₂ and 'Pseudo CO₂' diamonds significantly. The other five

NB: The stones were not repolished after the treatment, therefore they display matt surfaces.

stones exhibited a yellow hue after the treatment, some with a pale green and one with a pale pink modifying colour (Table I). The stones were not re-polished after HPHT, and display matt surfaces.

Colour distribution

Before: when discussing brown (and pink) diamonds, most people in the jewellery trade

BOX A: Summary of classification of brown diamonds

The proposed classification is based on the analysis and characterization of 900 brown diamonds between 0.03 and 4.09 ct by standard and advanced gemmological methods. Full details of the classification are in the Diplôme d'Université, Gemmologie (DUG) at the University of Nantes (Hainschwang, 2003). The basic characterization can be made by observation of the colour distribution and the infrared spectrum of each stone. The most important distinctions are made by the presence or the absence of an amber centre and by the presence or absence of coloured graining. The amber centre is a term describing a complex collection of peaks in the range ~ 8000 to 4065 cm^{-1} with a primary peak at 4165, 4115 or 4070 cm^{-1} , and this structure was observed in 97.4% of the analysed diamonds (see Figures 1 and 2). It has been found to be related to single atoms and A-aggregates of nitrogen (also known as C-centres and A-centres in some literature) combined with plastic deformation. Thus the amber centre cannot be found in type IaB, IIa and IIb diamonds nor in stones which have not experienced plastic deformation. Truly brown diamonds, which have not experienced such deformation, are rare and include stones containing solid CO_2 (Schrauder and Navon, 1995), 'Pseudo- CO_2 ' diamonds (Hainschwang, 2003), some very high nitrogen-containing type Ib diamonds and certain hydrogen-rich brown diamonds (Massi, 2003).

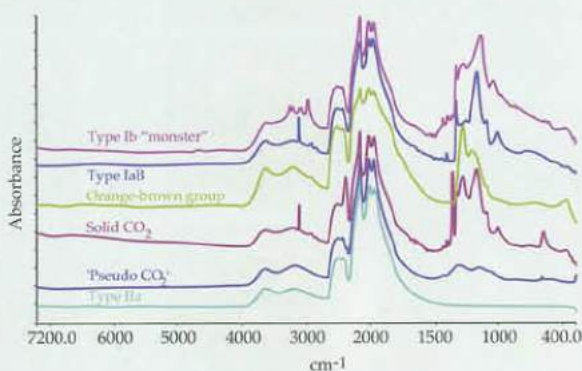


Figure 1: Spectra of the classes lacking the amber centre.

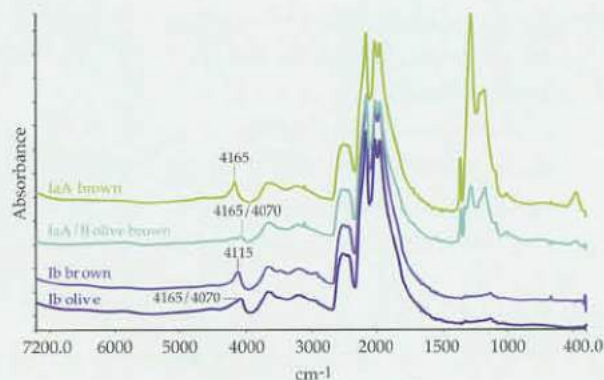


Figure 2: Spectra of the classes exhibiting an amber centre.

These rare stones were also found to show entirely different colour distribution, either patchy or around a phantom inclusion, and they have apparently a very different origin of colour (Figure 3). Around 98% of all brown diamonds have brown graining, i.e. parallel narrow planar brown bands (Figure 3). The list below contains all the determined classes; it must be mentioned that although hydrogen-rich brown diamonds were reported by Massi (2003), no such stones were found among our 900 brown diamonds.



Figure 3: Colour distributions of brown diamonds (left to right): graining, patchy colour, colour around phantom.

No	Class	Characterized by	Approx %
Exhibiting an amber centre			
1	Typical brown (Ia)	4165 cm ⁻¹ peak, brown 'graining'.	95%
2	Double amber centre (Ia+Ib)	4165 cm ⁻¹ /4070 cm ⁻¹ peaks, olive and brown graining.	2%
3	Regular Ib	4115 cm ⁻¹ peak, weak graining.	0.4%
Exhibiting no amber centre			
4	Orange-brown group (Ia/Ib)	Brown colour modified by orange, quite homogeneous.	Not represented in this study
5	Typical brown IaB pure	Colour usually distributed as 'graining'.	0.2%
6	Extreme Ib	Very high single nitrogen content. Colour around phantom.	0.3%
7	Type IIa	Generally little or no 'graining'.	0.6%
8	Solid CO ₂	2390 cm ⁻¹ and 645 cm ⁻¹ absorptions. Patchy colour.	0.9%
9	'Pseudo-CO ₂ '	Unusual nitrogen absorptions, no 2390 cm ⁻¹ / 645 cm ⁻¹ peaks. Patchy colour, 'colour banding'.	0.6%

will associate such diamonds with 'coloured graining'; this graining appears as sharp narrow parallel colour bands along octahedral growth directions (Figure 3). Five of the selected brown diamonds exhibited such brown graining albeit in variable strengths; the CO₂ diamond showed no graining but contained an irregular brown patch (Figure 3); the colour in the 'Pseudo CO₂' diamond was half irregular and patchy and half strongly developed brown graining.

After: Since the stones were not repolished they showed a burnt skin which did not permit an undisturbed view of the interior of the diamonds; immersion in methylene iodide helped but any faint colour irregularities could not be confirmed: nevertheless, immersion revealed that the graining had been practically eliminated and that the colour appeared quite homogeneous. The CO₂ diamond did not show any change and both before and after the HPHT run the same irregular brown patch was present. The colour distribution of the 'Pseudo CO₂'

diamond also did not change noticeably after annealing; after HPHT the colour bands reminiscent of brown graining were still present and thus are apparently different in nature from the graining in classic brown diamonds; thus these colour bands were called 'colour banding'.

Luminescence to UV radiation

The defects and changes of nitrogen aggregation, which are caused by the HPHT process, result not only in the formation of yellow to orange coloration, but also in a change of luminescence. This is also the case with the seven samples analysed in this study: all except the CO₂ and the 'Pseudo CO₂' diamond showed a very marked change in luminescence when excited by long-wave and short-wave ultraviolet radiation and a summary is given in Table II. Interestingly, none of our samples showed the typical strong 'pure' green luminescence, which has been described before (e.g. Reinitz *et al.*, 2000).

Table II: Luminescence of seven brown diamonds before and after HPHT treatment.

No(type)	Before HPHT		After HPHT	
	LW UV	SW UV	LW UV	SW UV
DUG 7 (Ib)	Faint reddish-orange	Weak reddish orange	Med. greenish blue	Strong chalky yellow
DUG 10 (IaA olive-brown)	None	None	Faint greenish yellow	None
DUG 18 (IaA/B)	Weak blue	Faint yellowish blue	Medium chalky blue	Medium chalky yellow
DUG 22 (IaB)	Weak chalky blue	Faint chalky blue	Strong chalky blue, lasting phosphorescence	Very strong greenish yellow, lasting phosphorescence
DUG 46 (IaA)	Faint yellow	None	Medium chalky blue	Medium chalky greenish yellow
DUG 3 (Ia CO ₂)	Medium yellow	Weaker yellow with weak lasting phosphorescence	Same as before	Same as before
DUG 30 (Ia'Pseudo-CO ₂ ')	Medium yellow	Weak yellow	Same as before	Same as before

Infrared spectroscopy

Changes of nitrogen aggregation: It was noted in all except the CO₂ and Pseudo-CO₂ diamonds that the treatment had changed the aggregation state of nitrogen to some degree; in the type IaA and IaA/B diamonds, the

amount of B-aggregates increased while the amount of A-aggregates decreased; thus it was concluded that the A-aggregates had been transformed into B aggregates. It was also notable that the type Ib brown diamond had been almost completely transformed into

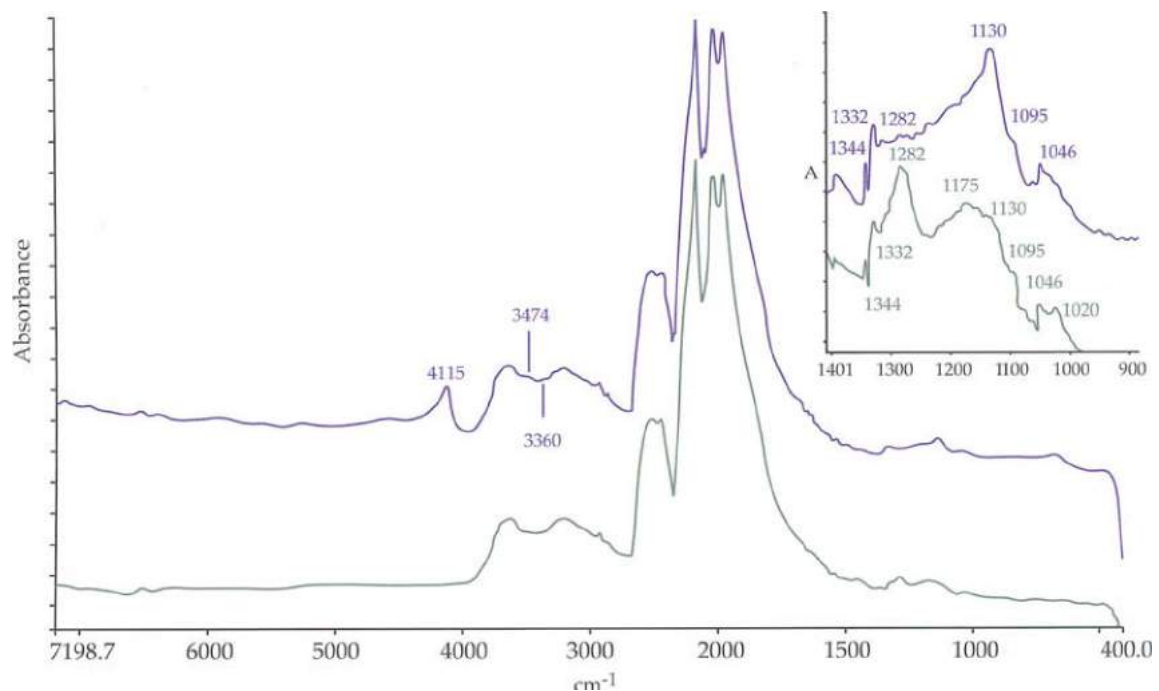
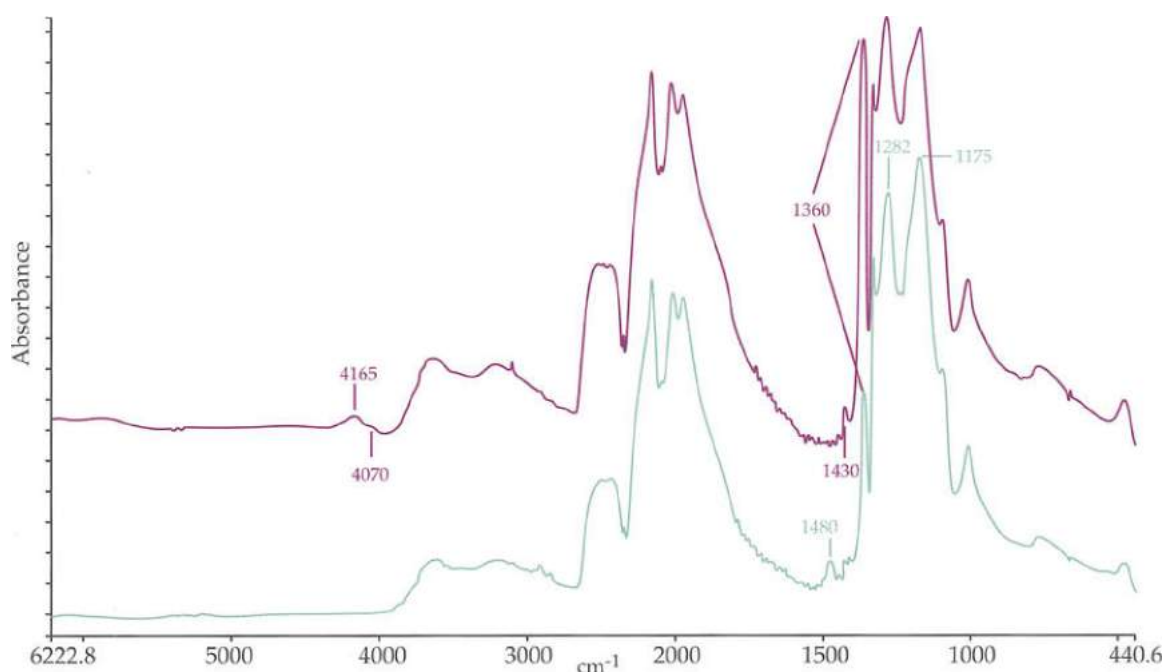


Figure 4: The FTIR spectrum of sample DUG 7, originally a brown type Ib diamond, before (blue trace) and after (green trace) HPHT treatment.

Figure 5: The FTIR spectrum of sample DUG 18, a brown IaA/B diamond, before (purple trace) and after (teal trace) HPHT treatment.



a type IaA/B diamond by aggregation of single nitrogen atoms into A- and B-aggregates (Figure 4).

Effects on other defect-induced absorptions

It has been described before that a defect called the 'amber centre' was eliminated by HPHT treatment (Reinitz *et al.*, 2000); Du Preez (1965) identified the main peak of this

complicated structure at 4165 cm⁻¹ in type I brown diamonds, but Hainschwang (2003) and Massi (2003) found that the main peak of this defect (the peak will be further referred to as the 'amber centre') was not only found at 4165 cm⁻¹ but could also be found at several different positions between 4070 and 4165 cm⁻¹ (see also Box A). During the HPHT experiment, all these peaks and the

Table III. Major changes observed in the FTIR spectra of the analyzed samples (CO₂ diamond not included [DUG 3]: no changes found)

Sample	Peak position, cm ⁻¹						Type
7 Before	4115	3474, 3360					Ib
7 After	none	none					IaA/B, some b
10 Before	4165	4070	1430	1405	1370	medium	IaA
10 After	none	none	none	1405	1370	weak	IaA, some B
18 Before	4165	4070	none	1430		1360 strong	IaA/B, A>B
18 After	none	none	1480	none		1360 weak	IaA/B, A<B
22 Before	4668	4494	4165	1430	1405	1362 strong	IaB, some A
22 After	none	none	none	none	none	1362 weak	IaB, less A
46 Before			4165			1360 medium	IaA
46 After			none			1360 very weak	IaA, some B
30 Before			none	615		1360 medium	Ia, A>B
30 After			2415	615		1360 weak	No changes CO ₂ (?)

associated structure were eliminated by the treatment (Figures 4 and 5). A strong reduction of the platelet peak, which can be found in the vicinity of 1360 cm^{-1} , was apparent (Figure 5) and has been reported before (e.g. Reinitz *et al.*, 2000).

Other defects, which were reduced or eliminated, include some of the hydrogen related features like the 3307 , 4494 , 4667 , 1405 and 1430 cm^{-1} absorptions. In sample DUG 18, a type IaA/B diamond with a very strong platelet peak, an absorption at 1480 cm^{-1} was formed by the HPHT treatment (Figure 5). This feature has only very rarely been observed in untreated diamonds (S. McClure, pers. comm. 2004). In sample DUG 7, a pure type Ib diamond before HPHT, the bands seen in the diamond intrinsic at 3474 and 3360 cm^{-1} were eliminated (Figure 4). In the spectrum of the CO_2 diamond, practically no changes were observed. In the 'Pseudo- CO_2 ' diamond, a peak at 2415 cm^{-1} was formed and the broad band around 650 to 400 cm^{-1}

was strengthened. The major changes induced by the HPHT treatment in the IR spectra are summarized in Table III.

Vis/NIR Spectroscopy

The Vis/NIR spectra of the brown diamonds before HPHT were categorized as follows:

Ia with very weak to undetectable N3, very weak H3, 550 nm band

Ib with distinct NV^- centre absorptions, 550 nm band

CO_2 and 'Pseudo CO_2 ' with continuous absorption but without distinct absorption bands other than a weak broad band at 480 nm.

After the HPHT treatment, weak to strong N3, H3 and H2 absorptions were formed in all samples except the CO_2 and 'Pseudo CO_2 ' diamonds. In the samples with distinct to strong H2 absorption, a related peak at 871 nm was observed. Besides a distinct N3 absorption, the H3 and H2 defects were weak

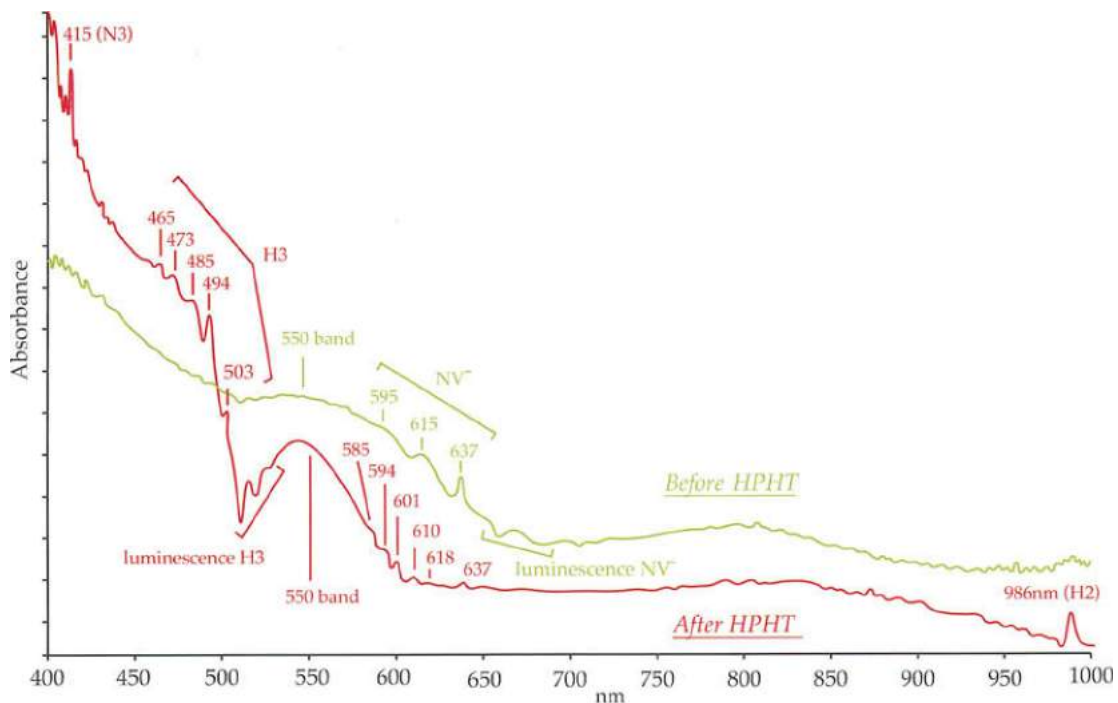


Figure 6: The Vis/NIR spectrum of sample DUG 7, originally a brown type Ib diamond, before and after HPHT. The spectrum before (green trace) exhibits only a distinct NV^- centre which causes the broad band at 550 nm. The aggregation of the single nitrogen by HPHT produced H3, H2 and distinct N3 absorption (red trace). Note that after HPHT, the NV^- centre was nearly eliminated and the stronger 550 nm band is due to the vibronic structure between 585 and 610 nm, and not to the NV^- centre.

Table IV. The changes observed in the Vis/NIR spectra of the analysed diamonds (CO₂ and 'Pseudo CO₂' diamonds not included: no changes observed).

Sample	Peak position, nm													
7 Before												550	615	637
7 After	415	465	485	494	503	550	585	601	610	618	637	871	986	
		473				594								
10 Before	415 weak	very weak H3			560									
10 After	415				494	503	871 986							
18 Before	415 weak	very weak H3			560									
18 After	415	473	485	494	503	560	871 986							
22 Before	415 weak	very weak H3			560									
22 After	415	473	485	494	503	560	986							
46 Before	415 weak	very weak H3			560									
46 After	415	473	485	494	503	560	871 986							

NB: The 494, 485, 473 and 465 nm peaks form the vibronic structure of the H3 centre with its ZPL at 503 nm; the 871 nm peak is part of the vibronic structure of the H2 centre with its ZPL at 986 nm; the 615 nm peak is a vibronic band of the NV⁻ centre with its ZPL at 637 nm; and the bands at 618, 610, 601, 594 and 585 are the vibronic structure forming the 550 nm band.

in sample DUG 10, which represents an olive-brown diamond of type IaA. Only a weak H2 centre combined with distinct H3 and N3 absorptions were present in sample DUG 22, a near-pure type IaB brown diamond. An interesting 'transformation' was observed in sample DUG 7, a pure type Ib brown diamond before HPHT: the apparent absorptions at 615 and 637 nm due to the NV⁻ centre present before HPHT were strongly reduced while rather strong H3 and

H2 defects and a vibronic structure between 585 and 618 nm were formed; it is notable that there was a strong N3 peak at 415 nm after the HPHT treatment (Figure 6). The observed changes seen by Vis/NIR spectroscopy are summarized in Table IV.

Photoluminescence (PL) spectroscopy

Before treatment, the emission of the brown diamonds excited by a green laser was mostly very weak; the only exception was the

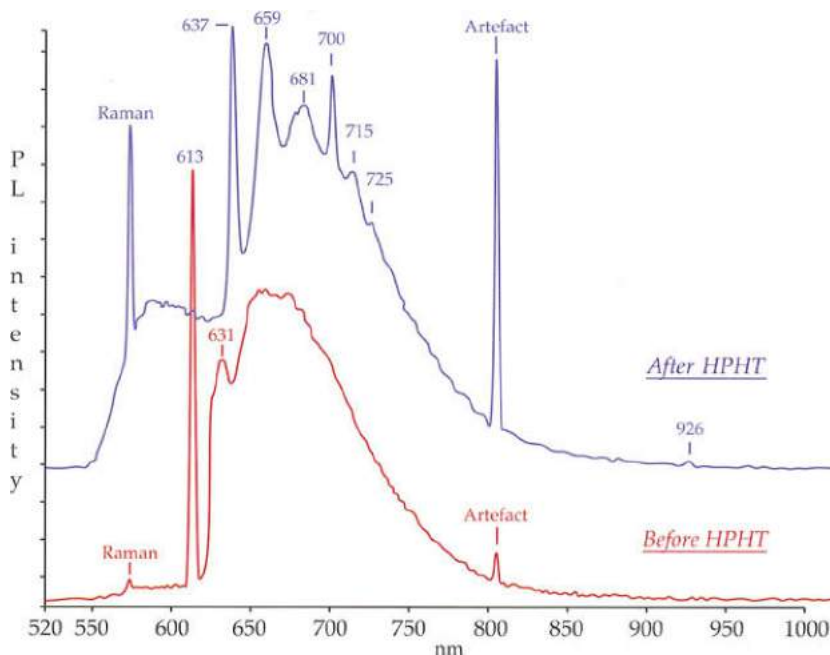


Figure 7: The PL spectra of sample DUG 10, an olive-brown type IaA diamond, before (red trace) and after (blue trace) HPHT. After HPHT, the spectrum indicates a clear type Ib character with strong peaks at 637, 659 and 681 nm.

The 659 and 681 nm peaks are the strongest bands of the vibronic structure of the NV⁻ center with its ZPL at 637 nm. The formation of the 700 nm centre with its 700 nm ZPL and vibronic bands at 715 and 725 nm plus the 926 nm feature tentatively indicate a nickel-nitrogen related defect.

Table V. The changes observed in the PL spectra of the analyzed diamonds (CO₂ and 'Pseudo CO₂' diamonds not included: no major changes observed).

Sample	Peak position, nm								
7 Before			587	600	620	637	659	681	707
After	566	575	587	600		637	659	681	707
10 Before				613	631				
After						637 strong	659	681	700 715 725 926
18 Before		575	596	613	626	637 weak			
After		575				637 strong	659	681	707
22 Before		575		600	613	620	637 weak		
After		575	588	596		620	637 strong	659	681 707
46 Before		575		600	613		637 weak	659	681
After		575					637 strong	659	681 707

NB: The 659, 681 and 707 nm peaks are the vibronic bands of the NV⁻ centre with its ZPL at 637 nm; and the 715 and 725 nm peaks are the vibronic bands of the 700 nm centre with its ZPL at 700 nm.

Ib diamond, which exhibited very strong photoluminescence. PL spectra of brown diamonds show a large variety of emissions; a typical PL spectrum for olive-brown diamonds is given in Figure 7 (red trace). Most peaks observed in brown diamonds have been described before, but some features present in CO₂ and 'Pseudo-CO₂' diamonds have not been described. Many of these emissions have been ascribed to brown diamonds but not explained so far (see for example Smith *et al.*, 2000). The NV⁻ centre peak at 637 nm was present in most samples, but except for the type Ib diamond, it was very weak. After HPHT treatment, all type Ia samples (except the CO₂ and 'Pseudo-CO₂' diamonds) showed PL spectra characteristic for type Ib diamonds with a very strong NV⁻ emission at 637 nm and peaks at 659 and 680 nm (Figure 7, blue trace); in contrast, the NV⁻ emissions in sample 7, the Ib diamond, were reduced. Some of the most interesting findings were made in the spectra of sample 10: besides distinct NV⁻ centres, the HPHT treatment resulted in a system with peaks at 700, 715 and 725 nm with an additional weak feature at 926 nm (Figure 7, blue trace).

Except for the reduction of certain emissions, no dramatic changes were observed in the PL spectra of the CO₂ and 'Pseudo-CO₂' diamonds. Table V summarizes

all noted changes in the PL spectra of the analyzed samples.

Discussion

The results of the HPHT treatment of seven brown diamonds indicate that they may be divided into at least two groups with distinctly different origins of colour. These include diamonds coloured by plastic deformation with an associated defect, and diamonds owing their brown colour to other defects such as solid CO₂ (Schrauder and Navon, 1993) or hydrogen (Massi, 2003). In the diamonds coloured by plastic deformation the brown colour is reduced by HPHT treatment while the treatment has little effect on other brown diamonds. The same conclusion can be drawn from fluorescence behaviour and from spectroscopic analysis: the observations and the interpretations are discussed in detail below.

FTIR spectroscopy

On treatment, changes in the aggregation state of nitrogen were observable; typically, B-aggregates increased at the expense of the A-aggregates, while single N atoms (C centres) were transformed into A- and even B-aggregates. It appears surprising that such changes in aggregation occur under the

HPHT conditions used in our experiments since A to B centre aggregation has been predicted to occur at temperatures of $>2600^{\circ}\text{C}$ (Kiflawi and Bruley, 2000), clearly above 2000°C . To explain the enhanced nitrogen aggregation in treated brown diamonds it may be proposed that aggregation at temperatures around 2000°C may be more likely with high concentration of dislocations and other defects in the brown diamonds; this is supported by the fact that the two diamonds not associated with plastic deformation did not show any apparent change of nitrogen aggregation. A similar effect has been described by Collins *et al.* (2000) who reported that A-aggregates could be formed in type Ib synthetic diamonds at temperatures as low as 1500°C , when the stones were irradiated prior to heating (vacancy-enhanced aggregation phenomenon). The temperatures indicated for the formation of A-aggregates from single nitrogen in untreated synthetic diamonds are in the proximity of 2000°C (Chrenko *et al.*, 1977). The changes in nitrogen aggregation have limited influence on the observed colour changes; the production of single nitrogen and of N3 aggregates by A to B centre aggregation or dissociation of A centres induce a yellow colour; unless elevated amounts of single nitrogen are produced, the main change of colour is not caused by nitrogen, but by a distinct H3 centre, which causes strong yellow colour and green luminescence.

The amber centre absorptions found between 4070 and 4165 cm^{-1} are one of the main features of interest. Apparently, the amber centre is very closely related to the defect responsible for the brown coloration of diamonds, and Hainschwang (2003) and Massi (2003) have found that it could be correlated either with the presence of single N atoms (C-centres) or with A-centres; B-centres were found not to be involved in this defect, since pure type IaB brown diamonds do not exhibit the amber centre. Also, since type IIa diamonds do not show this absorption, the defect is nitrogen-dependent. The absorption has only been observed in

brown to olive diamonds (both coloured by 'graining') or stones showing a brown to olive component, and it can be assumed that the defect responsible for the brown and olive colours is a component of the amber centre; thus the A centre or the single nitrogen combined with the defect, which is responsible for the brown colour, could possibly cause the amber centre absorption. Thus, if, the brown colour is indeed caused by graphitic or amorphous carbon, a combination of this sp^2 bonded carbon with the A or C centres may cause this feature; recrystallization of the sp^2 carbon into sp^3 carbon by HPHT treatment would accordingly eliminate the amber centre peaks, which would explain our findings. Another point to consider is one raised by Massi (2003) who reports that EPR measurements have indicated that the 4165 cm^{-1} absorption could be due to a deformed A-aggregate.

Vis/NIR spectroscopy

The increased absorption due to the H3 centre and the appearance of absorption due to H2 are well known effects of HPHT treatment. In our samples, weak to strong absorptions due to H3 and H2 were shown by all treated stones except the CO_2 and 'Pseudo CO_2 ' diamonds. The appearance of the absorptions H2, which is the negative charge state of the H3 centre, is believed to be caused by an electron transfer from single substitutional nitrogen to H3 centres (Buerki *et al.*, 1999). During HPHT treatment, substantial amounts of single nitrogen appear to be produced either as a by-product of the formation of B from A centres or simply by dissociation of the A-aggregates. The N3 absorption at 415 nm , which was generally weak or even undetectable before treatment of the brown diamonds clearly became more distinct. Most interesting is the fact that the type Ib diamond, which on treatment was transformed into a IaA/B stone, then exhibited a rather strong N3 absorption; the N3 aggregates were apparently formed as an intermediate product of A- to B-aggregation, as suggested by Kiflawi and Bruley (2000). The N3 absorption confirms our observation of the transformation from type Ib to type

IaA/B by HPHT. The vibronic structure between 585 and 618 nm has been observed by Shigley and Fritsch (1993) in a red diamond and has been interpreted as the vibronic structure of the 550 nm band. The formation of this structure in a formerly type Ib diamond, which originally showed a weak 550 nm band caused by the NV^- centre, is surprising and remains unexplained. The general formation of N3 and H3 has some influence on the observed colour; N3 will add pale yellow and a blue luminescence while H3 will add yellow and a green luminescence. The H2 absorption, if sufficiently strong, will give a green hue to a diamond (Collins *et al.*, 2000); none of our samples had strong enough H2 absorptions to exhibit a green face-up colour (which is not caused by H3 emission).

Photoluminescence spectroscopy

Photoluminescence spectra have clearly shown that significant amounts of single nitrogen were formed in the type Ia diamonds by the HPHT process, although this was not detected by FTIR spectroscopy. All stones which showed typical 'brown diamond PL spectra' before HPHT exhibited spectra characteristic of type Ib diamonds post HPHT; thus a very strong Ib character in PL, with strong NV^- and weak NV^0 emission, is typical for most of such treated diamonds. In the type Ib diamond, the NV^- centre emission was reduced due to the formation of A- and B-aggregates from single nitrogen atoms. The emission system with the zero phonon line (ZPL) at 701 nm and associated vibronic replicas at 715 and 725 nm plus the additional weak feature at 926 nm formed in sample DUG 10 (Figure 7) was identified by Iakoubovskii and Adriaenssens (2001) in natural hydrogen or nitrogen rich type Ia diamonds from Argyle, Australia. The 701 nm centre was tentatively assigned to a nickel-related defect. The same features were found by one author (TH) in similar Argyle stones and in chameleon diamonds. However, the PL spectra observed in the natural Argyle diamonds are very different and do not show strong 575 and 637 nm peaks. The appearance of these spectra

following HPHT may indicate that this centre is due to a nickel nitrogen defect; single substitutional nickel atoms are commonly bound to nitrogen atoms as found from annealing experiments of nickel-containing synthetic diamonds by Lawson and Kanda (1993).

Conclusions

Conclusions from the studies of the classification and origin of colour of brown diamonds indicate that there are four possible causes of the brown colour in natural diamonds: deformation with associated defect, CO_2+ 'Pseudo CO_2 ', high single nitrogen with associated defects, and hydrogen. Also, the absorption complex known as the amber centre is directly correlated with the cause of the brown colour in plastically deformed diamond; this feature is thus most important for the determination of the defect responsible for the colour in these stones.

From a gemmological standpoint, it can be stated, that a diamond with a type IaA/B infrared spectrum with an apparently unusually weak platelet peak and a 'type Ib' PL spectrum with 637 nm \gg 575 nm, may be strongly suspected of having undergone HPHT treatment. If additionally, H2 absorption is visible in the Vis/NIR spectrum, HPHT treatment must be assumed. In the experience of the authors the presence or absence of the H3 absorption cannot be used as an indication for the HPHT treatment.

A PL spectrum with a 'type Ib' character, with the 701 nm centre and vibronic sidebands at 715 and 725 nm, plus a 926 nm absorption has not so far been observed in an untreated diamond.

In rare cases, especially at higher annealing temperatures of 2400° to 2500°C, we observed 1344 cm^{-1} peaks due to single substitutional nitrogen together with A- and B-aggregates, even at standard resolution of 4 cm^{-1} ; the presence of all three A, B, and C

centre absorptions in one stone, although mentioned as a personal communication in a paper by Collins (2000), seems extremely unlikely in natural green to yellow to orange diamonds, and again, could be an indication of a treated stone. Some very rare and unusual diamonds exhibiting A, B and C-centres and H2 absorption have been identified by Hainschwang, Notari and Fritsch (in prep.) but these stones have properties very different from those shown by diamonds treated by HPHT.

Acknowledgements

The authors are grateful to the following persons for very fruitful discussions concerning the complex subject of brown diamonds: Emmanuel Fritsch (Institut des Matériaux Jean Rouxel, (IMN), Nantes, France), Franck Notari (Gemtechlab, Geneva, Switzerland) and Laurent Massi (Nantes, France).

References

- Bienemann-Kuespert, E., Brennecke, E., Flachsbart, I., Pietsch-Wilke, G., Stiess, P., and Wagner, J., 1967. *Gmelins Handbuch der Anorganischen Chemie*. Verlag Chemie GmbH, p. 237
- Buerki, P.R., Reinitz, I.M., Muhlmeister, S., and Elen, S., 1999. Observation of the H2 defect in gem-quality type Ia diamond. *Diamond and related materials*, **8**, 1061-6
- Chrenko, R.M., Tuft, R.E., and Strong, H.M., 1977. Transformation of the state of nitrogen in diamond. *Nature*, **270**, 141
- Collins, A.T., Kanda, H., and Kitawaki, H., 2000. Colour changes produced in natural brown diamonds by high-pressure, high temperature treatment. *Diamond and related materials*, **9**, 113-22
- Du Preez, L., 1965. *Electron paramagnetic resonance and optical investigations of defect centres in diamond*. Thesis, University of the Witwatersrand, Johannesburg
- Ewels, C.P., Wilson, N.T., Heggie, M.L., Jones, R., and Briddon, P.R., 2001. Graphitization at diamond dislocation cores. *Journal of Physics: Condensed Matter*, **13**, 8965-72
- Hainschwang, T., Notari, F., and Fritsch, E. Natural, untreated diamonds showing the A, B and C infrared absorptions ('ABC diamonds'), and the H2 absorption. *In prep.*
- Hainschwang, T., 2003. *Classification and Color Origin of Brown Diamonds*. Diplôme d'Université de Gemmologie (DUG), University of Nantes, France
- Iakubovskii, K., and Adriaenssens, G.J., 2001. Optical characterization of natural Argyle diamonds. *Diamond and related materials*, **11**, 125-31
- Katrusha, A.N., Vollstaedt, H., Zanevskyy, O.A., and Ivakhnenko, S.A., 2003. High pressure high temperature treatments (HPHT) for color changes of natural gem diamonds. *Jewellery Business, Kiev*, **2** (4), 42-7
- Kiflawi, I., and Bruley, J., 2000. The nitrogen aggregation sequence and the formation of voidites in diamond. *Diamond and related materials*, **9**, 87-93
- Lawson, S.C., and Kanda, H., 1993. An annealing study of nickel point defects. *J. Appl. Phys.* **73** (8), 3967-73
- Massi, L., 2003. *Défauts responsables de la couleur brune dans les diamants*. Mémoire de stage du Diplôme d'Etudes Approfondies « Sciences des Matériaux », University of Nantes, France
- Reinitz, I.M., Buerki, P.R., Shigley, J.E., McClure, S.F., and Moses, T.M., 2000. Identification of HPHT treated yellow to green diamonds. *Gems & Gemology*, **36** (2), 128-37
- Schrauder, M., and Navon, O., 1993. Solid carbon dioxide in a natural diamond. *Nature*, **365**, 42-4
- Shigley, J.E., and Fritsch, E., 1993. A notable red-brown diamond. *Journal of Gemmology*, **23**(5), 259-66
- Smith, C.P., Bosshart, G., Ponahlo, J., Hammer, V.M.F., Klapper, H., and Schmetzer, K., 2000. GE POL diamonds: before and after. *Gems & Gemology*, **36** (3), 192-215

Describing diamond beauty – assessing the optical performance of a diamond

Michael D. Cowing, FGA

AGA Certified Gem Laboratory

Abstract: *A diamond's optical performance is the visual interaction of the diamond reflecting and refracting the surrounding light to the viewer. It is this performance of the diamond that results in its beauty. This work advances the idea that the best diamond cuts 'evolved' to have the highest optical performance in a variety of typical viewing and illumination circumstances.*

Current and historical descriptors of diamond beauty and performance are reviewed. The rationale is put forward for the need to augment the current, single, quantitative measure of brilliance - light return intensity with the qualitative aspect of 'contrast brilliance'. Contrast brilliance is explained, and illustrated with diamond photography. The relationship between contrast brilliance and scintillation is also examined.

Introduction

When a gemmologist or appraiser evaluates a diamond, it is rated in four categories: cut, colour, clarity and carat weight. Known as the '4 Cs', these characteristics, which are related to the diamond's beauty and rarity, are assessed when arriving at its value. Of the four Cs there is general agreement that cut has the greatest influence on the diamond's beauty. The term cut may bring to mind any of three features of a polished diamond.

1. Shape such as round, pear, oval, cushion or rectangular.
2. Style of facet pattern such as radiant, step cut or princess cut.
3. The angles and proportions of a particular style and shape.

This article confines the meaning of cut to the angles and proportions of a particular shape and style of a diamond, such as the familiar 57-facet round brilliant.

There are several elements to the quality of

cut. Judgement of these elements falls in two distinct categories.

The first category is craftsmanship. Examples of craftsmanship are perfection of polish, facet meet points, facet alignment, symmetry, facet angles and proportions. Most grading of diamond cut being done today makes judgements that fall within this category.

The second category is an assessment of the extent to which all the various factors of craftsmanship have or have not actually resulted in a beautiful diamond. This category is 'direct assessment' of aspects of diamond beauty as opposed to the indirect assessments of beauty in the first category. Two important examples that fall in this second category are measures of brilliance and fire.

The quantity together with the 'quality' of the light returned from a diamond to the eye of the viewer is critical to the viewer's judgement of the diamond's performance and beauty.

Diamond beauty – brilliance, fire and sparkle

A well-cut diamond has the ability to reflect colours and light from a broad range of surrounding directions and angles. A well-cut round brilliant diamond reflects and refracts the surrounding panorama of light to the viewer in a mosaic – even artistic – composition possessing vibrancy and vitality.

This article refers to the visual interaction of the diamond reflecting and refracting the surrounding light to the viewer as the diamond's 'optical performance'. This optical performance results in the diamond's beauty. The beauty that results from this unique performance has stirred emotions and engendered devotion unsurpassed by any other gemstone.

Historical and contemporary terms describing diamond beauty

Brilliance, fire and scintillation (sparkle with movement) are three words that have evolved to describe diamond beauty. These are the terms currently used in the diamond industry by gemmologists, diamond cutters and sellers to convey aspects of diamond beauty with simplicity and clarity.

The most beautiful diamonds have 'the most vivid fire and the greatest brilliancy,' proclaimed Marcel Tolkowsky (1899-1991), the historically influential Belgian diamond cutter and mathematician who was credited with the key design proportions of the ideal round brilliant. Both he and his contemporaries used these two terms, brilliance and fire, to describe the beauty of a diamond. The third descriptor of diamond beauty called scintillation has since been added.

Combined with 'contrast brilliance', a related fourth aspect of diamond beauty introduced by this article, the jeweller is armed with the necessary vocabulary to convey the beauty of one diamond cut compared to another.

Brilliance

The *Diamond Dictionary* (Gaal, 1977) defined brilliance as: 'the intensity of the internal and external reflections of white light to the eye from a diamond or other gem in the face up position.' It is important to note here that brilliance was being defined as the intensity of light return. This 'brightness' measure which is a single value lacks any detail of the important variations in intensity across the diamond. This intensity variation or 'contrast' is needed to complete the picture of the historical meaning of brilliance.

Fire

Called the diamond's fire, an important aspect of the quality of light return is the diamond's dispersion of light into rainbow colours.

Scintillation or sparkle

Characterization of diamond beauty by fire and brilliance leaves all features other than fire as aspects of brilliance. A definition of brilliance narrowed to the single quantitative measure of average brightness necessitates additional descriptors of other quality aspects of diamond brilliance.

Scintillation is one such descriptor. Scintillation is the word used to describe a quality aspect of brilliance historically referred to as the diamond's 'life'. It is the diamond's sparkle occasioned by movement of the diamond, the illumination or the observer. This quality of light return is the sharp, on-off, bright-dark sparkle or flashes of light 'dancing' from the crown of the diamond.

These three terms used today to describe diamond beauty - brilliance, scintillation and fire - were the respective qualities that Tolkowsky noted in *Diamond Design* (Tolkowsky, 1919, p.24). He said: "The general trend of European diamond polishing is the constant search for greater brilliancy, more life, a more vivid fire in the diamond, regardless of the loss of weight." These are the qualities that diamond cutters of his day were seeking in their search for the most beautiful diamond cut. Maximizing these qualities of diamond beauty has remained the goal of diamond cutters from that time to the present.

Contrast quality of brilliance

In addition to scintillation, another descriptor is needed to augment the single, quantitative definition of brilliance as average brightness.

Why is this additional descriptor of brilliance needed? Human perception of brilliance goes beyond the brightness of the light returned from the crown of a diamond.



Figure 1: Photograph of a scene printed with less contrast.



Figure 2: Photograph of Figure 1 printed with greater contrast.

Intensity variation or contrast in light and dark areas across the diamond gives it an aspect of brilliance that has been described as 'snappy', 'dramatic' and by Bruton (1978, p.227) as 'hard' or 'sharp'.

These descriptions are the opposite of 'watery' and 'glassy' used in *The Diamond Dictionary* (Gaal, 1977) to describe the weak appearance of a poorly cut, 'fish-eye' diamond.

In this article the term 'contrast brilliance' is adopted to describe this aspect of brilliance. The term is needed because this aspect of diamond beauty influences our judgement of which diamond cuts are the most brilliant. Recognizing this contrast aspect of brilliance gives us a means for explaining why one diamond cut may be perceived as less brilliant than another even though it may have had an equal or greater average brightness.

It is worth noting that an emerald cut diamond is normally perceived to be less brilliant than a round cut mainly because it has less contrast brilliance even though it may have a similar brightness.

A second need for introducing contrast brilliance involves its relationship to scintillation. Scintillation will be shown to be the dynamic form of contrast brilliance. Because of its dynamic nature, scintillation eludes measurement, while contrast can be measured from static diamond images. The relationship between contrast and scintillation enables an assessment of both, through the characteristics they have in common.

Simultaneous contrast

The contrast aspect of brilliance is linked to a property of human vision called 'simultaneous contrast'. When a bright reflection is close to a darker one, our vision enhances the perception of the difference, and the bright reflection looks brighter because of its proximity to the dark reflection. The greater the contrast in a diamond, the brighter it appears to our eye.

One consequence of this phenomenon is our attention to variation or contrast in a scene. For example, we are generally attracted to greater contrast in a picture. Note the example in *Figures 1 and 2*. Most people would agree that the greater contrast in *Figure 2* makes the photograph more appealing.

The following experiment is designed to illustrate and support the idea that contrast in a diamond influences the perception and

judgement of brilliance. The diamond image in *Figure 3* was printed with maximum contrast. The same diamond image in *Figure 4* was printed with less contrast between the bright reflections and the adjacent dark reflections.

Using the current quantitative definition of light return intensity, the *Figure 4* image would emerge as having the greater brilliance. However, we would probably all perceive the *Figure 3* diamond image as more brilliant. The perception of greater brilliance in *Figure 3* is due to the white reflections in that diamond appearing brighter and more intense because of greater contrast with the dark reflections. Actually, the white reflections in both *Figures 3* and *4* have the same intensity.

This demonstration illustrates and supports the influence and importance of contrast to the perception and judgement of brilliance.

Dependence of diamond beauty upon viewer and illumination circumstances

Both the brightness and contrast aspects of brilliance depend not only upon the cut of the diamond, but also its illumination and viewer circumstances.

Figures 5 and *6* are two photographs of the same diamond illuminated in different ways. In *Figure 5* the diamond was uniformly illuminated from above with no obstruction from the presence of the viewer. This resulted in a diamond image with high light return intensity but low contrast. This type of uniform illumination, lacking contrast, results in an unfamiliar and undesirable diamond appearance, which also lacks contrast.

The illumination of the diamond in *Figure 6* consisted of high contrast lighting. As a result this particular diamond cut exhibited a high contrast aspect of brilliance.

Figures 5 and *6* have demonstrated that the brightness and contrast aspects of brilliance are interrelated with the diamond's illumination. It is often overlooked that the perception of diamond beauty in all its aspects is influenced by the character of the illumination.

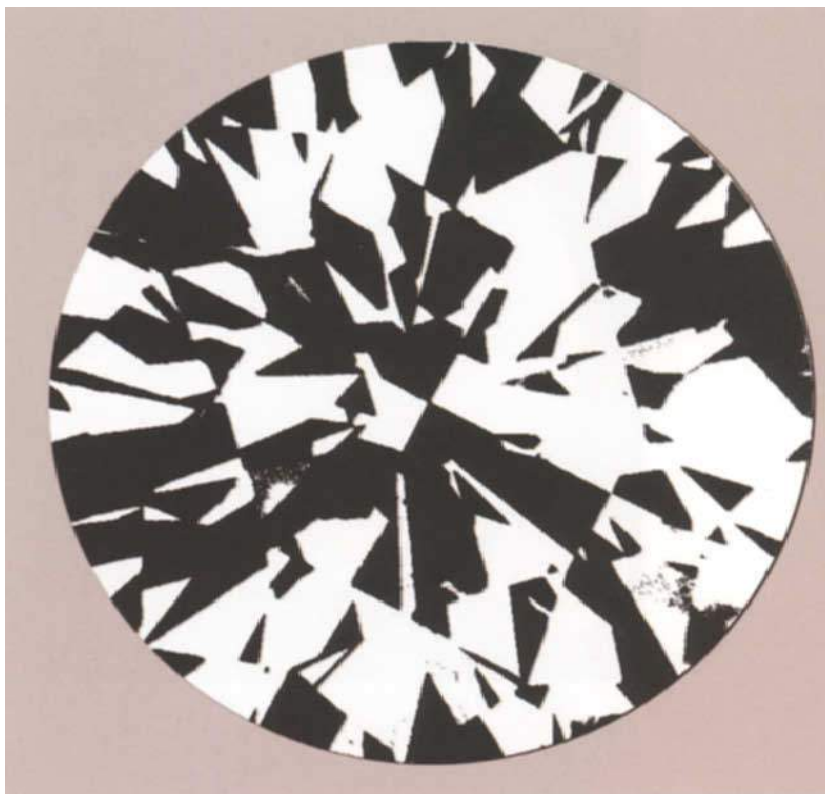


Figure 3: Diamond image printed with maximum contrast; it has a lower light-return intensity than the image in Figure 4.

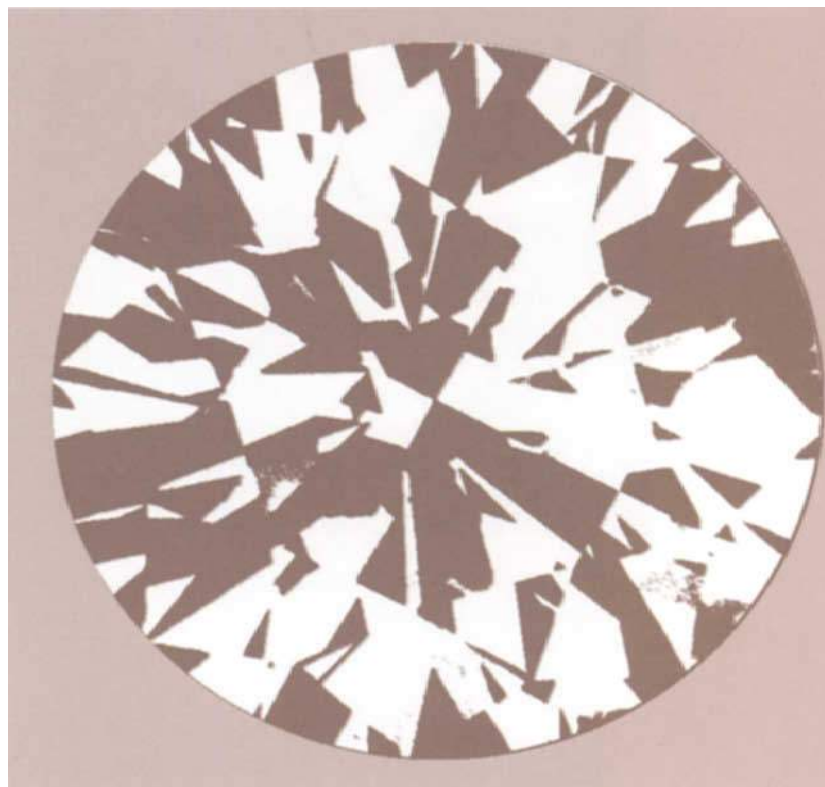


Figure 4: Diamond image printed with less contrast but a greater intensity of light return than that in Figure 3.

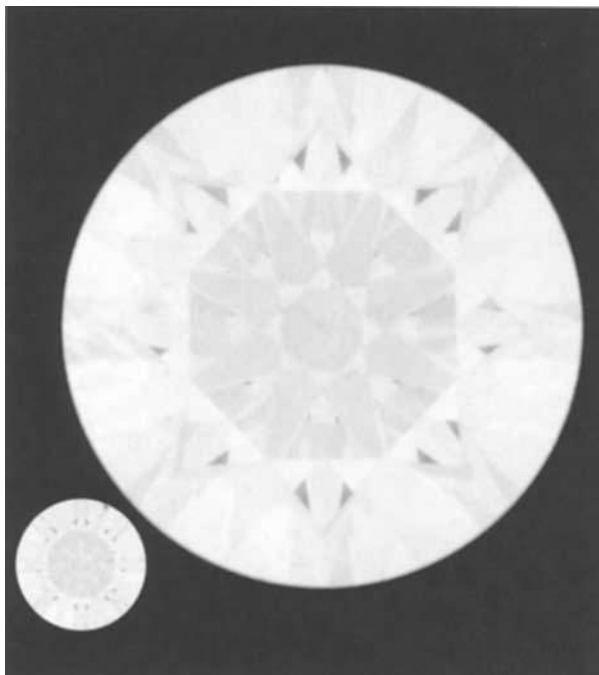


Figure 5: Diamond exhibiting high light return brilliance but low contrast brilliance.



Figure 6: Same diamond as that in Figure 5 exhibiting high contrast brilliance.

It is crucial to note that the perception that a diamond is beautiful depends upon the ability of the cut to take full advantage of the lighting under which it is being viewed.

Evolution of excellence in diamond cutting

The development of diamond cutting judged most beautiful evolved through 'cut and try' experimentation. Because success was judged under standard or typical illumination (discussed below), which was not uniform, the finest cutting inevitably evolved to have the greatest beauty in those typical viewing and non-uniform illumination circumstances.

This article advances the idea that diamond cuts judged to have ideal optical performance and beauty possess brighter, more evenly distributed, higher contrast reflections in a variety of typical illumination circumstances.

The worth of a measure of diamond beauty depends upon how well it agrees with human judgement.

'Perception of beauty is everything.' To be meaningful, measurements of diamond beauty should be made in illumination typical of circumstances in which human judgement of that beauty is made. Measurements of beauty in atypical lighting can give high scores to cuts that have lower scores in typical illumination. For example, measurements of brilliance in uniform lighting (such as that illuminating the diamond in Figure 5) can give high brilliance scores to cuts that have lower perceived brilliance in typical illumination.

Typical illumination and viewer obstruction

There is a short list of key characteristics of typical viewing circumstances that has influenced the evolution of the most beautiful and highest performing diamond cuts. One key, ever-present feature of typical viewing circumstances is the influence of the presence of the viewer on the illumination of a diamond.

Although this 'viewer obstruction' at first sounds disadvantageous, in well-cut diamonds it most often adds contrast to the illumination that is favourable to beauty. That same viewer obstruction results in poor optical performance in a badly cut diamond. For



Figure 7: Face-up photograph of a 2.25 ct diamond exhibiting brilliance and blue fire occasioned by bright, overcast sky partially obscured by the viewer.



Figure 8: The pattern of illumination of the diamond in Figure 7 as seen mirrored in the ring's prong. The overcast sky is partially obscured by the silhouette of the viewer's head, torso and outstretched hand and arm.



Figure 9: Tilted round brilliant cut diamond displaying fire and contrast brilliance under the partially obscured illumination of bright, overcast sky.



Figure 10: Face-up view of a round brilliant cut diamond displaying fire and contrast brilliance under the partially obscured illumination of bright, overcast sky.

example, in Figures 7, 9 and 10, where there is open sky illumination, it is the viewer obstruction that introduces contrast to otherwise diffuse illumination. This illumination is seen mirrored in the ring's prong in Figure 8. The prong acts as a convex mirror reflecting the entire panorama of illumination.

The dark appearance of the viewer in the prong is the factor providing the primary contrast in illumination. It is the synergy of the diamond's cut taking advantage of this contrast in illumination that produces the contrast and fire present in the diamonds in Figures 7, 9 and 10. Without contrast in its

illumination even the best diamond cut will lack contrast brilliance and fire, as *Figure 5* demonstrates.

The factors that characterize this contrast quality of brilliance are the sharpness, number, sizes and uniformity of the distribution of the diamond's mosaic-appearing pattern of reflections.

How can we assess this contrast aspect of brilliance?

The answer is simple. All these aspects may be observed and evaluated from stationary images or 'snapshots' of a diamond under a representation of typical viewing and illumination circumstances. Because diamonds are most often viewed in the face-up position, the most important snapshot to examine for contrast brilliance is this normal, face-up view (see *Figure 10*). Snapshots at other angles of observation representing usual tilts of the diamond also need to be examined.

Relationship between the contrast quality of brilliance and scintillation

What is the difference between contrast brilliance and scintillation? Clearly, the diamond's mosaic pattern of reflections has aspects common to both contrast and scintillation such as those already mentioned. However, the contrast quality of brilliance is the diamond's 'static contrast', whereas scintillation is the 'dynamic contrast' due to movement. Contrast brilliance is one frame or snapshot of the moving picture of scintillation. In fact, the change in contrast brilliance with movement from one moment to the next is scintillation. Contrast brilliance and scintillation are perceptually and mathematically related in this way. (Mathematicians may recognize scintillation as the partial derivative of contrast brilliance with respect to movement.)

Conclusions

These examples, illustrations and photographs support the need for the additional descriptor of contrast brilliance. Contrast bril-

liance complements the light return intensity aspect of brilliance, which is the current widely used definition.

Recognizing this stationary aspect of brilliance gives us a means for explaining why one diamond cut may be perceived as less brilliant even though it has an equal or greater intensity of light return.

The established language for describing diamond beauty includes the principal terms brilliance, fire and scintillation or sparkle. Contrast brilliance adds another dimension to the measure of brilliance, which is currently confined to the average brightness or intensity of light return. In addition, evaluation of contrast in snapshots of diamonds provides a way to deal with the more difficult to measure, dynamic aspect of scintillation.

Recognition and judgement of this additional quality aspect of brilliance helps complete our understanding of why one diamond cut is preferred over, and is seen as more beautiful than, another.

References

- Bruton, E., 1978. *Diamonds*. 2nd edn. Chilton Book Co. Radnor, PA. 532 pp
- Gaal R.A.P., 1977. *The Diamond Dictionary*. 2nd edn. Gemological Institute of America, California. 342 pp
- Tolkowsky M., 1919. *Diamond Design*. Spon & Chamberlain, New York. 104 pp

Gem-quality musgravite from Sri Lanka

Dr Karl Schmetzer¹, Dr Lore Kiefert²,
Dr Heinz-Jürgen Bernhardt³ and Murray Burford⁴

1. Taubenweg 16, D-85238 Petershausen, Germany

2. SSEF Swiss Gemmological Institute, Falknerstr. 9, CH-4001 Basel, Switzerland

Present address: AGTA-GTC, New York

3. Central Microprobe Facility, Ruhr-University, D-44780 Bochum, Germany

4. 136 Beechwood Avenue, Victoria, British Columbia V8S 3W5, Canada

Abstract: Gemmological, chemical and spectroscopic properties of a transparent, gem-quality rough musgravite from Sri Lanka are presented. A detailed analysis of musgravite samples reveals that applying X-ray diffraction and/or electron microprobe analysis and/or micro-Raman spectroscopy are decisive in establishing the identity of this rare gemstone. The greyish-blue pebble of 1.42 ct consists of a musgravite crystal with lamellar inclusions of spinel. With refractive indices of 1.721 (n_e) and 1.717 (n_o) and a specific gravity of 3.61, the musgravite has an iron content of 0.91 wt.% FeO, while the spinel exsolution lamellae reveal higher amounts of 1.89 wt.% FeO.

Introduction

Over the last few years, the gem island of Sri Lanka has supplied some new and extremely rare gem materials such as bromellite, serendibite and grandidierite (McClure and Muhlmeister, 2002; Schmetzer *et al.*, 2002, 2003). From all these gem minerals, only a limited number of faceted samples are known. Another gem species from Sri Lanka which could be placed on a list of extremely rare gem materials is musgravite, a beryllium-magnesium-aluminium oxide, which is chemically and structurally related to taaffeite. Both minerals, taaffeite $\text{BeMg}_3\text{Al}_8\text{O}_{16}$ and musgravite $\text{BeMg}_2\text{Al}_6\text{O}_{12}$, were originally regarded as polytypes of one single mineral species. Chemical and structural examinations proved the existence of two independent mineral

species with different chemical formulae, unit cell dimensions, space groups and crystal structures (Schmetzer, 1983 a, b; Nuber and Schmetzer, 1983). Due to a recently published nomenclature, the two minerals are now regarded as so-called polysomatic members of the taaffeite group, in which taaffeite is designated as magnesiotaaffeite-2N'2S and musgravite becomes magnesiotaaffeite-6N'3S (Armbruster, 2002).

Since the discovery of the first taaffeite as a cut gemstone in 1945, faceted and rough taaffeites of gem quality have come predominantly from Sri Lanka, with only a few rare samples reported to come from Myanmar and Tanzania. In 1993 two faceted 'taaffeites', probably from Sri Lanka, weighing



Figure 1: This water-worn pebble of 1.42 ct, size about 8.4×5.5 mm, represents the first rough gem-quality musgravite found in Sri Lanka.



Figure 2: Needle-like structures form a characteristic inclusion pattern in the musgravite pebble. Magnified $200 \times$.

0.30 and 0.37 ct, were identified as musgravites by means of X-ray single crystal diffraction. The colour of this material was described as greyish-mauve with a greenish cast (Demartin *et al.*, 1993).

Because the difference in BeO content between taaffeite and musgravite is only 1.56 wt.%, similar physical properties such as refractive indices and specific gravity are observed for both mineral species. Due to the overlapping ranges of gemmological properties an examination by X-ray diffraction (powder or single crystal techniques) or a quantitative chemical analysis (e.g. by

electron microprobe) was necessarily applied for an unambiguous distinction of musgravite and taaffeite. More recently, micro-Raman spectroscopy has also been found to be useful as a non-destructive routine technique for identification of both species (Kiefert and Schmetzer, 1998; McClure, 2001).

Subsequent to the first description of the two faceted samples by Demartin *et al.* (1993), a number of 'possible musgravites' were examined in gemmological laboratories and determined as taaffeites. In this search to find other musgravites of gem quality, to the knowledge of the present authors, the finds of only two faceted gemstones have so far been published, both of unknown provenance. These two stones of 0.60 and 0.36 ct, brownish-purple and greenish-grey respectively, were identified in the GIA Trade Lab and described briefly by Johnson and Koivula (1997) and by McClure (2001).

In addition to Sri Lanka, musgravite is known from a limited number of localities in only three countries: Australia, Greenland and Madagascar, as well as Antarctica (see the detailed compilation of data by Grew, 2002). The colour of the samples is described in the Musgrave Ranges, Australia (type locality) as pale olive green (Hudson *et al.*, 1967), at Casey Bay, Antarctica, as dark green (Grew, 1981; Grew *et al.*, 2000), at Dove Bugt, Greenland, as black (Chadwick *et al.*, 1993) and at Sakeny, Madagascar, as light grey to colourless (Rakotondrazafy, 1999). In these localities, musgravite occurs in high-grade metamorphic rocks and is not of gem quality.

The rough musgravite pebble of 1.42 ct to be described in this paper (Figure 1) was found among a group of mixed gem samples including some 'possible musgravites' which were submitted for examination to one of the authors (MB) by W. Molligoda, a gem collector residing in Kohuwela, Sri Lanka. According to the information obtained from Molligoda (pers. comm., 2003), the water-worn pebble was bought in 2000 and, most probably, came from the Horana area, which is about 37 km west of Ratnapura.

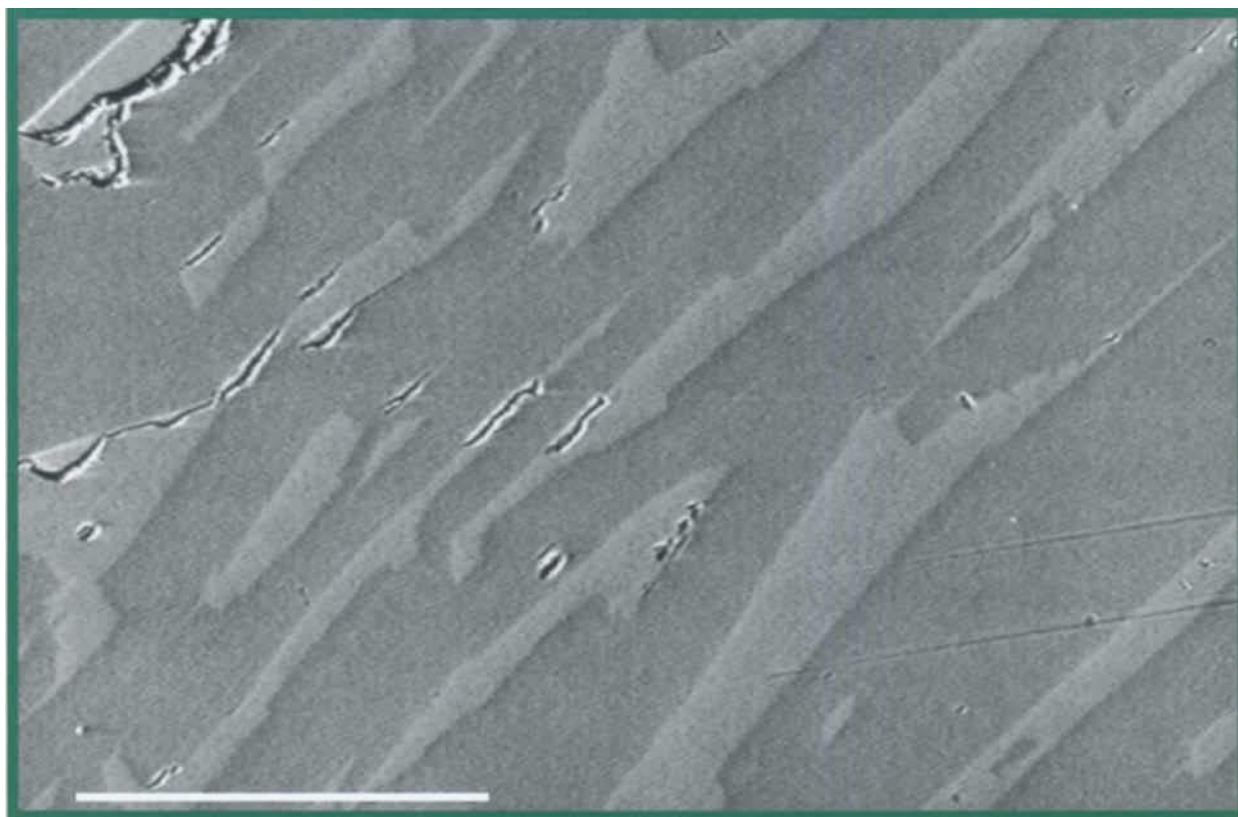


Figure 3: Back-scattered electron (BSE) image of spinel lamellae (pale grey) in a matrix of musgravite (dark grey); the length of the bar represents 200 μm .

Materials and methods

The water-worn pebble received for further examination and identification was provided with a polished window to measure refractive indices. Standard gemmological methods were used to determine refractive indices (RI), optic character, specific gravity (SG) and fluorescence under long- and short-wave ultraviolet radiation. Standard microscopic techniques were used to examine the internal features under different lighting conditions, both with and without immersion liquids.

To perform X-ray powder diffraction analysis a minute amount of material was scraped from the rough surface of the specimen. In order to obtain adequate resolution, a Gandolfi camera with a diameter of 114.6 mm and $\text{CuK}\alpha$ radiation was used.

To further characterize the sample, a Cameca Camebax SX 50 electron microprobe was used to obtain 15 point analyses from a traverse across the polished window of the

gemstone. In order to be sure of obtaining quantitative data of both the host and its inclusions (i.e. to analyse single mineral phases), the different points of the traverse were located by means of back-scattered electron (BSE) images. These are sensitive to composition, with darker greys indicating lower average atomic number elements and lighter greys, those of higher atomic number (see Figure 3).

Non-polarized UV-Vis (300-800 nm) absorption spectra were recorded using a Cary 500 Scan spectrophotometer. In addition, we analyzed the sample and its solid inclusions by laser Raman microspectrometry using a Renishaw 1000 system. Although it was impossible to recognize clear differences between the host and its inclusions by microscopic examination of the polished surface, we obtained different spectra of both phases using a simple trial and error procedure, by examining numerous points on the polished face.

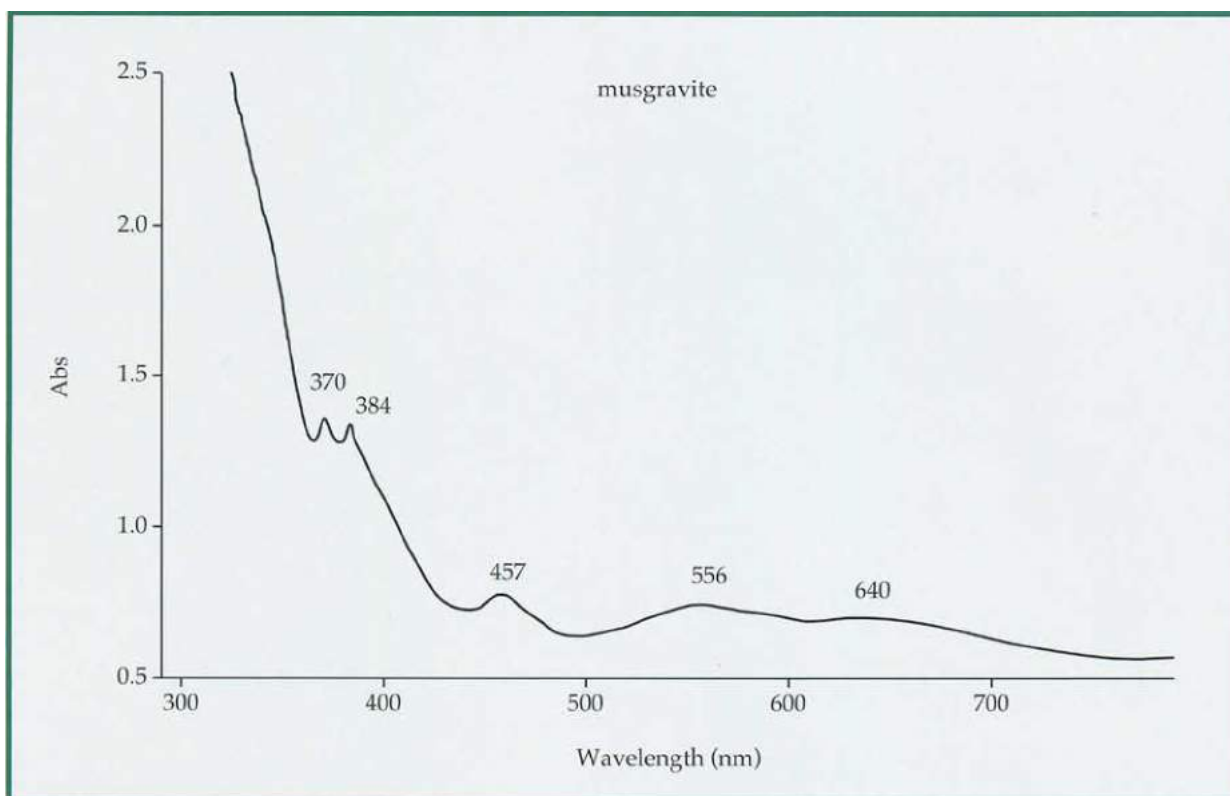


Figure 4: Non-polarized UV-Vis absorption spectrum of musgravite with lamellar spinel inclusions from Sri Lanka; direction of the incident beam is slightly inclined to the c-axis of the musgravite host.

Results

Gemmological properties

The colour of the transparent musgravite (Figure 1) is greyish-blue with a light green tint. The stone is uniaxial negative and showed clear RI readings with n_o 1.721, n_e 1.717; pleochroism was not detected. The SG was determined as 3.61. The sample was inert to both long- and short-wave UV radiation.

Features observed with the microscope

In the immersion microscope, an undistorted interference figure of an optically uniaxial crystal was observed with crossed polarizers. The optic axis is slightly inclined to the polished window of the water-worn pebble. In reflected light, the polished surface of the sample does not show any structures such as phase boundaries, which could indicate the presence of two different phases. However, by means of a differential interference contrast device, the presence of lamellar structures within the host is visible (compare Figure 3). In the gemmological microscope, using different lighting

conditions with and without immersion, a special type of needle-like structure present throughout the whole stone (Figure 2), was detected. The exact nature of these needles has not yet been determined, but probably the needle-like pattern is related to edges or boundaries of the included spinel lamellae (see below).

X-ray diffraction

The powder pattern of the stone clearly indicates the presence of two mineral phases, namely musgravite and spinel. Additional lines that might indicate taaffeite were sought but not found.

Chemical composition

Although there are no clear optical differences between musgravite and spinel in reflected light, a back-scattered electron (BSE) image, obtained from the electron microprobe, revealed that the musgravite contains lamellar inclusions (Figure 3). Quantitative electron microprobe analyses of both phases, the musgravite host and lamellar spinel inclusions, are given in Table 1.

No distinct chemical zoning was observed in either of the minerals analysed. In detail, the range of iron in the musgravite host is 0.88-0.93 wt.% FeO (9 point analyses) and 1.79-1.94 wt.% FeO for the lamellar spinel inclusions (6 point analyses of different lamellae). It is clear that the average iron content of the spinel is distinctly higher than that in the musgravite host. Only small traces of other transition metals, especially zinc, are present in both minerals.

UV-Vis spectroscopy

The non-polarized absorption spectrum of the sample is shown in Figure 4. The relative intensity and position of the strongest iron-related absorption maxima observed at 640, 556, 457, 384, and 370 nm are almost identical with the spectrum of gem-quality taaffeite and spinel from Sri Lanka (Schmetzer 1983b; Schmetzer *et al.*, 1989, 2000). It must be emphasized, however, that this spectrum represents a combination of the individual

Table I: Chemical composition of musgravite with lamellar spinel inclusions from Sri Lanka.

Oxide (wt.%)	Musgravite ^c	Spinel ^d
Al ₂ O ₃	73.07	70.48
V ₂ O ₃	0.01	0.01
Cr ₂ O ₃	0.01	0.01
TiO ₂	0.01	0.01
MgO	19.09	26.34
FeO ^a	0.91	1.89
ZnO	0.04	0.09
MnO	0.02	0.03
BeO ^b	6.00	–
Sum	99.16	98.86
cation proportions	based on 12 oxygens (assuming Be = 1.000)	based on 4 oxygens
Al	5.979	2.007
V	0.001	–
Cr	0.001	–
Ti	–	–
Mg	1.976	0.949
Fe	0.053	0.038
Zn	0.002	0.002
Mn	0.001	0.001

- Total iron as FeO.
- Since beryllium is not detectable by microprobe analysis, the BeO figure has been calculated for 1 BeO per formula unit; for the theoretical composition of musgravite (BeMg₂Al₆O₁₂) an amount of 6.08 wt.% BeO is required.
- Average of 9 point analyses using a Cameca electron microprobe.
- Average of 6 point analyses using a Cameca electron microprobe.

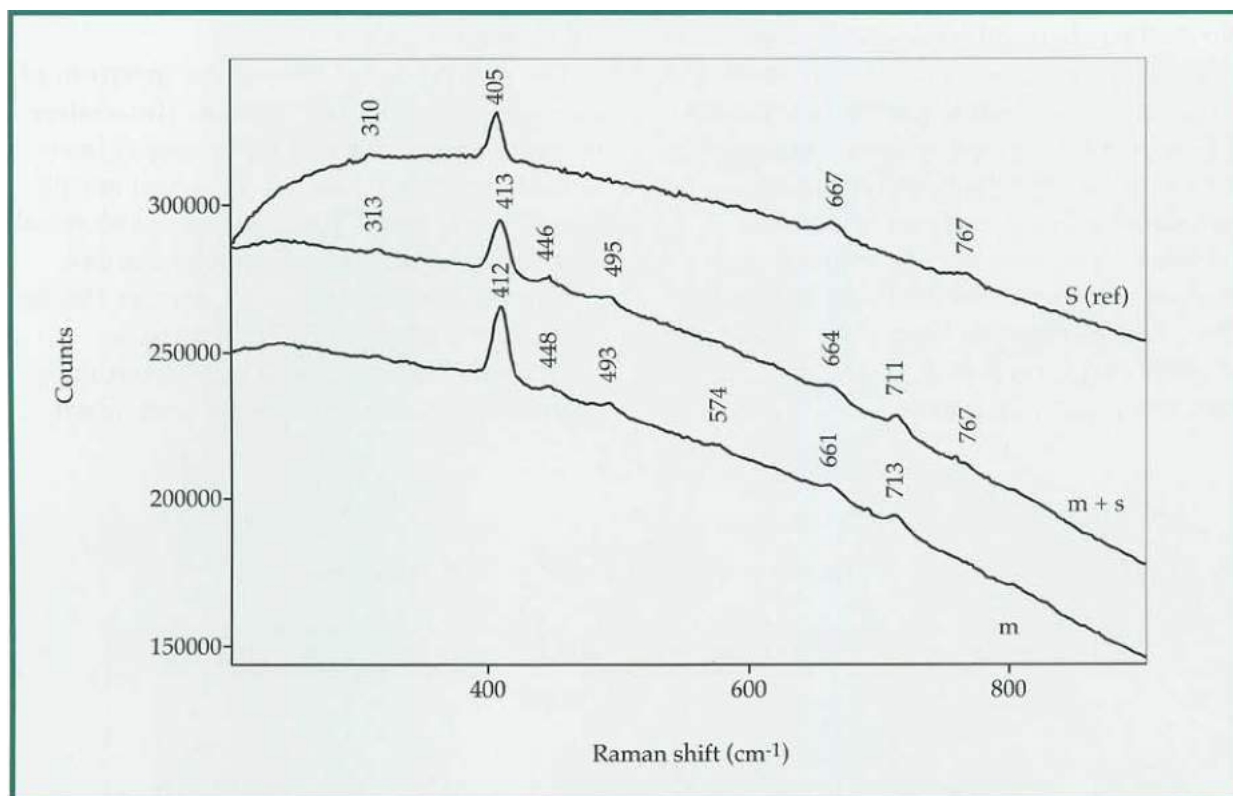


Figure 5: Raman spectra of musgravite (*m*), of a combination of musgravite and spinel (*m + s*), and for comparison, of a gem-quality spinel (*s(ref)*). The ordinate scale of Counts is arbitrary and the spectra have been moved vertically to avoid overlap.

spectra of the musgravite host and the lamellar iron-bearing spinel inclusions. Thus, it should not be quoted as a spectrum typical of pure musgravite.

Raman spectroscopy

The Raman spectrum of the musgravite host is almost identical with literature data (Kiefert and Schmetzer, 1998), with the strongest lines at 412, 448, 493, 574, 661 and 713 cm^{-1} (Figure 5). In several spectra taken at different points of the polished window, additional lines at 313 and 767 cm^{-1} were observed and these are due to the presence of lamellar spinel inclusions. Two Raman lines of spinel at 405 and 667 cm^{-1} overlap with those of musgravite. A Raman spectrum purely of spinel, i.e. without any characteristic lines of the musgravite host, was not obtained from this stone.

Discussion and conclusions

The various tests carried out on the transparent gem-quality pebble clearly indicate that it is another musgravite, albeit

the first to be confirmed from Sri Lanka. This water-worn crystal fragment contains inclusions of lamellar spinel. Some of the data obtained represent properties of the pure host (refractive indices, chemical composition, Raman spectrum) or the spinel inclusions (chemical composition). Other data have to be considered as values representing combinations of various proportions of host and inclusions (specific gravity, colour, UV-Vis absorption spectrum, part of the Raman spectra). These data indicate how complex the results obtained from different highly sophisticated techniques may be and how it still may be necessary to combine several different analytical methods for an adequate identification and characterization of a gem.

At present, no definite distinction of musgravite and taaffeite in the field, i.e. by means of ordinary gemmological properties and without a detailed laboratory examination, is possible. Among the gem-quality musgravites known to date (Table II), four samples show a slight green tint, which has not been observed in taaffeite. Non-gem-

Table II: Physical and chemical properties of musgravites.

Gem-quality musgravites					
Weight (ct)	0.30	0.37	0.60	0.36	1.42
Faceted/ rough	faceted	faceted	faceted	faceted	rough
SG	3.64	3.62	3.69	3.61	3.61
RI: n_o	1.726	1.725	1.728	1.726	1.721
n_e	1.720	1.719	1.721	1.719	1.717
Colour	greyish- mauve with greenish cast	greyish- mauve with greenish cast	brownish- purple	greenish- grey	greyish- blue with light green tint
X-ray diffraction	yes	yes	yes	yes	yes
Chemical analysis	no	no	yes	yes	yes
FeO ^a (wt.%)	n.d.	n.d.	present	present	0.91
ZnO (wt.%)	n.d.	n.d.	present	present	0.04
Raman spectra	no	no	no	yes	yes
Source/ locality	Sri Lanka?	Sri Lanka?	collector	collector	Sri Lanka
Reference	Demartin <i>et al.</i> (1993)	Demartin <i>et al.</i> (1993)	Johnson and Koivula (1997)	McClure (2001)	this paper

Non-gem-quality musgravites*				
Location	Musgrave Ranges, Australia	Casey Bay, Antarctica	Dove Bugt, Greenland	Sakeny, Madagascar
SG	3.68			
RI: n_o	1.739	1.754		
n_e	1.735	1.744		
Colour	pale olive green	dark green	black	light grey to colourless
Colour in thin section	almost colourless	pale green	grey	
FeO ^a (wt.%)	7.14	8.92-12.13	6.76-7.89	1.98-2.42
ZnO (wt.%)	n.d.	4.65-5.18	3.20-4.47	n.d.
Reference	Hudson <i>et al.</i> (1967)	Grew (1981); Schmetzer (1983b); Grew <i>et al.</i> (2000)	Chadwick <i>et al.</i> (1993)	Rakoton- drazafy (1999)

a. Total iron as FeO. n.d. = not determined. * See note (p. 288) added in proof.

quality musgravite is described as pale olive green, dark green, black or grey (see again *Table II*). These musgravites show higher iron and zinc contents than the gem material known from Sri Lanka or elsewhere – exact locality data are lacking for the faceted samples. Such differences in chemical composition are responsible for the higher refractive indices and, most probably, also for the different colours of non-gem-quality material.

For gem samples with typical gemmological properties of the taaffeite group of minerals, such as SG and RI, the slightly different colours of some musgravites might be a useful hint towards these species. An unambiguous determination of such samples, however, needs definite confirmation by X-ray crystallography and/or quantitative chemical analysis and/or Raman spectroscopy (Kiefert and Schmetzer, 1998; McClure, 2001).

Phase relationships in the BeO-MgO-Al₂O₃ system, especially along the chrysoberyl (BeAl₂O₄)-spinel (MgAl₂O₄) join, may be complex and are not completely understood. According to Kawakami *et al.* (1986), the two ternary phases along this join, namely taaffeite and musgravite, are incongruently melting compounds (for a new phase diagram of the pseudobinary system chrysoberyl-spinel see Franz and Morteani, 2002). At high temperatures, there is extensive solubility of BeAl₂O₄ and MgAl₂O₄. This high temperature compound, i.e. the Be-Mg-Al-oxide, exsolves taaffeite and/or musgravite and/or spinel with decreasing temperature. In other words: with decreasing temperature a homogeneous single phase may cool and transform into finely intergrown spinel and/or taaffeite and/or musgravite (see also Schmetzer *et al.*, 1999).

These known phase relationships may explain the composition differences and exsolution lamellae in the specimen described in this paper. A possible scenario is one where grains of a Be-Al-Mg-oxide with a composition close to musgravite, but with some excess of the spinel molecule were present at an elevated temperature in a high-

grade metamorphic environment, which is typical for all known musgravite-bearing host rocks. With decreasing temperature, the grains of a high temperature phase referred to above would cool to a musgravite host with the excess of the spinel molecule present as exsolution lamellae.

Acknowledgements

The authors are grateful to Dr O. Medenbach of Ruhr-University, Bochum, Germany, for obtaining X-ray diffraction data of several Be-Mg-Al-oxide minerals (taaffeite and musgravite). Professor E.S. Grew, University of Maine, Maine, USA, provided copies of special references and critical comments.

Note added in proof:

The authors have just received information about another occurrence of non-gem-quality musgravite at Costabonne Peak, Pyrenees, France. For further details see Schmetzer *et al.* (2005), *Neues Jahrbuch für Mineralogie, Abhandlungen (in press)*.

References

- Armbruster, T., 2002. Revised nomenclature of hōgbomite, nigerite, and taaffeite minerals. *European Journal of Mineralogy*, **14**(2), 389-95
- Chadwick, B., Friend, C.R.L., George, M.C., and Perkins, W.T., 1993. A new occurrence of musgravite, a rare beryllium oxide, in the Caledonides of North-East Greenland. *Mineralogical Magazine*, **57**(386), 121-9
- Demartin, F., Pilati, T., Gramaccioli, C.M., and de Michele, V., 1993. The first occurrence of musgravite as a faceted gemstone. *Journal of Gemmology*, **23**(8), 482-5
- Franz, G., and Morteani, G., 2002. Be-minerals: synthesis, stability, and occurrence in metamorphic rocks. In: Grew, E.S. (Ed.), *Beryllium: mineralogy, petrology, and geochemistry*. Reviews in Mineralogy & Geochemistry, **50**, 551-89
- Grew, E.S., 1981. Surinamite, taaffeite, and beryllian sapphirine from pegmatites in granulite-facies rocks of Casey Bay, Enderby Land, Antarctica. *American Mineralogist*, **66**, 1022-33
- Grew, E.S., 2002. Beryllium in metamorphic environments (emphasis on aluminous compositions). In: Grew, E.S. (Ed.), *Beryllium: mineralogy, petrology, and geochemistry*. Reviews in Mineralogy & Geochemistry, **50**, 487-549
- Grew, E.S., Yates, M.G., Barbier, J., Shearer, C.K., Sheraton, J.W., Shiraishi, K., and Motoyoshi,

- Y., 2000. Granulite-facies beryllium pegmatites in the Napier Complex in Khmara and Amundsen Bays, western Enderby Land, East Antarctica. *Polar Geoscience*, **13**, 1-40
- Hudson, D.R., Wilson, A.F., and Threadgold, I.M., 1967. A new polytype of taaffeite – a rare beryllium mineral from the granulites of central Australia. *Mineralogical Magazine*, **36**(279), 305-10
- Johnson, M.L., and Koivula, J.I. (Eds), 1997. Gem News – Musgravite: A rarity among the rare. *Gems & Gemology*, **33**(2), 145-7
- Kawakami, S., Tabata, H., and Ishi, E., 1986. Phase relations in the pseudo-binary system BeAl_2O_4 - MgAl_2O_4 . *Report of the Government Industrial Research Institute, Nagoya*, **35**(6), 235-9 (in Japanese)
- Kiefert, L., and Schmetzer, K., 1998. Distinction of taaffeite and musgravite. *Journal of Gemmology*, **26**(3), 165-7
- McClure, S.F., 2001. Another musgravite. *Gems & Gemology*, **37**(1), 60-2
- McClure, S.F., and Muhlmeister, S., 2002. Bromellite. *Gems & Gemology*, **38**(3), 250-2
- Nuber, B., and Schmetzer, K., 1983. Crystal structure of ternary Be-Mg-Al oxides: taaffeite, $\text{BeMg}_3\text{Al}_8\text{O}_{16}$, and musgravite, $\text{BeMg}_2\text{Al}_8\text{O}_{12}$. *Neues Jahrbuch für Mineralogie Monatshefte*, **1983**(9), 393-402
- Rakotondrazafy, R., 1999. *Les granulites alumineuses et magnésiennes de hautes températures et roches associées de sud de Madagascar*. Thèse, Université d'Antananarivo, Madagascar
- Schmetzer, K., 1983a. Taaffeite or taprobanite – a problem of mineralogical nomenclature. *Journal of Gemmology*, **18**(7), 623-34
- Schmetzer, K., 1983b. Crystal chemistry of natural Be-Mg-Al-oxides: taaffeite, taprobanite, musgravite. *Neues Jahrbuch für Mineralogie Abhandlungen*, **146**(1), 15-28
- Schmetzer, K., Bernhardt, H.-J., and Medenbach, O., 1999. Heat-treated Be-Mg-Al oxide (originally musgravite or taaffeite). *Journal of Gemmology*, **26**(6), 353-6
- Schmetzer, K., Bosshart, G., Bernhardt, H.-J., Gübelin, E.J., and Smith, C.P., 2002. Serendibite from Sri Lanka. *Gems & Gemology*, **38**(1), 73-9
- Schmetzer, K., Burford, M., Kiefert, L., and Bernhardt, H.-J., 2003. The first transparent faceted grandidierite, from Sri Lanka. *Gems & Gemology*, **39**(1), 32-7
- Schmetzer, K., Haxel, C., and Amthauer, G., 1989. Colour of natural spinels, gahnospinel, and gahnites. *Neues Jahrbuch für Mineralogie Abhandlungen*, **160**(2), 159-80
- Schmetzer, K., Kiefert, L., and Bernhardt, H.-J., 2000. Purple to purplish red chromium-bearing taaffeites. *Gems & Gemology*, **36**(1), 50-9

Iron- and zinc-rich gem-quality taaffeites from Sri Lanka

Dr Karl Schmetzer¹, Dr Lore Kiefert²,
Dr Heinz-Jürgen Bernhardt³, Murray Burford⁴
and Dunil Palitha Gunasekara⁵

1. Taubenweg 16, D-85238 Petershausen, Germany

2. SSEF Swiss Gemmological Institute, Falknerstr. 9, CH-4001 Basel, Switzerland*

*Present address: AGTA-GTC, New York, U.S.A

3. Central Microprobe Facility, Ruhr-University, D-44780 Bochum, Germany

4. 136 Beechwood Avenue, Victoria, British Columbia V8S 3W5, Canada

5. 28 Batugedara, Ratnapura, 7000, Sri Lanka

Abstract: Gemmological, chemical and spectroscopic properties of a semitransparent, gem-quality rough (water-worn) taaffeite crystal of 2.52 ct and of two transparent, faceted taaffeites of 1.48 and 0.30 ct from Sri Lanka were determined. The rough crystal was identified by X-ray single crystal diffraction and Raman spectroscopy. By electron microprobe analysis an extraordinarily high value of 5.62 wt.% FeO was determined. This high iron content is consistent with the high refractive indices and the high specific gravity of the taaffeite crystal. The two faceted gemstones were identified by Raman spectroscopy and electron microprobe analysis which revealed extraordinarily high zinc values of 8.87 and 5.27 wt.% ZnO. These high zinc contents are responsible for the high refractive indices and the high specific gravities of both taaffeites.

Introduction

The taaffeite group consists of three independent mineral species, namely taaffeite, musgravite and pehrmanite (Armbruster, 2002). Only taaffeite and musgravite are known in gem quality, especially from Sri Lanka. Taaffeite, $\text{BeMg}_3\text{Al}_8\text{O}_{16}$, is a rare collector's stone, and musgravite, $\text{BeMg}_2\text{Al}_6\text{O}_{12}$, is considered as one of the rarest gem species known to date. Due to the similar chemical composition and crystal structure of taaffeite and musgravite (Schmetzer, 1983 a,b; Nuber and Schmetzer, 1983), the gemmological properties of these independent species overlap. Consequently, for an unequivocal determination of faceted gems of this group a

combination of special physical techniques such as X-ray diffraction (powder or single crystal techniques) and/or quantitative chemical analysis (e.g. by electron microprobe) and/or micro-Raman spectroscopy is needed (see, e.g., Kiefert and Schmetzer, 1998; McClure, 2001; Schmetzer *et al.*, 2005).

Numerous localities in Sri Lanka are known as sources for gem-quality taaffeites (Gunawardene, 1984), but a correlation of individual properties and localities of origin has not been performed to date. Taaffeites from Sri Lanka, in general, contain minor amounts of transition metals, especially iron

and zinc. The maximum values reported so far are 2.59 wt.% FeO and 4.66 wt.% ZnO; in red to purplish-red specimens traces of Cr₂O₃ are also present (Schmetzer, 1983b; Schmetzer and Bank, 1985; Schmetzer *et al.*, 2000).

Gemmological properties of taaffeites such as specific gravity and refractive indices were found to be correlated with trace element contents of individual specimens (Schmetzer *et al.*, 2000).

In the course of a research project describing Sri Lankan gemstones of the taaffeite group (see Schmetzer *et al.*, 2005), the authors examined several samples with unusually high refractive indices. In order to exactly determine the mineral species and to understand the physical properties of these gem specimens, several different techniques to determine their physical and chemical properties were applied.

Materials and methods

The rough taaffeite crystal of 2.52 ct to be described in this paper (Figure 1) was purchased in 2004 by one of the authors (MB) in Sri Lanka. The sample was said to originate

from a gem pit near the small village of Delwela, south-east of the town Karawita, which is located about 11 km south of Ratnapura. The water-worn 2.52 ct crystal from Sri Lanka already had a window polished on it to enable internal examination and to measure refractive indices.

The two faceted gemstones of 1.48 and 0.30 ct (Figures 2 and 3) were recognized by one of the authors (DPG) as members of the taaffeite group with special properties due to their high refractive indices and, thus, submitted for further examination. The 1.48 ct specimen originates from the Mudunkotuwa area, the 0.30 ct taaffeite from the Ratnapura area of Sri Lanka.

Standard gemmological methods were used for all three samples to determine refractive indices (RI), optical character, specific gravity (SG) and fluorescence under long- and short-wave ultraviolet radiation. Standard microscopic techniques were used to examine the internal features under different lighting conditions, both with and without immersion liquids.



Figure 1 (Specimen A): This water-worn crystal of 2.52 ct with pyramidal habit, size 5.9 × 9.1 × 4.9 mm, is a high ferrous iron-bearing taaffeite from Sri Lanka. The c-axis of the crystal is approximately north-south and its base (not shown) is a polished window.



Figure 2 (Specimen B): This faceted taaffeite of 1.48 ct from Sri Lanka, size $6.9 \times 8.5 \times 3.4$ mm, has the highest zinc content known to date for gem-quality and non gem-quality taaffeites.



Figure 3 (Specimen C): This faceted taaffeite of 0.30 ct, size $3.9 \times 4.6 \times 2.6$ mm, is a high zinc-bearing taaffeite from Sri Lanka.

Non-polarized UV-Vis (300–800 nm) absorption spectra were recorded using a Cary 500 Scan spectrophotometer. In addition, we analysed all three samples and their solid inclusions by laser Raman microspectrometry using a Renishaw 1000 system.

To perform X-ray diffraction analysis a small fragment of the rough 2.52 ct crystal was removed and examined with an Excalibur automatic single crystal diffractometer from Oxford Diffraction using $\text{MoK}\alpha$ radiation, a graphite monochromator and a CCD-detector.

To further characterize the specimens, a Cameca Camebax SX 50 electron microprobe was used to obtain several point analyses from traverses across the polished window of the rough or the table facets of the two faceted gemstones.

Results

1. Iron-rich rough taaffeite of 2.52 ct Gemmological properties

The water-worn 2.52 ct crystal (Figure 1) showed pyramidal habit similar to that in other water-worn taaffeite crystals reported from Sri Lanka (Kampf, 1991). Our sample was broken diagonally and, thus, showed only three complete and two broken pyramidal faces. At the opposite end to the pyramids and parallel to

its basal face the sample is terminated by a polished face.

In the immersion microscope and using crossed polarizers, an undistorted interference figure of an optically uniaxial crystal was observed. The optic axis is slightly inclined to the normal of the polished window of the water-worn crystal. The stone is uniaxial negative and showed clear RI readings with n_o 1.732, n_e 1.726. The colour of the semitransparent (translucent) taaffeite is a very dark purplish violet and pleochroism was not detected. The SG was determined as 3.69. The crystal was inert to both long- and short-wave UV radiation.

Identification, X-ray crystallography and spectroscopy

The crystal was identified as taaffeite by a combination of X-ray single crystal diffraction and laser Raman microspectrometry. Unit cell dimensions were determined as 5.69 \AA for a_o and 18.35 \AA for c_o ; they are consistent with known crystallographic data of taaffeite (Schmetzer, 1983b; Nuber and Schmetzer, 1983). The major peaks of the Raman spectrum of the specimen were also identical with the taaffeite data published by Kiefert and Schmetzer (1998), and Schmetzer *et al.* (2005).

The UV-Vis absorption spectrum of our specimen, although of somewhat low quality because of the low transparency of the taaffeite crystal, showed the known iron-related absorption bands of purplish violet samples of this mineral species (see, e.g., Schmetzer, 1983b; Schmetzer *et al.*, 2000). The absorption spectrum reveals several maxima in the green to red part allowing more transmission in the blue-violet range.

Features observed with the microscope

Under the gemmological microscope, using different lighting conditions with and without immersion, the taaffeite crystal appears extremely clean without major fractures or healing feathers. Only two small mineral inclusions are present: these were identified by laser Raman microspectrometry as feldspar (Figure 4) and as a carbonate mineral such as dolomite or magnesite.

Chemical composition

The results of electron microprobe analysis are presented in Table I. No distinct chemical zoning was observed in a traverse across the polished window of the sample. In addition to the principal components of taaffeite, Al_2O_3 , MgO and BeO (which is not detectable directly by electron microprobe), the sample contains major percentages of iron. In addition, there are minor amounts of zinc and smaller traces of other transition metals such as chromium and manganese.

Theoretically, the oxide percentages obtained by electron microprobe (which cannot be used to determine the valence state of iron), can be calculated as cations for a formula with 16 oxygens (related to taaffeite) or for a formula with 12 oxygens (related to musgravite). For our specimen, a calculation for 12 oxygens would fit to a musgravite formula, but would require a high percentage of the iron present as Fe^{3+} (ferric iron). This indicates that for such a sample with high iron contents, the quantitative microprobe analysis alone is not always sufficient for an identification of the gem.

However, according to the results of X-ray crystallography and Raman spectroscopy, which both identified the sample as taaffeite,

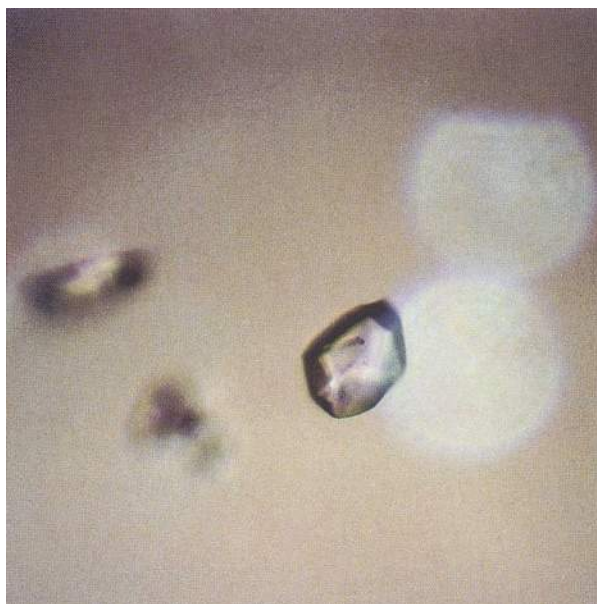


Figure 4: Feldspar inclusion in iron-rich taaffeite crystal of 2.52 ct from Sri Lanka; magnification 200 ×.

cation proportions were calculated for 16 oxygens per formula unit (Table I). The figures obtained are in good agreement with the theoretical formula of taaffeite, which – in addition to 1 Be per formula unit – requires 8 trivalent cations (Al, Cr, V) and 3 bivalent cations (Mg, Fe, Zn, Mn) per formula unit. The calculated values, 7.970 and 3.046 cations, respectively, indicate, that the larger percentage of iron is present as Fe^{2+} (ferrous iron) and only a smaller percentage of iron is present in the ferric state. A calculation of the taaffeite formula with both ferric and ferrous iron would require 0.30 wt. % Fe_2O_3 for our sample.

II. Zinc-rich faceted taaffeites of 1.48 and 0.30 ct *Gemmological properties*

Both samples (Figures 2 and 3) are uniaxial negative with, compared to 'normal' taaffeites from Sri Lanka, relatively high refractive indices of n_o 1.735, n_e 1.730 (specimen B) and n_o 1.729, n_e 1.724 (C). The colours were a greyish violet (B) or light violet (C). Both stones were cut with the table facet almost perpendicular to the optic axis. Pleochroism is extremely weak in specimen B and invisible in C. The SG was determined as 3.78 for B and 3.69 for C. The two faceted taaffeites are inert to both long- and short-wave UV radiation.

Table I: Physical properties and chemical composition of iron- and zinc-rich taaffeites from Sri Lanka.

Physical properties

Specimen	A	B	C	D ^a
Locality	Delwela, Sri Lanka	Mudunkotuwa, Sri Lanka	Sri Lanka	Sri Lanka
Weight (ct)	2.52, rough	1.48, faceted	0.30, faceted	1.25, faceted
Size (mm) diameter	5.9 × 9.1	6.9 × 8.5	3.9 × 4.6	6 × 7
height	4.9	3.4	2.6	
Colour	very dark purplish violet	greyish violet	light violet	intense reddish violet
Specific gravity	3.69	3.78	3.69	3.71
Refractive indices n_o	1.732	1.735	1.729	1.730
n_e	1.726	1.730	1.724	1.726
Birefringence	- 0.006	- 0.005	- 0.005	- 0.004

Chemical composition (microprobe analysis, average, wt.%)

Number of analysis points	13	20	15	5
Al ₂ O ₃	70.58	70.13	71.05	71.10
V ₂ O ₃	bdl	0.02	0.01	n.d.
Cr ₂ O ₃	0.02	0.01	0.01	0.15
TiO ₂	0.03	0.01	0.01	n.d.
MgO	17.74	15.63	17.80	17.69
FeO ^b	5.62	1.76	1.40	1.88
ZnO	0.82	8.87	5.27	4.66
MnO	0.05	0.06	0.04	0.06
BeO ^c	4.35	4.31	4.36	4.37
Sum	99.21	100.79	99.95	99.91
Sum of transition metal contents (wt.%)	6.54	10.73	6.74	6.75

Cation proportions based on 16 oxygens

Al	7.966	7.980	7.988	7.990
V	-	0.001	0.001	-
Cr	0.002	0.001	0.001	0.011
Ti	0.002	0.001	0.001	-
Sum trivalent cations	7.970	7.983	7.991	8.001
Mg	2.533	2.249	2.531	2.515
Fe	0.450	0.142	0.112	0.150
Zn	0.059	0.633	0.371	0.328
Mn	0.004	0.005	0.004	0.005
Sum divalent cations	3.046	3.029	3.018	2.998
Be	1.000	1.000	1.000	1.000

bdl = below detection limit n.d. = not detected

a. Schmetzer and Bank (1985).

b. Total iron as FeO.

c. Since beryllium is not detectable by microprobe analysis, the BeO figure has been calculated for 1 BeO per formula unit; for the theoretical composition of taaffeite (BeMg₃Al₈O₁₆) an amount of 4.52 wt.% BeO is required.

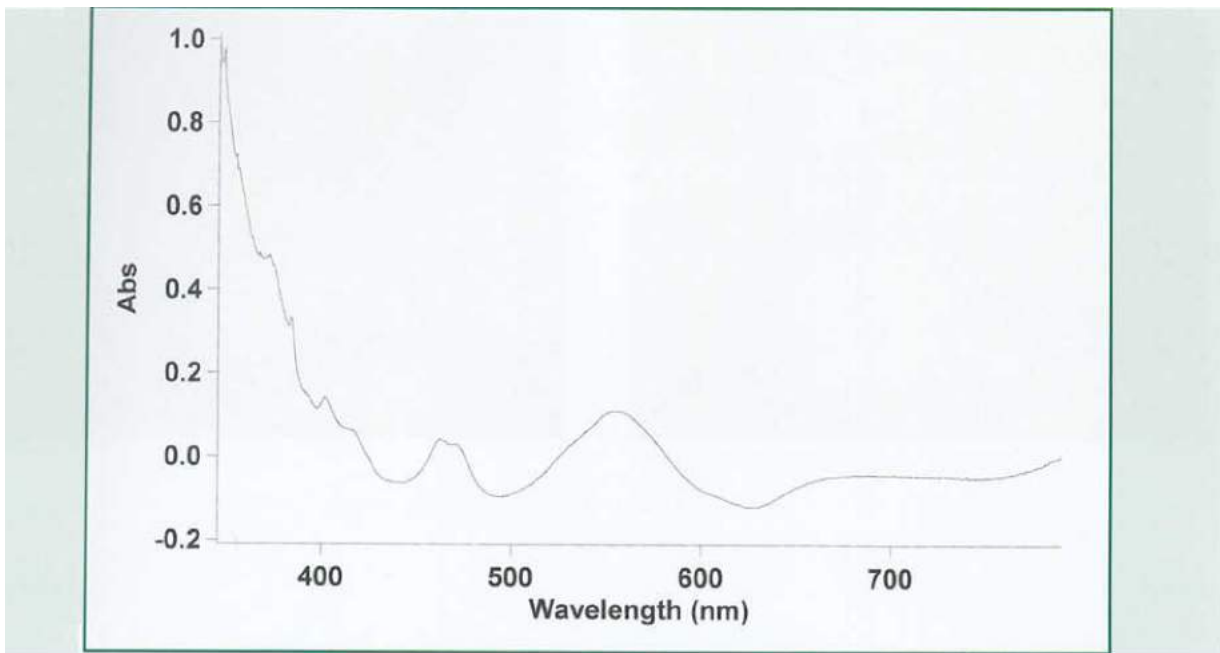


Figure 5: The non-polarized absorption spectrum of a zinc-rich taaffeite of 1.48 ct from Sri Lanka reveals the iron-related absorption bands consistent with those in low zinc-bearing taaffeite samples; the direction of the incident beam is almost parallel to the *c*-axis; the most characteristic absorption maxima are located at 555, 471, 462, 417, 402, and 370 nm.

Identification and spectroscopy

The major peaks of the Raman spectra of both stones are consistent with the taaffeite data published by Kiefert and Schmetzer (1998), and Schmetzer *et al.* (2005). Consequently, these results and the quantitative chemical data described later confirm identification of both faceted stones unequivocally as taaffeites.

Absorption spectra in the UV-Vis range (Figure 5) are identical with those of violet to greyish violet taaffeites from Sri Lanka with lower zinc contents as described by Schmetzer (1983b) and Schmetzer *et al.* (2000).

Features observed with the microscope

Both taaffeites are extremely clean gemstones. Specimen B contains a healed fracture with two-phase (solid and liquid) inclusions. The minute birefringent material in these cavities was too small for a determination by laser Raman microspectrometry. The smaller stone C revealed another healed fracture with similar appearance. The elongated negative crystals with multiphase fillings (either two-phase, solid and liquid, or three-phase, solid, liquid and gas; Figure 6) contain somewhat larger birefringent components (Figure 7 a,b).

Any distinctive Raman peaks which these mineral inclusions may have shown were masked by an extremely strong continuous background fluorescence signal of the taaffeite host. In several taaffeites from Sri Lanka the birefringent inclusions in healed fractures have been determined as magnesite (Schmetzer *et al.*, 2000). Thus, since the minerals in the healed fractures of stones B and C are of similar appearance, they may also be magnesite.



Figure 6: Negative crystals with multiphase fillings in zinc-rich taaffeite of 0.30 ct from Sri Lanka; magnification 100 ×.

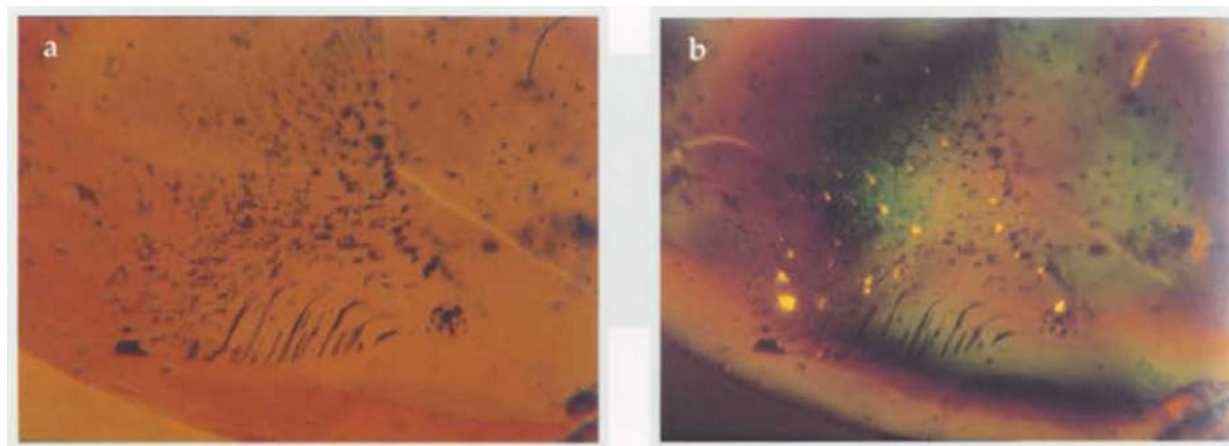


Figure 7: Healed fracture with multiphase inclusions in zinc-rich taaffeite of 0.30 ct from Sri Lanka (a); tiny birefringent crystals are visible with crossed polarizers (b). Immersion, magnification 80 ×.

Chemical composition

The two stones contain elevated zinc contents of 8.87 and 5.27 wt.% ZnO (Table I). These values exceed the highest zinc content of 4.66 wt.% ZnO measured to date in taaffeite from Sri Lanka (Schmetzer and Bank, 1985; see column D in Table I). Iron contents, on the other hand, are in the range frequently found in Sri Lankan taaffeites.

The chemical composition calculated according to the chemical formula of taaffeite for 16 oxygen atoms and 1 beryllium atom per formula unit is close to ideal cation proportions. The sum of trivalent cations is only slightly below the theoretical value of 8.000 and the sum of bivalent cations is slightly above the ideal value of 3.000. These data indicate that only a small fraction of total iron is present as Fe^{3+} with the majority of iron replacing magnesium as Fe^{2+} .

Discussion and conclusions

The various tests carried out on the semi-transparent gem-quality crystal and the two transparent faceted stones clearly indicate that all three gemstones are taaffeites. The refractive indices of our samples (n_o between 1.729 and 1.735, n_e between 1.724 and 1.730) as well as the specific gravities (3.69 to 3.78) are distinctly higher than normally found for gem taaffeites from Sri Lanka.

For numerous Sri Lankan taaffeites analysed, the iron values obtained to date have been distinctly lower with a maximum

value obtained in one sample of 2.59 wt.% FeO (Schmetzer, 1983b; Schmetzer *et al.*, 2000). Zinc contents determined in taaffeites from Sri Lanka, in general, were up to 2.24 wt.% ZnO with one exception of 4.66 wt.% ZnO described by Schmetzer and Bank (1985). The values of this sample are quoted in Table I, column D, for comparison. Our new data consequently expand the compositional range and the range of physical properties, e.g. specific gravity and refractive indices, known so far for gem-quality taaffeites from Sri Lanka. In addition to zinc-bearing spinel (gahnospinel) which has been known for a long time as gem material from Sri Lanka (Schmetzer and Bank, 1986), zinc-bearing taaffeite is another gem mineral from this country which shows an extensive isomorphic replacement of magnesium and zinc.

The zinc value of 8.87 wt.% ZnO determined for the faceted stone of 1.48 ct, represents the highest zinc content of gem-quality and non gem-quality taaffeites found to date. The zinc content of stone C of 5.27 wt.% ZnO is also considered as extraordinarily high for samples from Sri Lanka, but is not too different from the 4.66% ZnO in the stone analysed by Schmetzer and Bank (1985). A comparable high zinc content of 4.27 wt.% ZnO was determined for a taaffeite from Pitkäranta mining district, Lake Ladoga, Russia (Schmetzer, 1983b).

The iron content of 5.62 wt.% FeO in stone A is, up to now, considered as extraordinarily

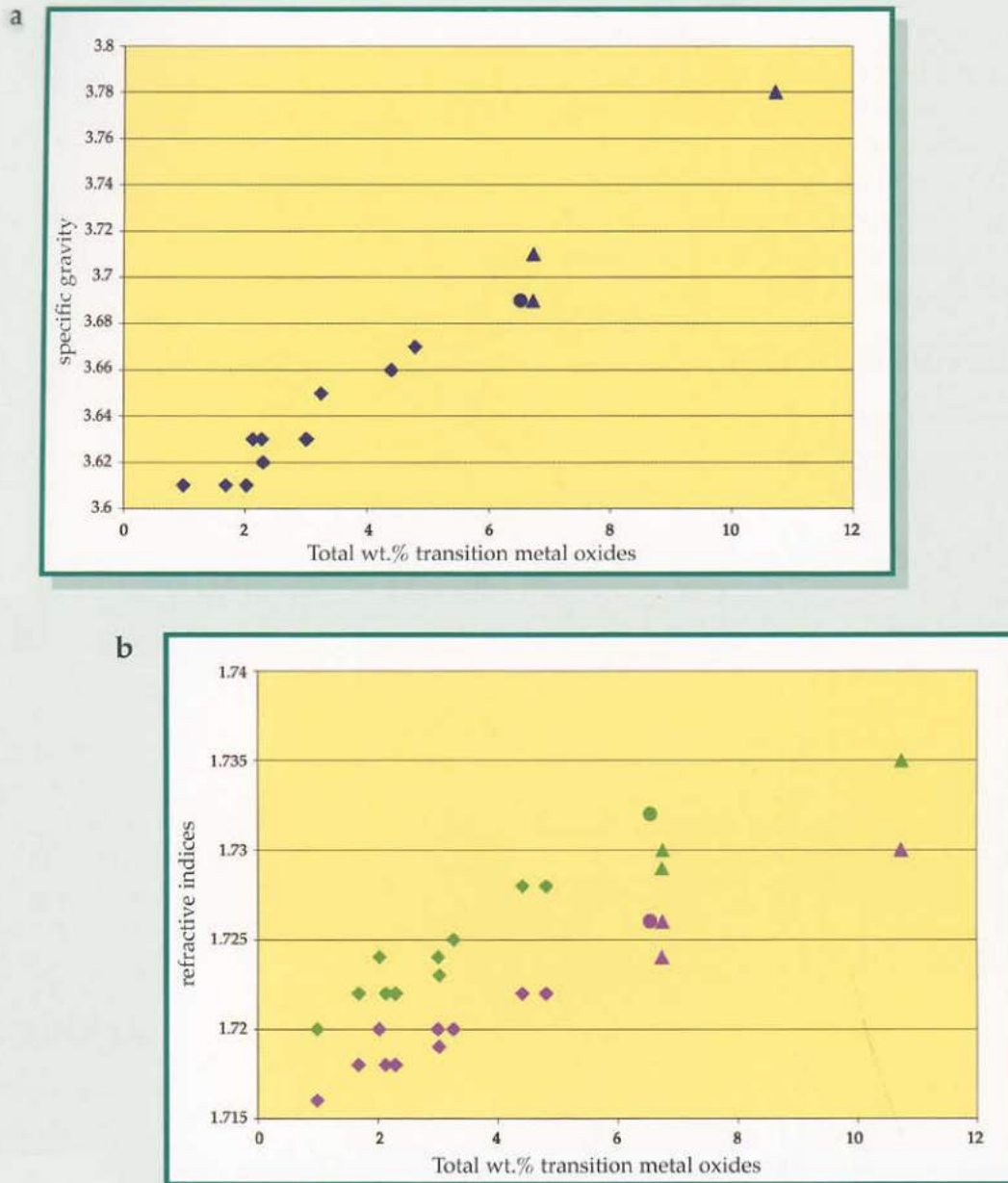


Figure 8 a,b: A correlation of the sum of transition metal contents (wt.% oxides) with specific gravity (a) and refractive indices (b) such as n_D (green) and n_e (purple) indicates the influence of chemical composition on gemmological properties of taaffeite samples from Sri Lanka; data from Schmetzer and Bank (1985), Bank and Henn (1989), Schmetzer et al. (2000), and this paper. The specimens which are the subject of the present study are indicated by full circles (iron-rich taaffeite) or triangles (zinc-rich taaffeites).

high for gem-quality taaffeites from Sri Lanka. Similar iron values, on the other hand, have already been obtained by electron microprobe from non gem-quality taaffeites from other localities, e.g. between 5.52 and 5.88 wt.% FeO for samples from China which also contained from 1.89 to 2.78 wt.% ZnO (Schmetzer, 1983b).

RIs and SGs of taaffeites from Sri Lanka are compared with the individual sum of

transition metal contents ($\text{TiO}_2 + \text{V}_2\text{O}_3 + \text{Cr}_2\text{O}_3 + \text{MnO} + \text{FeO} + \text{ZnO}$) of different samples in Figures 8a and b. In addition to iron, higher zinc contents distinctly increase the refractive indices and specific gravity of taaffeite (Schmetzer *et al.*, 2000). The data obtained and plotted for the crystal (A) and the two faceted stones (B and C) are consistent with these conclusions. Most probably, the taaffeite with similar refractive indices

and specific gravity described by Burford (1997) but not chemically analysed is also a sample with high iron and/or zinc contents.

The extremely dark, translucent purplish-violet coloration of specimen A is also explained by its high iron content. In contrast, specimens B and C with high zinc but distinctly lower iron values, are transparent gemstones with little colour.

Acknowledgement

The authors are grateful to Dr O. Medenbach of Ruhr-University, Bochum, Germany, for obtaining X-ray diffraction data.

References

- Armbruster, T., 2002. Revised nomenclature of hōgbomite, nigerite and taaffeite minerals. *European Journal of Mineralogy*, 14(2), 389-95
- Bank, H., and Henn, U., 1989. Changierender Taaffeit aus Sri Lanka. *Zeitschrift der Deutschen Gemmologischen Gesellschaft*, 38(2/3) 89-94
- Burford, M., 1997. Two zincian rarities. *Canadian Gemmologist*, 18(4), 108-10
- Gunawardene, M., 1984. Inclusions in taaffeites from Sri Lanka. *Gems & Gemology*, 20(3), 159-63
- Kampf, A.R., 1991. Taaffeite crystals. *Mineralogical Record*, 22(5), 343-7
- Kiefert, L., and Schmetzer, K., 1998. Distinction of taaffeite and musgravite. *Journal of Gemmology*, 26(3), 165-7
- McClure, S.F., 2001. Another musgravite. *Gems & Gemology*, 37(1), 60-2
- Nuber, B., and Schmetzer, K., 1983. Crystal structure of ternary Be-Mg-Al oxides: taaffeite, $\text{BeMg}_3\text{Al}_8\text{O}_{16}$ and musgravite, $\text{BeMg}_2\text{Al}_6\text{O}_{12}$. *Neues Jahrbuch für Mineralogie Monatshefte*, 1983(9), 393-402
- Schmetzer, K., 1983a. Taaffeite or taprobanite – a problem of mineralogical nomenclature. *Journal of Gemmology*, 18(7), 623-34
- Schmetzer, K., 1983b. Crystal chemistry of natural Be-Mg-Al-oxides: taaffeite, taprobanite, musgravite. *Neues Jahrbuch für Mineralogie Abhandlungen*, 146(1), 15-28
- Schmetzer, K., and Bank, H., 1985. Zincian taaffeite from Sri Lanka. *Journal of Gemmology*, 19(6), 494-7
- Schmetzer, K., and Bank, H., 1986. A re-investigation of gahnospinel from Sri Lanka. *Journal of Gemmology*, 20(3), 157-60
- Schmetzer, K., Kiefert, L., and Bernhardt, H.-J., 2000. Purple to purplish red chromium-bearing taaffeites. *Gems & Gemology*, 36(1), 50-9
- Schmetzer, K., Kiefert, L., Bernhardt, H.-J., and Burford, M., 2005. Gem-quality musgravite from Sri Lanka. *Journal of Gemmology*, 29(5/6), 281-9

Note on nephrite jade from Val Faller, Switzerland

Dr Douglas Nichol¹ and Herbert Giess²

1. 39 Buckingham Road, Wrexham, Wales

2. Geeringstr. 60, 8049 Zürich, Switzerland

Abstract: In the Oberhalbstein area of southeastern Switzerland, 12 occurrences of nephrite jade are recorded in intimate association with serpentized peridotite within an alpine ophiolite complex of Mesozoic age. These include two roadside localities in Val Faller that have been enlarged as a result of highway improvement schemes through the valley. Fresh rocks exposed in new rock cuttings reveal the contact alteration zones between serpentinites and the country rocks. The small pods and irregular patches of nephrite jade are classed as orthonephrite in type. Predominant colours are of uneven greyish-green hue, grain size varies from fine- to coarse-grained and the surface is rough with vitreous lustre in parts.

The nephrite jade formed as a result of metasomatism and high-pressure effects following the emplacement of the ultrabasic rocks and serpentization.

Although the occurrences of nephrite are of insufficient size to warrant mining operations, the sites in Val Faller have considerable historical significance and remain popular with collectors of mineral specimens.

Introduction

From the time of their discovery around 1910, the nephrite jade occurrences within the valley of Val Faller in southeastern Switzerland have been the subject of widespread interest not only because they crop out at readily accessible positions alongside a public road but also because of their histori-

cal significance as the first *in-situ* deposits of nephrite jade found in Switzerland (Figure 1).

During recent highway improvement schemes in the lower valley of Val Faller, the excavation of road cuttings through two nephrite jade localities has created fresh exposures and provided the opportunity to collect geological specimens as well as samples for lapidary testing.

The valley of Val Faller forms part of the geological and geographical area referred to as Oberhalbstein. The valley itself lies some 35 km south of the town of Chur and near the village of Mulegns which is situated on the Julier Pass road between Tiefencastel and St Moritz. Here, the eastern Swiss Alps form steep terrain with spectacular and rugged mountain scenery.

The writers carried out field investigations at Val Faller during September 2003 as part of a wider study of nephrite jade in Europe.



Figure 1: Location of Val Faller in the Oberhalbstein area, southeastern Switzerland.

Table 1: Nephrite jade occurrences associated with serpentinite in the Oberhalbstein area (see Figure 2).

Ref No.	Locality name	Nephrite occurrence	Swiss National Grid co-ordinates	Reference
1	Salux	Boulder found at roadside	not known	Welter (1910)
2	Piz Martegnas	Rockfall material on northern slope of mountain	760.000 / 160.590	Streiff (1939)
3	Crap Farrèras	Thin band (~200 mm) between serpentinite and basalt	761.500 / 159.920	Streiff (1939)
4	Sblocs	Pod associated with serpentinite	766.715 / 155.260	Dietrich and de Quervain (1968)
5	Val Faller - locality A	Patches at contact of sheared serpentinite	767.170 / 154.850	Welter (1911); this paper
6	Val Faller - locality B	Lens at contact of pillow basalts and serpentinite	767.060 / 154.820	Welter (1911); this paper
7	Furschela	Lenses and veins in serpentinite	765.950 / 152.950	Welter (1910)
8	Marmorea Castle dam	Band (~250 mm) at contact of basalt and serpentinite	767.940 / 152.710	Dietrich and de Quervain (1968)
9	Muntognas digls Lajets	Lenses in sheared serpentinite	765.680 / 150.530	Staub (1926)
10	Seeflüe	Nephrite layers with sheared serpentinite and gabbro	765.140 / 147.630	Dietrich and de Quervain (1968)
11	Cuolms	Lenses (<400 mm) in sheared serpentinites	769.790 / 145.800	Dietrich and de Quervain (1968)
12	Fuorcla da la Valletta	Thin lenses in sheared serpentinite	766.350 / 144.190	Staub (1926)

This paper provides a brief review of the nephrite jade occurrences in the Oberhalbstein area and describes the two sites at Val Faller.

Geological setting

Geologically, the central feature of the Oberhalbstein area is an extensive ophiolite complex of Mesozoic age that crops out within the Platta nappe (Upper Penninic), an oceanic nappe with relicts of continental crust. The Oberhalbstein ophiolite is exposed discontinuously for a distance of some 30 km between the Albula Valley to the north and the Engadine Line to the south (Figure 2).

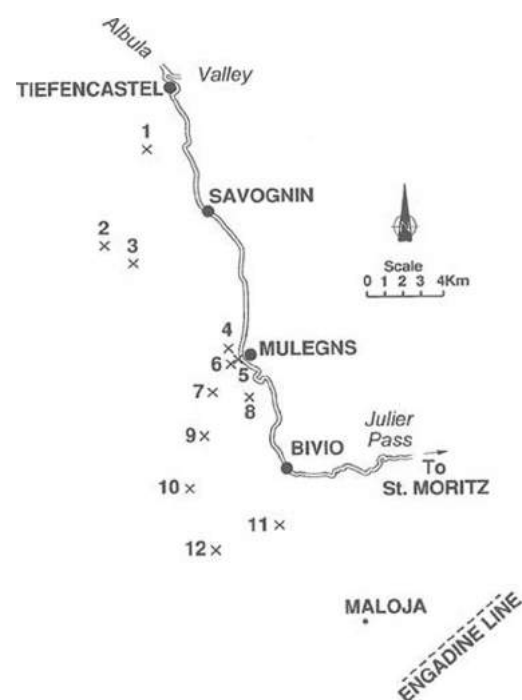


Figure 2: Nephrite jade occurrences associated with serpentinite in the Oberhalbstein area (see Table I).

It comprises the close association of serpentinized peridotites, gabbroic rocks, and pillow basalts overlain by marine sedimentary sequences, including radiolarian cherts and pelagic limestones, the whole having been affected by mild metamorphism. The serpentinized peridotites are interpreted as subcontinental mantle rocks that were exhumed along low-angle detachment faults in Cretaceous to early Tertiary time (Desmurs *et al.*, 2001, and references therein).

A total of 12 occurrences of nephrite jade have been identified within the dismembered blocks of the Oberhalbstein ophiolite belt (Table 1 and Figure 2). Detailed descriptions and discussions of these nephrite occurrences and their significance are given by Dietrich and de Quervain (1968) and Giess (1994). However, the two localities in Val Faller (Table 1 and Figure 2, Sites 5 and 6) are perhaps the best known and observationally accessible sites.

In the neighbourhood of Val Faller, massive serpentinites and pillow basalts underlie the hilly ground and are to be found together with associated metasediments in the rock cuttings alongside the road through the valley.

The Val Faller occurrences

Welter (1910,1911) reported the first discovery of primary deposits of nephrite jade in Switzerland in the valley of Val Faller. He identified two localities approximately 200 m

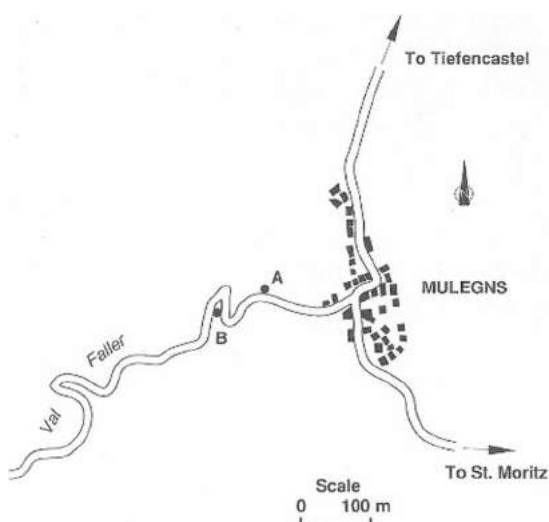


Figure 3: Val Faller nephrite jade sites at A and B near Mulegns.

apart along a short stretch of road within the lower reaches of the narrow valley (Figure 3). From Mulegns, access is westwards for 0.25 km. Stony ground and vegetation of conifer forest characterize the surrounding country.

Locality A

According to Welter (1911), this locality originally comprised an irregular outcrop alongside the road with bare rocky hillside above. He observed a wide variety of rock types and identified two minor patches of nephritic material.

A new road cutting was excavated at the site during 2002-2003 (Figure 4). It measures over 30 m long by up to 3 m high and exposes a sharp tectonic contact between serpentinite and metasedimentary strata. The serpentinite forms a sheet-like body that ranges from black and massive to dark green and foliated. Its main constituents are

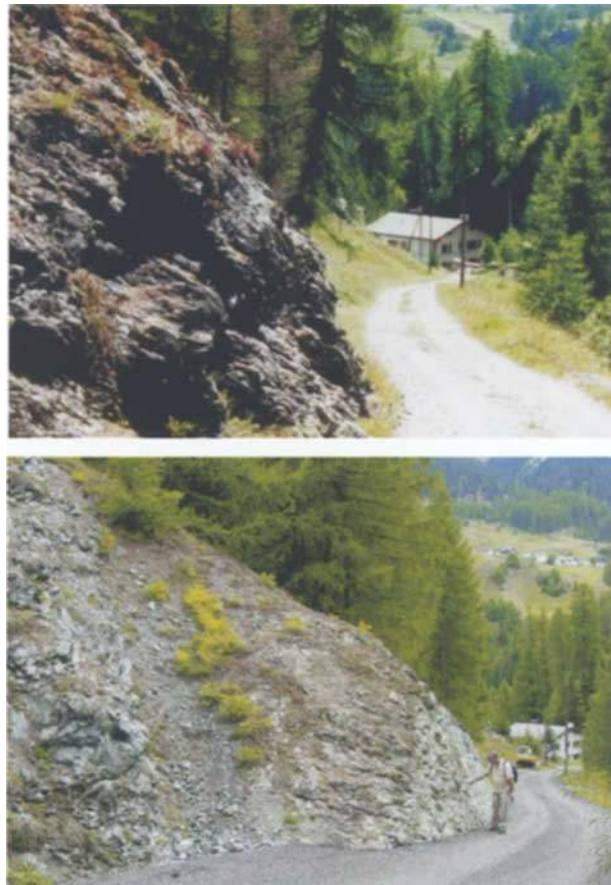


Figure 4: Locality A. Views looking southeastwards. (Upper) small roadside cutting in summer 1993 and (lower) new road cutting in autumn 2003. Serpentinite crops out in the left of the picture whereas metasedimentary rocks form the face in the fresh rock cutting on the right of the picture. Photos by Herbert Giess.

lizardite and chrysotile plus minor quantities of chlorite and magnetite.

The metasediments are mainly grey, green and red variegated, calcareous and pelitic phyllites and schists (Bündnerschiefer) with minor veins of milky quartz and veinlets of white asbestiform tremolite-actinolite. The nephrite jade is present in very small patches within the contact alteration zone but good specimens are uncommon.

Locality B

According to Welter (1911), this locality originally comprised a large outcrop of nephrite at the contact between serpentinite and pillow basalt. Part of the site was disturbed during road-widening operations carried out in 1972 but relatively unaffected by the recent road improvements (Figure 5). Here



Figure 5: Locality B. Views looking southwards. (Upper) roadside sketch by Welter (1911) and (lower) the same outcrop site in autumn 2003. Photos by Herbert Giess.



Figure 6: Locality B. Roadside outcrop of white weathered nephrite. Photo by Herbert Giess.

the nephrite jade crops out discontinuously on the upslope side of the road over a stretch of some 20 m. The cutting slope ranges up to 3 m high. The near surface material is highly weathered to a soft and friable, white, powdery schistose material containing talc, tremolite, chlorite and clay minerals (Figure 6).

Outcrops of serpentinite, pillow basalt and metasedimentary rocks (Bündnerschiefer) are to be found nearby.

Using the Munsell notation (Rock-Colour Chart Committee, 1980), the nephrite jade ranges from pale green (5G 7/2) through greyish green (10G 5/2) to dark yellowish green (10GY 4/4) but is predominantly greyish green (10G 5/2). Colours generally are

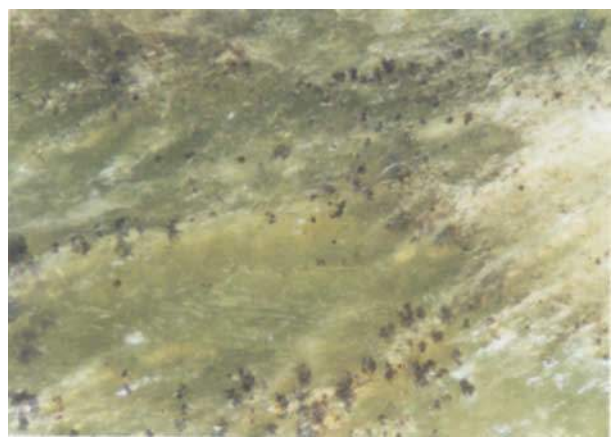


Figure 7: Specimen of nephrite jade from Locality B, Val Faller. Natural surface of greyish-green nephrite with black dendrites of secondary manganese. Field of view approximately 10mm across. Photo by Russell J. Beck.



Figure 8: Specimen of nephrite jade from Locality B, Val Faller. Approximately 40 x 20mm. Photo by Herbert Giess.

patchy and uneven and surface lustre typically appears vitreous in parts and somewhat sheared. Almost invariably, textures show very fine fibrous crystals of microcrystalline tremolite-actinolite and incipient preferred orientation (Figure 7).

Nephrite classification and origin

The nephrite jade localities throughout Oberhalbstein are all spatially associated with serpentinites. Based on the field relationships between the nephrite bodies and the ophiolite belt, the occurrences are all classed as orthonephrite in type (Nichol, 2000). The nephrite jade formed as a result of metasomatism and high-pressure effects following the emplacement of the ultrabasic rocks and serpentinization.

Production

In several parts of Switzerland, archaeologists have unearthed a considerable number of nephrite jade axes, chisels and other cutting tools at the sites of Neolithic lake

dwelling. Indeed, several thousand nephrite artifacts were discovered on the shores surrounding Lake Constance and are held in museum collections in Germany and Switzerland. Although some uncertainty remains about the sources of nephrite jade exploited by the Neolithic lake-dwellers, it is considered likely that a certain proportion of their material was collected as cobbles and boulders from the rivers in the Oberhalbstein area (Giess, 1994).

In modern times, no commercial mining has taken place at the nephrite jade occurrences in the Oberhalbstein area. This was probably due to the dispersed distribution of the material through the serpentinite and the apparent lack of a single mass of sufficient dimensions to warrant mining operations or to encourage deeper exploration beneath the ground surface. Consequently, output has been limited to fossicking for loose material on the ground surface and knapping of small pieces from outcrops. These fragments are suitable only for mineral specimens (Figure 8). Another consideration is quality, which appears generally low for most gemmological purposes.

Conclusions

The Val Faller nephrite occurrences formed within the contact alteration zones associated with serpentinites in the Oberhalbstein ophiolite complex of Mesozoic age. The nephrite jade is categorised as an ortho-nephrite and occurs mainly in narrow patches and irregular pods. Colour is predominantly greyish green (10G 5/2), texture ranges from fine- to coarse-grained and surface lustre is typically vitreous.

Although surface indications of nephrite are widely scattered throughout the serpentinites in the Oberhalbstein area, the occurrences generally appear small in size and poor in quality. No commercial production is recorded but the region remains highly regarded as a significant nephrite jade province for historical, mineralogical and geological reasons.

Acknowledgements

We are much indebted to Russell J. Beck for helpful discussions and to Angela Hughes for assistance in preparing the diagrams.

References

- Desmurs, L., Manatschal, G., and Bernoulli, D., 2001. The Steinmann Trinity revisited: mantle exhumation and magmatism along an ocean-continent transition: the Platte nappe, eastern Switzerland. In: Wilson, R. C. L., Whitmarsh, R. B., Taylor, B. and Froitzheim, N. (eds.), Non-volcanic rifting of continental margins: a comparison of evidence from land and sea. *Geological Society, London, Special Publication*, **187**, 235-66
- Dietrich, V., and de Quervain, F., 1968. Die Nephrit-Talklagerstätte Scortaseo (Puschlav, Kanton Graubünden). *Beiträge zur Geologie der Schweiz, Geotechnische Serie, Lieferung* **46**
- Giess, H., 1994. Jade in Switzerland. *The Bulletin of the Friends of Jade*, **8**, 1-30
- Nichol, D., 2000. Two contrasting nephrite jade types. *Journal of Gemmology*, **27**, 193-200
- Rock-Colour Chart Committee, 1980. *Rock-Colour Chart*. Geological Society of America, New York.
- Staub, R., 1926. Geologische Karte des Avers (Piz Platta-Duan), 1:50000. *Swiss Geological Commission, Special Map*, No 97
- Streiff, V., 1939. Geologische Untersuchungen im Ostschams (Graubünden). *University of Zürich, PhD thesis* (unpublished)
- Welter, O.A., 1910. Über anstehenden Nephrit in den Alpen. *Verhandl. Naturwissenschaftlicher Verein Karlsruhe*, **32**, 3-5
- Welter, O. A., 1911. Ein Beitrag zur Geologie des Nephrits in den Alpen und im Frankenwald. *Neues Jahrbuch für Mineralogie, Geologie und Paläontologie*, **2**, 86-106

Nephrite jade from Mastabia in Val Malenco, Italy

Douglas Nichol¹ and Herbert Giess²

1. 39 Buckingham Road, Wrexham, Wales

2. Geeringstr. 60, 8049 Zürich, Switzerland

Abstract: At Mastabia in Val Malenco, northern Italy, a major deposit of nephrite jade was recently identified at the site of an abandoned talc mine. Geologically, the talc orebody comprises a series of steeply dipping lenses associated with a fault wedge of dolomitic marble and calc-silicate rocks of Triassic age. The nephrite jade is hosted within massive tremolitite in the central core of the talc orebody and the nephrite and tremolitite were both discarded as waste material during talc mining operations. Recovery of nephrite from the spoil heaps is now underway. Predominant colours of the nephrite jade are of uneven pale green and yellow-green hue. Grain size ranges from fine- to coarse-grained and accessory constituents include calcite, talc and opaque iron minerals. The nephrite jade is classified as para-nephrite in type and formed together with talc and tremolitite by intense hydrothermal alteration and decarbonation of dolomitic marble along shear zones related to thrust structures. The quantity of nephrite jade available remains uncertain but appears substantial. The nephrite is fashioned into a range of jewellery and ornamental pieces.

Introduction

Recently, a major new source of nephrite jade in Europe was identified at Mastabia in Val Malenco, northern Italy (Figure 1). The discovery, announced in January 2002 at the Fourth Symposium of the Federation for European Education in Gemmology, stimulated widespread interest not only because of the considerable quantities of nephrite apparently available but also because of its unusual geological setting (de Michele *et al.*, 2002).

Discovery of the nephrite jade is attributed to Pietro Nana of Sondrio who first noticed an attractive green stone in the discarded waste materials at an abandoned talc mine

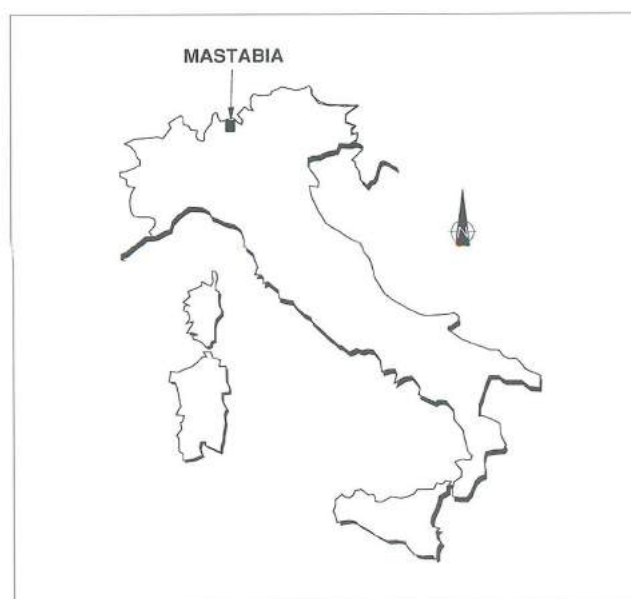


Figure 1: Location of Mastabia in Val Malenco, northern Italy.



Figure 2: Photo of Pietro Nana (left) and Douglas Nichol with a typical block of Mastabia nephrite jade. Photo by Herbert Giess.

(Figure 2). The old mine lies near Mastabia, some 20 km north-north-west of the town of Sondrio, 4 km north-west of Torre di Santa Maria and 4 km south-west of Chiesa in Val Malenco. Here, the Italian Alps form steep terrain with spectacular and rugged mountains.

The writers visited Val Malenco during September 2003 as part of a wider study of nephrite jade in Europe. This paper provides a preliminary review and a description of the geological setting of the deposit of nephrite jade in Mastabia.

Geological setting

The geology of the Val Malenco district has been described in detail by Bonsignore *et al.* (1971) and the solid geology is outlined in a simplified form in Figure 3. The regional geology appears complex due to extensive tectonic disruptions associated with a stack of Alpine nappes (Penninic and Austroalpine nappe systems).

The Malenco Serpentinite is part of an ophiolite complex of Mesozoic age that forms the central feature of the district. The complex covers an area of some 200 km². It comprises a tectonic sheet around 2 km thick that dips at moderate angles eastwards and consists of serpentinitized peridotite with minor relicts of lherzolite and harzburgite. Two other groups of igneous intrusions are present; the Fedoz Gabbro forms a series of irregular bodies emplaced during Permian time whereas the Bergell Granite, a pluton of mainly granodiorite and tonalite was intruded during Tertiary (Oligocene) time. The country rocks surrounding these igneous masses include pre-Mesozoic crystalline basement rocks (mainly schists and gneisses) together with dismembered blocks of Triassic carbonate strata.

The Val Malenco district has a long history as a major mining centre for a wide variety of rocks and minerals. In relation to talc mining operations, at least 15 mine sites are recorded throughout the valley (Conti, 1956; Beaulieu,

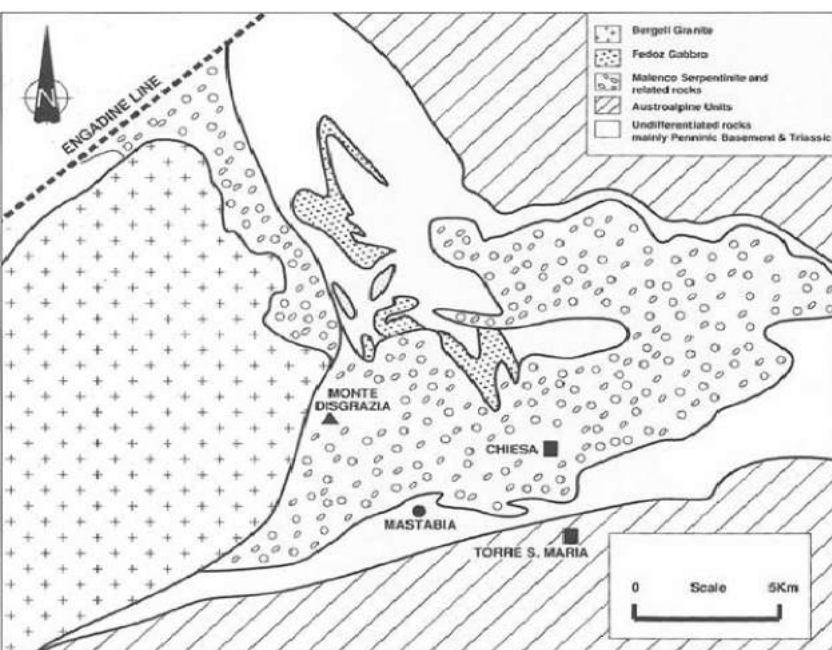


Figure 3: Simplified geological map of the Val Malenco district.

1985). Almost invariably, they are situated either within the Malenco Serpentinite or in the dismembered blocks of Triassic carbonate rocks around its margins.

In the neighbourhood of Mastabia, the bedrocks occupy a narrow tectonic zone sandwiched between the massive Malenco Serpentinite to the north and Austroalpine strata to the south. The principal rocks around the old talc mine at Mastabia comprise tectonic slivers of schists and gneisses of the pre-Mesozoic crystalline basement together with fault wedges of Triassic dolomitic marble and calc-silicate rocks, all closely associated with the thrust-slide boundary between the Margna nappe and the Malenco Serpentinite.

The Mastabia Talc Mine

The Mastabia Talc Mine is situated at elevation 2077 m above ordnance datum on the steep south-eastern mid-slopes of Monte Disgrazia and on a ridge between Valle Airale and Valle Giumellino.

From Chiesa in Val Malenco, access to the site is south-westwards for 1.5 km along the Primolo Road thence 6.5 km on a rough track via Alpe Lago to Alpe Mastabia. From here, a path leads north for some 600 m up to the mine entrance. The surrounding country is characterised by stony ground (Figure 4).

The early history of the mine remains uncertain but operations were apparently established around 1952 on an irregular talc orebody cropping out on the mountainside. Access to the orebody was gained by a series of adits into the hillside and extraction was carried out using conventional underground methods. The mined talc was brought to the surface by means of a number of galleries and tunnels and then transported down the steep mountainside by aerial cableway. It was



Figure 4: Mastabia Talc Mine (circa 1965). View looking northwards. Mine entrance in centre left of picture (after Andreis 1970).

then taken to a milling plant in the lower valley and processed primarily for use in the paper manufacturing industry. Mining operations ceased around 1985 due to an unacceptably high fibre content (acicular tremolite) in the talc product. When the mine closed, the adit entrances were barricaded.

According to Andreis (1970), the talc ore is predominantly massive with a waxy sheen and varies from white and pale green to greenish yellow in colour. It also contains a relatively high proportion of calcite as well as radial fibrous rosettes of tremolite.

Individual talc veins range up to about 10 m wide. However, massive tremolitite frequently forms prominent, tough and hard bands typically about 1 m wide in the middle of the lodes (Figure 5). Not surprisingly, these hard bands posed persistent problems during mining and so, wherever possible, they were avoided by the miners. Nonetheless, significant quantities were encountered during ore extraction and discarded to the waste heaps. In certain places, the tremolitite bands contain a core of moderately intense green fine-grained nephrite that graduates almost imperceptibly outwards into coarser-grained material of progressively paler tones. Not infrequently, the centre of the core is marked by a distinctive stripe up to 10 mm wide characterized by inclusions of opaque iron minerals.

Table I: Chemical composition of Mastabia nephrite and comparisons.

Identifier No.	1	2	3	4	5	6	7
Analysis (Wt.%)							
SiO ₂	59.17	43.91	59.65	56.34	63.36	32.59	40.30
TiO ₂	-	0.03	0.02	-	-	-	-
Al ₂ O ₃	-	0.27	0.18	0.34	-	-	1.45
Fe ₂ O ₃	-	0.26	0.16	0.71	-	0.72	5.80
MnO	-	0.01	0.04	0.12	-	-	0.11
MgO	24.81	18.34	23.74	22.59	31.89	18.64	39.90
CaO	13.80	26.51	12.44	14.92	-	23.35	1.20
Na ₂ O	-	0.52	-	0.19	-	0.10	-
K ₂ O	-	0.53	-	0.07	-	0.02	-
P ₂ O ₅	-	0.01	0.07	-	-	-	-
LOI	2.22	8.05	3.00	4.20	4.75	22.56	10.50
Total	100.00	98.44	99.30	99.48	100.00	97.98	99.26
Trace elements (ppm)							
Co	-	11	<1	-	-	-	-
Cr	-	76	28	-	-	-	1100
Ni	-	124	2	-	-	-	2400
Identifier No.	1. Theoretical pure composition of tremolite - nephrite. 2. Nephrite jade from Mastabia (analysis by staff at the National Museum of Wales). 3. Nephrite jade from Mastabia (analysis by Alcontrol Geochem). 4. Nephrite jade from Mastabia (courtesy G. Liborio). 5. Theoretical pure composition of talc. 6. Talc ore from Mastabia (Andreis, 1970). 7. Malenco serpentinite from quarry Chiesa (Trommsdorff and Evans, 1972).						

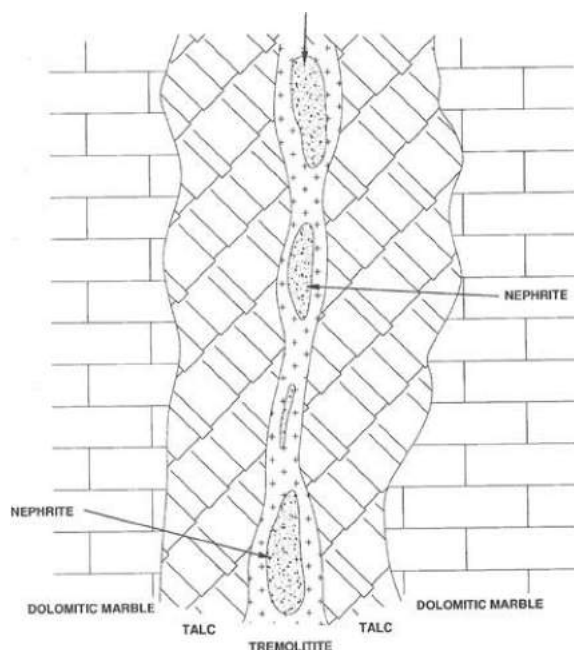


Figure 5: Schematic section illustrating rock relations at Mastabia Talc Mine (not to scale).

The nephrite jade is found exclusively within the massive tremolite and the material discarded during talc mining operations is currently being salvaged for its nephrite content.

Nephrite jade

X-ray, chemical and petrographic examinations of representative samples of Mastabia nephrite have revealed that it consists of microcrystalline tremolite-actinolite which is intimately associated with minor but variable quantities of calcite, talc and pyrite. The principal impurity is calcite.

Mineralogically, nephrite is a monoclinic amphibole of variable chemical composition between the end members tremolite



Figure 6: Slab specimens of nephrite jade from Mastabia. Slab size approximately 10 mm wide. Foreground specimen contains inclusions of opaque iron minerals. Photo by Herbert Giess.

($\text{Ca}_2\text{Mg}_5\text{Si}_8\text{O}_{22}(\text{OH})_2$) and ferroactinolite ($\text{Ca}_2\text{Fe}_5\text{Si}_8\text{O}_{22}(\text{OH})_2$). The magnesium in tremolite is often partially replaced by iron.

However, Mastabia nephrite features very low iron contents, typically less than one percent, placing it closer in composition to the tremolite end member (Table 1).

Using the Munsell notation (Rock-Colour Chart Committee, 1980), the nephrite jade ranges from light greenish grey (5G8/1 & 5GY 8/1) through moderate yellow green (5GY 7/4) to greyish yellow green (5GY 7/2) but is predominantly moderate yellow green (5GY 7/4).

Localized zones contain an unusual variety of nephrite peppered with black flecks of opaque iron minerals, mainly pyrite (Figure 6).

Colours generally are patchy and uneven and surface lustre typically appears greasy and somewhat sheared. Variations in colour are ascribed to minor variations in iron content with higher Fe_2O_3 values producing greener hues and darker tones. Interestingly, Mastabia nephrite contains less than 100 ppm

chromium, in marked contrast to other deposits elsewhere in the world with chromium contents of 1000 to 10000 ppm; chromium is responsible for imparting their emerald green colours (Nichol, 2000).

Texture controls the toughness and hence the durability of the gemstone as well as its polishing characteristics. Toughness is due to an interlocking mesh of fine fibre or needle like crystals which are commonly 0.1 to 5 μm in diameter and 20 to 150 μm long (Figure 7).

Variations in toughness depend upon the length and diameter of the fibres, and the size and orientation of the fibre bundles. The toughest nephrite has randomly oriented fibre bundles and a very fine grain size. The presence of foliation as aligned fibres or fibre bundles as well as coarse-grained tremolite reduces toughness.

Nephrite classification and origin

The nephrite jade at Mastabia is spatially associated with Triassic dolomitic marble and calc-silicate rocks of metasedimentary

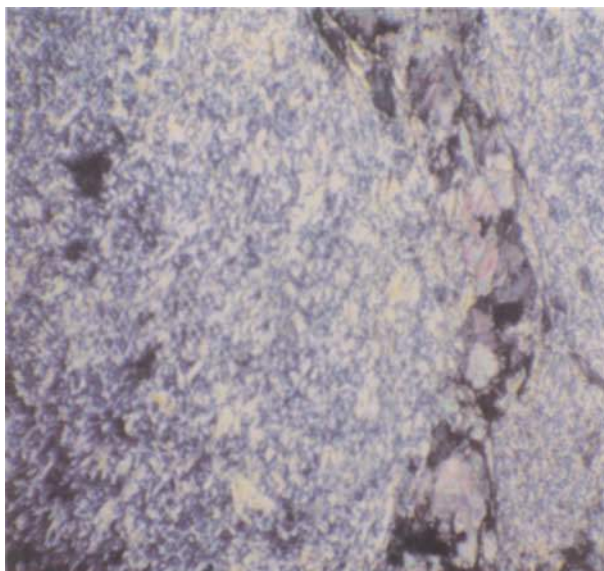


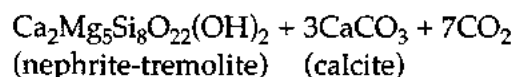
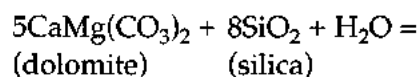
Figure 7: Photomicrograph of Mastabia nephrite under polarized light, with coarse grained vein of calcite on the right. Length of photo 1.1 mm. Photo by Dr Vincenzo de Michele.



Figure 8: Necklace fashioned from Mastabia nephrite jade. Photo by Pietro Nana.

derivation. Based on the field relationships between the nephrite bodies and the country rock together with the subdued chromium and nickel contents, the deposit is classed as para-nephrite in type (Nichol, 2000).

The origin of the Mastabia nephrite may be ascribed to metamorphism, metasomatism and decarbonation of impure dolomitic strata involving reactions of the form:



Generally, the mixed compositions and varied textures indicate intense fluid-rock reactions by hydrothermal solutions percolating within the shear zones.

It is also noteworthy that the geological features evident at Mastabia, as well as the close association of the nephrite with a talc orebody, appear remarkably similar to the geological environment reported by Dietrich and de Quervain (1968) for the Scortaseo nephrite jade deposit in south-east Switzerland. Indeed, the colour and general appearance of Mastabia nephrite also closely resemble Scortaseo nephrite.

Production practice

Output of Mastabia nephrite is still in the early stages of development and adequate stocks for immediate requirements are salvaged from mining wastes outside the talc mining adits.

Boulders of raw jade are transported from the mine site to Chiesa and Sondrio for sawing and grading according to colour and quality. Some jade is consigned to lapidary workshops in China and Idar-Oberstein to be processed further into carved pieces and items of jewellery (Figure 8). Jade for hardstone carving is first trimmed with a diamond saw, carved using diamond tipped tools and then polished with diamond paste to achieve its characteristic final lustre (Figure 9). Sondrio provides the principal outlet for finished articles.

Conclusions

The Mastabia nephrite deposit formed in hydrothermally altered zones of intense deformation associated with a fault wedge of metamorphosed dolomitic marble and calc-silicate rocks. As well as nephrite jade, the alteration zone also contains talc and

tremolite. The nephrite jade occurs as irregular pods exclusively within lenticular masses and bands of tremolite in the central core of the talc orebody.

The material is categorised as a para-nephrite jade (Nichol, 2000). Colour is predominantly moderate yellow green (5GY 7/4), and texture ranges from fine- to coarse-grained microfibrous.

Much nephrite jade was originally extracted from the Mastabia Talc Mine in conjunction with tremolite as waste material produced during talc mining operations. Substantial quantities of nephrite are understood to exist in the vicinity of the old workings but detailed geological investigations are required to provide quantitative assessments.

Lapidaries and artisans fashion the nephrite jade into a variety of jewellery pieces and ornamental hardstone carvings.

Acknowledgements

The authors are grateful to Pietro Nana for guidance during our visit to Val Malenco and also for providing Figures 8 and 9. We also thank Dr Vincenzo de Michele, Istituto Gemmologico Italiano for helpful advice and for providing Figure 7. Laboratory testing of specimens of Mastabia nephrite was carried out by the Department of Geology, National Museum of Wales, Cardiff and by Alcontrol Geochem, Chester. In addition, Professor Giuseppe Liborio, Department of Earth Sciences at University of Milan kindly provided one chemical analysis of Mastabia nephrite (Table I, Sample No 4).

References

- Andreis, C., 1970. *Il talco di Mastabia in Val Malenco (Prov. Di Sondrio)*. Thèse Faculty Science, University of Milan
- Beaulieu, P., 1985. Les gisements de talc du Val Malenco (Italie du Nord). *Chronique de la recherche minière*, 478, 5-20
- Bonsignore, G., Casati, P., Crespi, R., Fagnani, G., Liborio, G., Montrasio, A., Mottana, A., Ragni, U.,

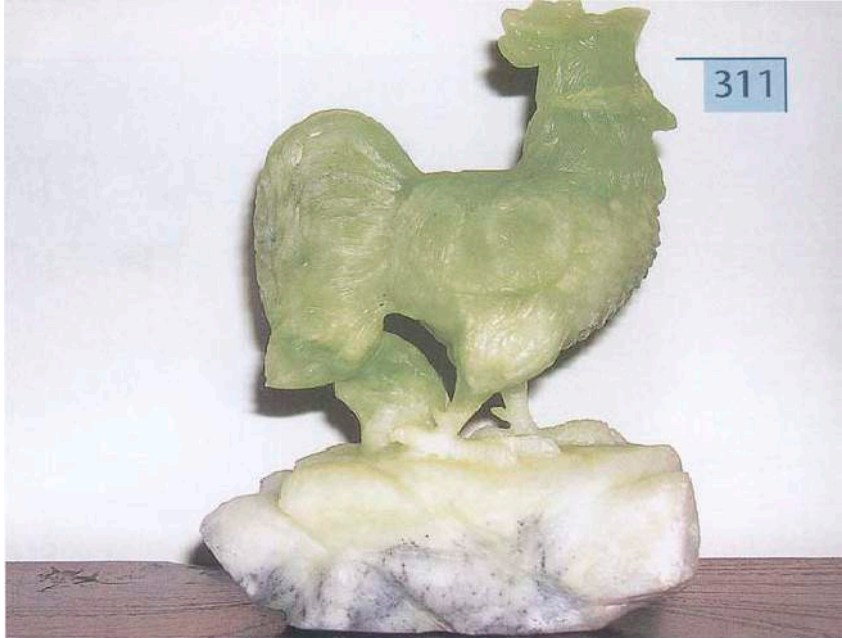


Figure 9: Ornamental carving fashioned from Mastabia nephrite jade. Size approximately 200 mm in height. Photo by Pietro Nana.

- Schiavinato, G., and Venzo, S., 1971. Note illustrative della carta geologica d'Italia, Pizzo Bernina e Sondrio. *Fogli 7 e 18*
- Conti, U., 1956. Il talco e la steatite della Valmalenco. *L'industria Mineraria*, 459-70
- Dietrich, V., and de Quervain, F., 1968. Die Nephrit-Talklagerstätte Scortaseo (Puschlav, Kanton Graubünden). *Beiträge zur geologie der Schweiz, Geotechnische Serie, Lieferung*, 46
- De Michele, V., Liborio, G., Nana, P., and Piacenza, B., 2002. Nefrite della Val Malenco (Provincia di Sondrio, Lombardia, Italia). *Bollettino dell'Istituto di Mineralogia "F. Grazioli"*, 1/2002, 13-15
- Nichol, D., 2000. Two contrasting nephrite jade types. *Journal of Gemmology*, 27(4), 193-200
- Rock-Colour Chart Committee, 1980. *Rock-Colour Chart*. Geological Society of America, New York
- Trommsdorff, V., and Evans, B. W., 1972. Progressive metamorphism of antigorite-schist in the Bergell tonalite aureole (Italy). *American Journal of Science*, 272, 423-37

Stereoscopic effect in asterism and chatoyancy

Harold Killingback FGA
Oakham, Rutland

Abstract: *The optical effect of a star displayed by rose quartz which appears to be located above the stone is described. An explanation of the phenomenon using ray diagrams is proposed. This analysis applies to all star and cat's-eye stones.*

Introduction

I recently purchased a star rose quartz sphere. At first there seemed to be nothing remarkable about it. True, it was big – 105 mm in diameter - and as is commonly the case, it was heavily fissured and had many growth features which made it non-transparent, so there was no diasterism. Although epiasterism was present, it appeared somewhat vague, but after continuous observation for about 20 seconds, to my amazement the star appeared to float about 40 mm above the surface of the ball! The effect was quite dramatic. Those who saw it tried to touch the star. I had not read about such a phenomenon, and determined to find out more.

Observations

One of the arms of the star, though it had a discontinuity, was brighter than the others and I concentrated on that. I noticed that, when I looked with my right eye, the arm appeared further to the left than it did when viewed with the left eye. This is shown in *Figure 1* taken with the camera in two positions having the same angle of view as the eyes at normal reading distance. *The conclusion is that the two rays cross above the stone.* The brain seeks to meld the two images of the arm into one, i.e. it causes the eyes to focus on the point where the rays cross and so a stereoscopic view is obtained. This is why the star appears to float in space. I then attempted to trace the light rays to the ball and from it to the eye. I

arranged the ball such that the sun shone from directly behind me and the brightest arm of the star was vertical. In this position, the reflective needles in the quartz are perpendicular to my line of sight when looking with one eye down the line of the incident ray. I then ascertained the path of the incident and emergent rays as seen first from the position of the right eye and then from that of the left. (This is not easy, partly because of the fuzziness of the star.) *Figure 2* is the result of such an experiment.

It will be noticed that the emergent rays which reach the pupils appear to come from the sphere at points virtually coincident with



Figure 1: Star rose quartz sphere as seen by the left eye (a) and the right eye (b). The prominent arm of the star is vertical and just to the right of centre in (a), and to the left in (b).

In order to 'see' the sphere in *Figure 1* in three dimensions without the aid of a stereoscope:

1. Place the images flat on a desk or table;
2. Stand above the images with your eyes 50-60 cm above looking vertically down;
3. Allow your eyes to relax, like gazing into the distance. Your eyes momentarily defocus and images of the sphere float sideways; one image from the left and one from the right will coalesce and you should then focus on this image that lies at the centre of the three.
4. You should see this central image clearly and with a distinct depth to it, with the arm of the star appearing to be above the surface of the sphere.

the points of entry of the incident rays. The conclusion is that the light is reflected from needles very close to the surface. The rays converge about 45 mm above the sphere.

In order better to understand what is happening inside the sphere, I constructed a schematic diagram (*Figure 3*) in which the region of refraction and reflection is greatly enlarged. Starting with the observed angle of incidence and a (mean) refractive index of

1.55, the path of the ray can be calculated by the usual methods. The theoretical approach agrees very well with the results observed.

I am grateful to J R Fletcher of Nottingham for pointing out that the situation can be likened to a plano convex lens backed by a plane mirror. (Indeed if, instead of a mirror, one attaches a parallel array of polished wires one gets a reasonable cat's-eye! This is shown in *Figure 4*.) As the light passes twice through

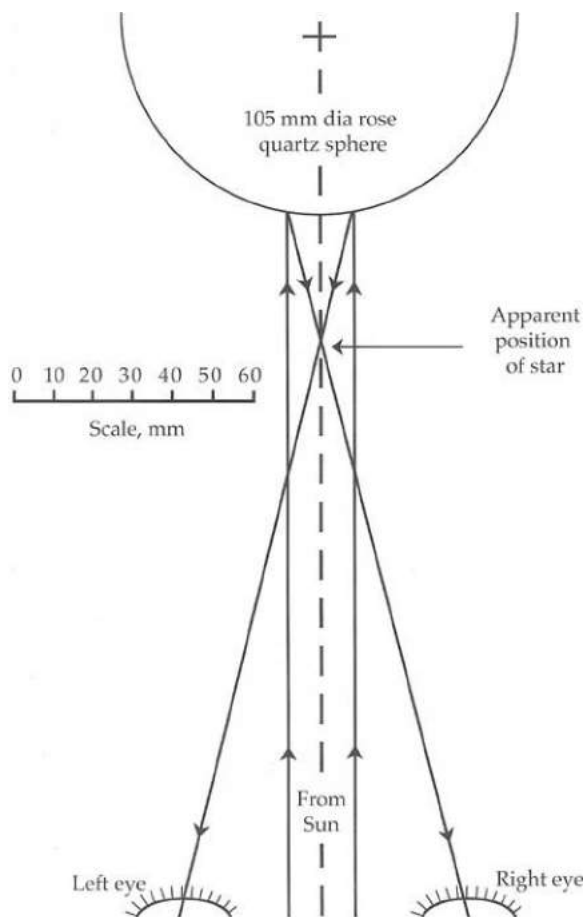


Figure 2: Schematic diagram of paths of the sun's rays to each eye.

the lens, the effective focal length is halved (Fletcher, pers. comm.). The thin lens equation is $1/U + 1/V = 1/F = 2(N-1)/R$. Here, the source distance U is effectively infinite and its reciprocal zero. Consequently the image distance V is equal to the effective focal length F and so $V = R/2(N-1)$ where R is the lens radius and N the refractive index. Consequently, we would expect the image to be at a distance from the lens equal to $52.5 / 2(1.55-1)$ i.e. 47.7 mm. Within the accuracy of the assumptions and observations, this is in very good agreement with Figure 2.

Discussion

Although the above has been based on a particular example, the argument is quite general. It must, therefore, apply to all star stones and cat's-eyes that have ever been and ever will be.

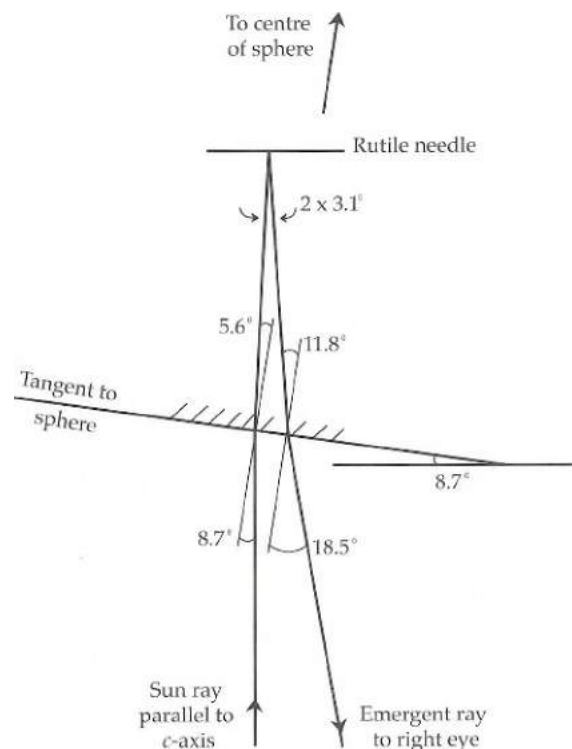


Figure 3: Schematic diagram of ray path. The angles are calculated for a 105 mm diameter sphere and for an inter-pupillary distance of 65 mm.



Figure 4: Cat's-eye effect produced by pins taped to the flat underside of a plano-convex lens.

The only reference I have found to this phenomenon is in *Identification of Gemstones* by O'Donoghue and Joyner, page 72, who quote a GIA report (Mayerson, 2001) of blue cabochons having stars which appeared to float over the surface, and am surprised that this startling effect has not received more attention.

I have looked at smaller stars and cat's-eyes. In examples of moderate size the effect can be seen (though I had not noticed it before). In small stones the effect seems too small to attract attention. Tests, however, confirm that it is still there. In one respect, the fissures in rose quartz help by providing a background against which the stereoscopic effect is more obvious than in the case of stones with few visible inclusions, where the surface level is less obvious.

I conclude that the stereoscopic effect is of academic rather than practical interest but I hope that understanding of it extends the enjoyment to be had from gemmology. I only hope that it is not used by charlatans asking inflated prices for star rose quartz spheres 'containing a force field so powerful it projects the star outside the sphere'!

References

- Mayerson, W., 2001. Sapphires with diffusion-induced stars. In Gem Trade Lab notes. *Gems & Gemology*, 37(4), 324-5, and Errata, 38 (3), 275
- O'Donoghue, M.J., and Joyner, L., 2002. *Identification of gemstones*. Butterworth-Heinemann, Oxford. 313 pp

Identification of an imitation of pearl by FTIR, EDXRF and SEM

T.L. Tan¹, T.S. Tay², S.K. Khairoman¹ and Y.C. Low¹

1. Natural Sciences Academic Group, National Institute of Education, Nanyang Technological University, 1 Nanyang Walk, Singapore 637616, Singapore

2. Far East Gemological Laboratory, 400 Orchard Road 03-10, Orchard Towers, Singapore 238875, Singapore

Abstract: Pearl is an organic gem and its popularity is basically due to the beauty of its natural lustrous and iridescent surface. Most of the pearls in the market are now grown ('cultured') in farms containing thousands of molluscs. Each mollusc deposits a nacreous layer on an inserted bead of mother-of-pearl material. For superior quality pearls, it may take up to two years or more to harvest and the yield is usually low, and these factors account for their high price and the proliferation of pearl imitations. Pearl imitations which are developed in laboratories are not easily identified using conventional gemmological methods. In this investigation, the surface structures of the cultured pearls and its imitations were studied using a scanning electron microscope (SEM) at magnification of up to 2000 \times . Energy-dispersive X-ray fluorescence (EDXRF) and Fourier transform infrared (FTIR) spectroscopy were employed to study the chemical composition of the pearl layer and the bead for naturally-coloured cultured pearls, dyed cultured pearls and pearl imitations. EDXRF results show that the cultured pearls and their beads are basically CaCO₃, while the detection of only C and O in the pearl imitations indicates that they are consistent with a polymeric composition. The presence of Si, O, Na and Al in the bead of the pearl imitation is consistent with it being glass. In FTIR experiments, the absorption peaks of 700 cm⁻¹, 713 cm⁻¹, 862 cm⁻¹ and 1083 cm⁻¹ are observed in both naturally-coloured and dyed cultured pearls, which confirm that they are CaCO₃ with aragonite structure. However, the infrared spectra of pearl imitations are very different and are typical of polymers. In addition, studies on fluorescence using short and long wave ultraviolet radiation indicate that cultured pearls can be effectively distinguished from their imitations.

Keywords: Pearl Imitation, Pearls, FTIR, EDXRF, SEM

Introduction

Pearls are one of the more desirable gemstones in the world (Clark, 2000; Landman *et al.*, 2001). Unlike other gemstones, pearls are produced biologically by molluscs such as clam, oyster or snail. Molluscs form pearls naturally when an irritant affects their soft parts (Shirai, 1994). As a defence mechanism, the mollusc secretes a fluid to coat the irritant and layer upon layer of this nacreous coating is deposited on the irritant until a lustrous pearl is formed. These radiant layers of coating consist mainly of aragonite and conchiolin (Landman *et al.*, 2001; Shirai, 1981), the same substances deposited by the molluscs in building their shell. A cultured pearl undergoes a similar process of growth. The only difference is that the irritant is a surgically-implanted mother-of-pearl bead or a piece of shell (Wada, 1999). However, imitation pearls are produced very differently. In most cases, a glass bead is dipped into a solution made from fish scales, which then dries as a skin, (Landman *et al.*, 2001). This coating is thin and may eventually wear off. Recently, pearl imitations have been constructed of more recently developed materials to give good iridescent surface effects. These imitations can be easily mistaken for good-quality pearls as basic gemmological tests are not adequate for differentiating them.

Among recent studies on cultured pearls, the following are noteworthy. Studies of Chinese cultured pearls in relation to their production and colour-treatment using Raman spectroscopy have been made by Li and Chen (2001) and Li (2001). Formation and quality of pearls have been investigated and described in detail using optical and scanning electron microscope by Wada (1999). These structural studies are useful in understanding the formation of cultured pearls in molluscs. The history, production and yield of Australian pearls have been studied by Brown (2002), and the structure of non-nacreous pearls (Safar and Sturman, 1998) and Bangladeshi pearls (Kennedy, 2001) have also been described.

In the present investigations, studies on naturally-coloured and dyed cultured pearls and pearl imitations using accurate spectroscopic techniques as in Fourier transform infrared (FTIR) and energy-dispersive X-ray fluorescence (EDXRF) have been made. These techniques are useful for the identification of the chemical compositions of cultured pearls for comparison with these of pearl imitations. The usefulness of these techniques was discussed with examples by Hayashi (1999). Although some properties of pearl imitations were mentioned by Landman *et al.* (2001), accurate spectroscopic studies on them remain very limited. Furthermore, the pearl imitations abundant in the market show strong iridescence on their surfaces, and may not easily be distinguished by visual observation. Therefore, a systematic study of the chemical compositions using FTIR and EDXRF techniques of both cultured pearls and their imitations has been carried out. Surface structural studies have also been made using the scanning electron microscope (SEM) at magnifications up to 2000 \times , and fluorescence using short and long wave ultraviolet radiation has been observed. The results of these experiments show that pearl imitations can be differentiated effectively from cultured pearls.

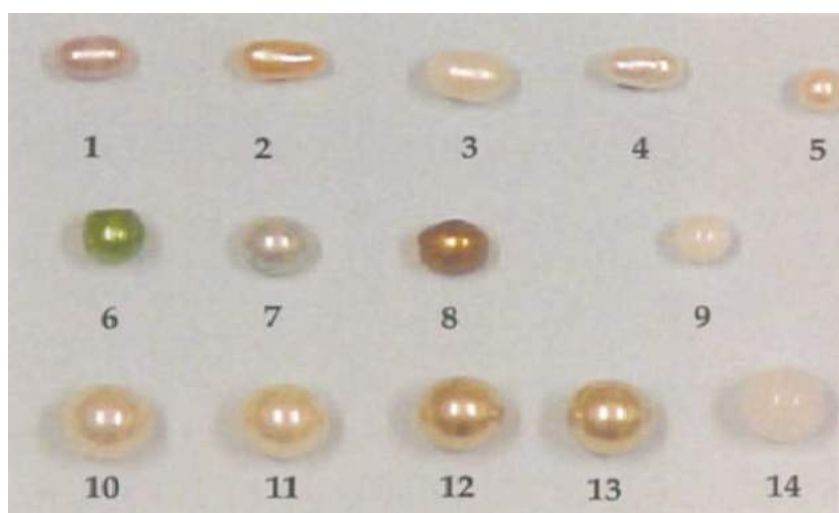


Figure 1: The photograph shows five samples of naturally-coloured cultured pearls (numbered 1 to 5, top row, from left to right); three samples of dyed cultured pearls and one sample of a cultured pearl bead (numbered 6 to 9, middle row, from left to right) and four samples of pearl imitations and one sample of a pearl imitation bead (numbered 10 to 14, bottom row, from left to right).

Table I: Gemmological and spectroscopic properties of naturally-coloured cultured pearls (samples 1 to 5), dyed cultured pearls (samples 6 to 8), cultured pearl bead (sample 9), pearl imitations (samples 10 to 13) and pearl imitation bead (sample 14).

Sample	Description and (SEM) observations	UV fluorescence		FTIR absorption peaks (cm ⁻¹)	EDXRF elemental peaks
		short wave (254 nm)	long wave (265 nm)		
Cultured pearls					
1	natural pink; baroque; layered, flaky surface	inert	weak blue	700, 713, 862, 1083, 1469, 1788, 2499, 2522, 2547, 2920	C, O, Ca
2	natural orange; baroque; layered, flaky surface	inert	inert	700, 713, 863, 1083, 1472, 1788, 2499, 2522, 2547, 2919	C, O, Ca
3	natural white; oval-shaped; layered, flaky surface	weak bluish white	very strong bluish white	700, 713, 862, 1083, 1467, 1788, 2500, 2522, 2547, 2918	C, O, Ca
4	natural white, strong iridescence; baroque; layered, flaky surface	weak bluish white	very strong bluish white	700, 713, 862, 1083, 1462, 1788, 2500, 2522, 2547, 2918	C, O, Ca
5	natural white; spherical; layered, flaky surface	weak bluish white	very strong bluish white	700, 713, 862, 1083, 1463, 1788, 2500, 2522, 2547, 2918	C, O, Ca
6	green-dyed; spherical; layered, contoured surface	inert	green	700, 713, 863, 1083, 1469, 1788, 2500, 2522, 2547, 2918	C, O, Ca
7	blue-dyed; spherical; layered, contoured surface	weak purple	very strong bluish white	700, 713, 862, 1083, 1469, 1788, 2500, 2522, 2546, 2917	C, O, Ca
8	gold-dyed; spherical; layered, contoured surface	inert	inert	700, 713, 861, 1083, 1469, 1788, 2499, 2522, 2547, 2918	C, O, Ca
9	bead for cultured pearls; spherical; layered, flaky surface	weak bluish white	strong bluish white	700, 713, 861, 1083, 1424, 1788, 2499, 2522, 2546, 2918	C, O, Ca
Imitation pearls					
10	cream-white; spherical; small cubic particles on surface	inert	weak dark purple	751, 840, 1068, 1161, 1280, 1376, 1654, 1732, 2554, 2929, 2964, 3466	C, O
11	cream-white; spherical; small cubic particles on surface	inert	weak dark purple	750, 840, 1067, 1161, 1280, 1375, 1654, 1732, 2553, 2929, 2964, 3468	C, O
12	gold; spherical; small cubic particles on surface; visible cracks and lines	inert	weak dark purple	752, 841, 1068, 1161, 1280, 1378, 1655, 1733, 2554, 2929, 2964, 3468	C, O
13	gold; spherical; small cubic particles on surface; visible cracks and lines	inert	weak dark purple	751, 840, 1067, 1161, 1281, 1376, 1654, 1732, 2553, 2929, 2963, 3469	C, O
14	bead for imitation pearls, cloudy grey; spherical	weak yellowish white	inert	3511, Highly opaque to IR	Si, O, Na, Al, Ca

Materials and experimental methods

Five samples of naturally-coloured cultured pearls (samples 1-5), three samples of dyed cultured pearls (samples 6-8), one sample of the beads used for a great number

of cultured pearls (sample 9), four samples of pearl imitations (samples 10-13) and one sample of the beads used for pearl imitations (sample 14) were used in this investigation, as shown in *Figure 1*.

All samples of the naturally-coloured cultured, dyed cultured pearls, and their

beads (samples 1-9) were produced from a freshwater mollusc (*Hyriopsis cumingi* or *tritogonia*) in China (Li and Chen, 2001; Li, 2001). The pearl imitations and their bead (samples 10-14) are commercially available and have a Japanese brand-name. Scanning electron microscope (SEM) observations, ultraviolet fluorescence, Fourier transform infrared (FTIR) spectroscopy and energy-dispersive X-ray fluorescence (EDXRF) measurements were carried out on these samples and the results are summarized in *Table I*. Before every experiment, the surfaces of the cultured pearl samples were cleaned using ethanol solution in order to remove any contaminant derived from handling. However great care was taken with the pearl imitations and their surfaces were only very lightly cleaned with ethanol to prevent possible chemical reaction of the surface material with the solvent.

Ultraviolet (UV) fluorescence was the initial test carried out on all the samples. The UV lamp used is UVGL-58 (Mineralight, USA), with a short wave source of 254 nm and long wave of 365 nm. Cultured pearls normally have a weak whitish fluorescence under short wave and strong bluish white fluorescence under long wave (Matlins and Bonanno, 1997).

All the samples were tested using FTIR spectroscopy. The Perkin Elmer Instruments, Model Spectrum One - Fourier transform infrared spectrometer was used to record the spectra of all samples in the wavelength range of 400 cm^{-1} to 4000 cm^{-1} . The accuracy of the absorption peaks was $\pm 1 \text{ cm}^{-1}$. Since cultured pearl material is basically opaque to infrared radiation, a diluted sample of pearl in an infrared-transparent matrix of potassium bromide (KBr) is needed for detailed FTIR work. In preparing cultured pearl pellets for FTIR work, the samples were wiped clean with ethanol, and their surfaces were scraped to obtain some pearl material which was then ground to a fine powder, mixed with KBr, and pressed in a 2-tonne press to make flat circular pellets. These pellets are sufficiently translucent to allow collection of infrared transmission spectra

and the recording of absorption peaks for identification of materials.

Following the FTIR work, EDXRF experiments and SEM observations were carried out using JEOLSM - 5600LV SEM/EDX microscopy with a working voltage of 20kV. Surface analysis by EDXRF was accomplished by bombarding a sample with high-energy electrons and detecting, and analysing the energy of the emitted X-rays (Potts, 1993). These electrons have penetrating power in a solid extending 1 to 5 μm depending on their energy and the nature of the substance. Since EDXRF is a surface-sensitive technique for chemical characterization of the surface of a solid, care is taken to ensure that the surfaces of the samples are clean. EDXRF helps to identify the elements present in the samples, while SEM observations reveal the surface structure of the samples. Both are useful in distinguishing cultured pearls from their imitations.

Results and Discussion

The results of short wave UV fluorescence, FTIR spectroscopy, EDXRF elemental analysis, and SEM surface observations are summarized in *Table I* for all 14 samples.

Ultraviolet (UV) fluorescence

For naturally-coloured cultured pearls (samples 1 to 5), there was no consistent distinction between fluorescence under UV in short and long wave. However, samples 3, 4 and 5 all being white cultured pearl, show very strong bluish white in the long-wave and weak bluish white in the short wave. In contrast, samples 1 and 2 do not show such strong fluorescence. The results of samples 3, 4 and 5 agree well with the observations given in Matlins and Bonanno (1997) which showed that cultured white pearls show weak white fluorescence in short wave and strong bluish white in the long wave. Similarly, the bead (sample 9) of the kind used in the cultured pearls shows weak white fluorescence in short wave and strong bluish white in the long wave. This indicates that the bead and the white cultured pearl could be of similar composition.

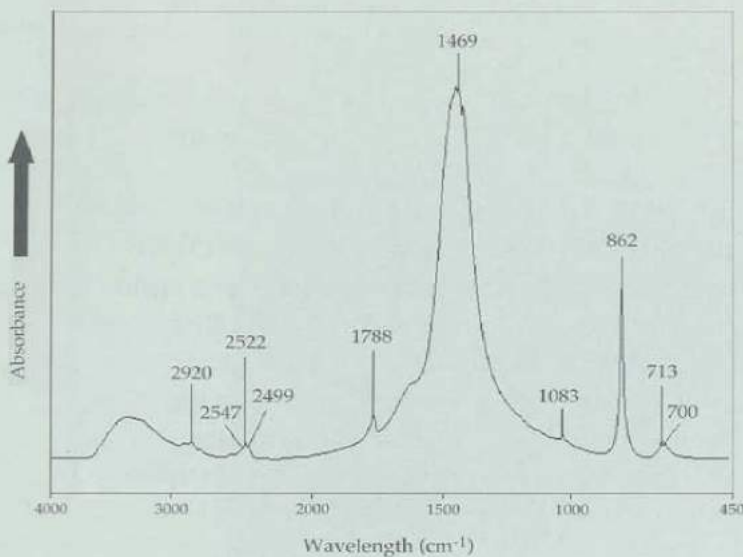


Figure 2: FTIR absorption spectrum typical of naturally-coloured and dyed cultured pearls (samples 1 to 8), and cultured pearl bead (sample 9).

For dyed cultured pearls (samples 6 to 8) there were no obvious trends in their UV fluorescence. Any fluorescent effects must depend on the presence of dye materials on the surface. The pearl imitations (samples 10 to 13) are inert in short wave and show weak dark purple fluorescence in long wave, whereas the bead used in the pearl imitations (sample 14) is inert in long wave and weak yellowish white in short wave. This shows that there is a clear difference in behaviour between the bead and its coating in the pearl imitation. Although fluorescence patterns are not conclusive enough for differentiation between cultured pearls and pearl imitations, the weak dark purple fluorescence in long wave shown by imitation pearls is a useful indicator.

Fourier transform infrared (FTIR) spectroscopy

All naturally-coloured and dyed cultured pearls (samples 1 to 8) and the bead used in cultured pearls (sample 9) have strong infrared absorption peaks at around 700 cm^{-1} , 713 cm^{-1} , 862 cm^{-1} , 1083 cm^{-1} , 1469 cm^{-1} , 1788 cm^{-1} , 2499 cm^{-1} , 2522 cm^{-1} , 2547 cm^{-1} and 2920 cm^{-1} . A typical FTIR spectrum is shown in Figure 2. These are typical infrared absorption peaks for calcium carbonate, CaCO_3

structure as given in Smith (1999). The peaks at 700 cm^{-1} , 713 cm^{-1} , 862 cm^{-1} , 1083 cm^{-1} show that CaCO_3 in the cultured pearls and pearl bead is of aragonite crystal structure, with a pattern similar to that shown by turtle eggshell (Baird and Soloman, 1979). The result shows that the pearl bead is made from the shell of a mollusc similar to that which produces the cultured pearls. Since the FTIR spectra of samples 1 to 8 give the same absorption peaks, it was not possible to use the FTIR method to differentiate naturally-

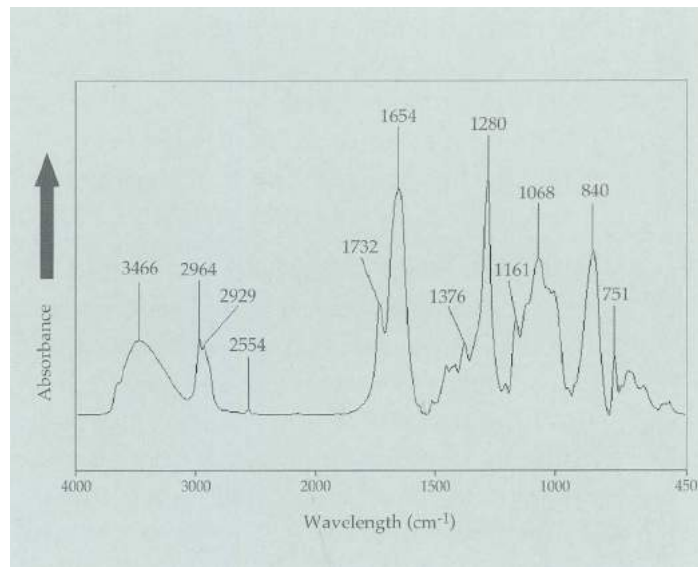


Figure 3: FTIR absorption spectrum typical of pearl imitations (samples 10 to 13).

coloured cultured pearls from the dyed ones. This agrees with the findings of Li (2001).

The infrared spectra of pearl imitations (samples 10 to 13) and the bead used in pearl imitations (sample 14) are very different from those of cultured pearls. Figure 3 shows the typical strong absorption peaks of pearl imitations at around 751 cm^{-1} , 840 cm^{-1} , 1068 cm^{-1} , 1161 cm^{-1} , 1280 cm^{-1} , 1376 cm^{-1} , 1654 cm^{-1} , 1732 cm^{-1} , 2554 cm^{-1} , 2929 cm^{-1} , 2964 cm^{-1} and 3466 cm^{-1} . These peaks indicate that pearl imitations are basically made up of polymeric material. In contrast to Figure 2, the absence of peaks due to CaCO_3 in Figure 3, especially that at 1469 cm^{-1} , clearly shows

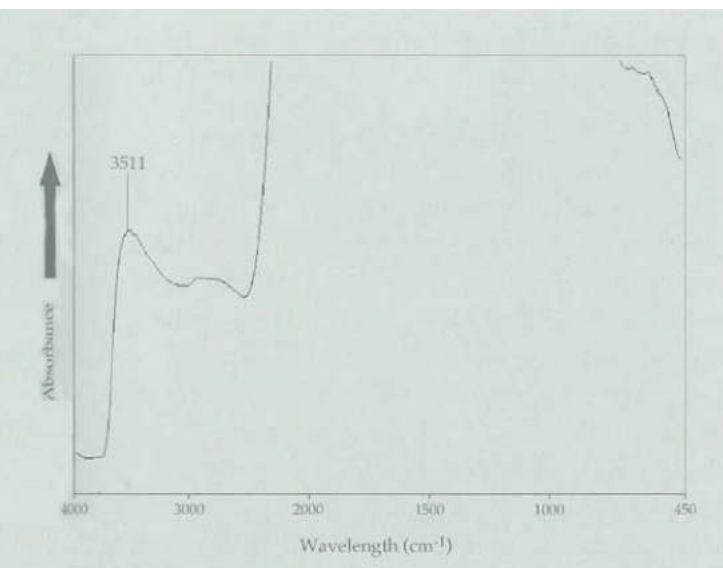


Figure 4: FTIR absorption spectrum typical of pearl imitation bead (sample 14).

that pearl material (nacre) is not used in imitations. In Figure 3, the peak at 3466 cm^{-1} is due to an O-H stretch, peaks at 2929 cm^{-1} and 2964 cm^{-1} are from C-H vibrations, strong peaks at 1654 cm^{-1} and 1732 cm^{-1} are due to C=O stretch, a strong peak at 1280 cm^{-1} is possibly due to a C-C-O asymmetric stretch in a phenol group, and the peak at 840 cm^{-1} is due to a C-C-O symmetric stretch (Smith, 1999 and Socrates, 1994). The presence of C, H and O atoms in these vibrations can be explained by the high polymeric content of pearl imitations. The bead for pearl imitations is opaque to infrared below 2500 cm^{-1} and has a broad peak at 3511 cm^{-1} as seen in Figure 4. This shows that the substance used in the bead is different from that used in cultured pearls.

The measurements of the various FTIR absorption peaks given in Table 1 are useful and effective in differentiating naturally-coloured and dyed cultured pearls from their imitations. The beads used in cultured pearls and the pearl imitations are also different. One shortcoming of the method is that it does not enable distinction between the naturally-coloured and dyed cultured pearls. In addition, the technique is not sensitive enough to detect the low levels of dye used in the dyed pearls.

Energy dispersive X-ray fluorescence (EDXRF).

An EDXRF spectrum typical of naturally-coloured and dyed cultured pearls, is shown in Figure 5. The strong X-ray energy peaks of carbon, C $K\alpha_1$ at 0.277 keV ; oxygen, O $K\alpha_1$ at 0.525 keV ; calcium, Ca $K\alpha_1$ at 3.69 keV and Ca $K\alpha_2$ at 3.92 keV , and gold, Au $M\beta$ at 2.205 keV are present (see Blake, 1990). The spectrum recorded in the X-ray energy range of 0 to 9 keV can provide identification of all major elements with atomic number higher than boron, i.e. carbon and above, that are present on the surface of the pearls. The element hydrogen which is normally present in organic material as in pearl cannot be detected because of the small mass of hydrogen. EDXRF is a surface analysis technique with detection of elements to

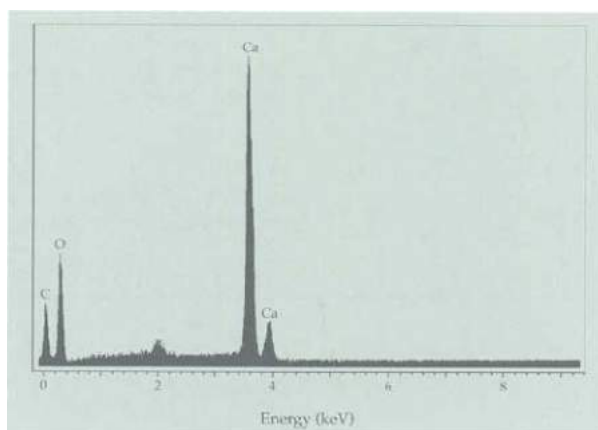


Figure 5: EDXRF spectrum typical of naturally-coloured and dyed cultured pearls (samples 1 to 8), and cultured pearl bead (sample 9).

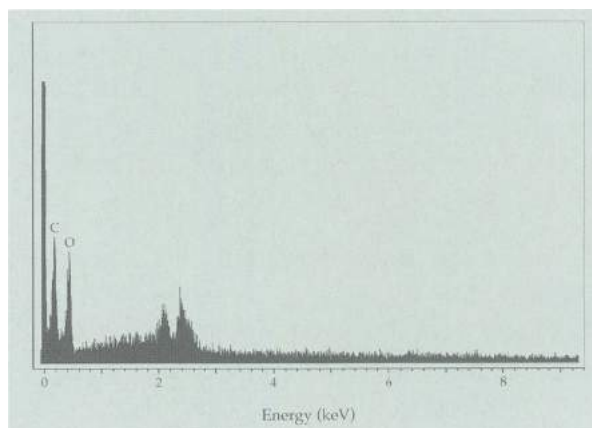


Figure 6: EDXRF spectrum typical of pearl imitations (samples 10-13).

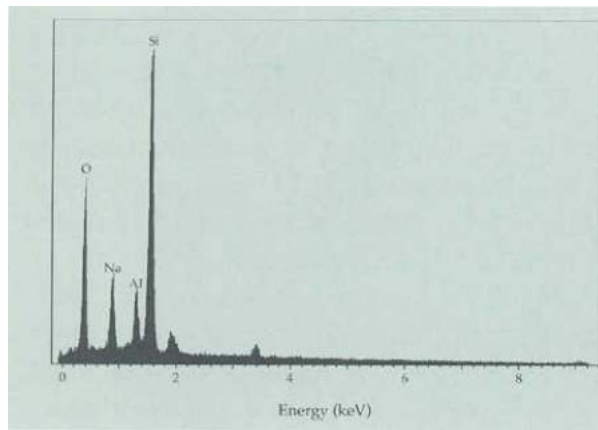


Figure 7: EDXRF spectrum typical of bead of pearl imitation (sample 14).



Figure 8: SEM micrograph typical of naturally coloured and of dyed cultured pearls (samples 1-8). Magnification 2000 \times .

a depth of 5 μm , indicating that it may not be accurate for bulk studies. The gold peak comes from a thin layer of gold on the sample surface which is coated prior to the EDXRF scan to conduct away electrons from the electron beam and prevent a negative charge on the surface. The detection of Ca, C and O is consistent with the composition of cultured pearls, which is calcium carbonate, CaCO_3 .

EDXRF spectra of dyed cultured pearls are similar to that in Figure 5. Elements other than Ca, C and O and Au are not found. This indicates that the dyes are not detectable by the EDXRF method. The EDXRF spectrum obtained from the cultured pearl bead is

indistinguishable from those of samples 1-8 and is consistent with that of a mollusc shell.

The EDXRF spectrum typical of pearl imitations (samples 10-13) is shown in Figure 6 and reveals the presence of C and O, and absence of Ca. The C and O peaks are consistent with the presence of polymers. Unfortunately, the EDXRF technique is unable to detect the lightest element, hydrogen which is an important component of polymers. The analysis of the bead (sample 14) used in pearl imitations is shown in Figure 7 and indicates the presence of oxygen (O), silicon (Si), aluminium (Al) and sodium (Na). The energy

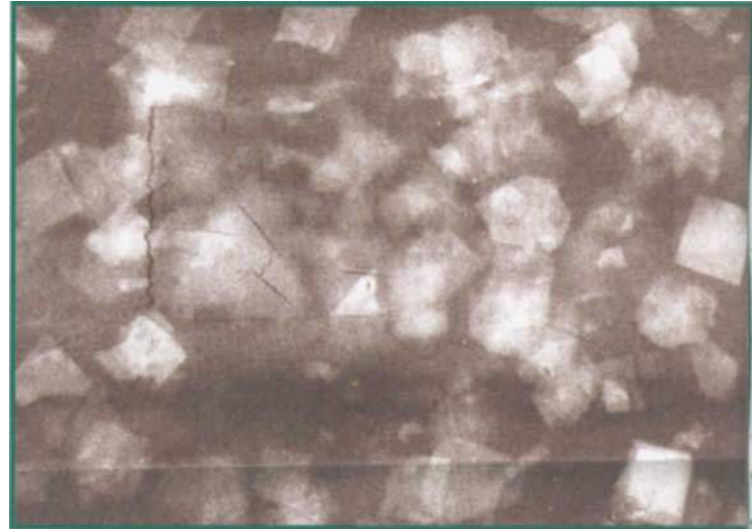


Figure 9: SEM micrograph typical of pearl imitations (samples 10 to 13). Magnification 2000 \times .

pattern of the bead reveals that it cannot be CaCO_3 . The high energy peaks of Si and O show that the bead is possibly made of glass as mentioned in Landman *et al.*, 2001. Further measurements on the bead give specific gravity as 2.2 and refractive index of 1.5, which are consistent with a glass material.

The elemental analysis of the samples using EDXRF provides useful information of the chemical composition of the surfaces of the samples. The detection of major elements can be used to distinguish cultured pearls from their imitations. The non-destructive

nature of EDXRF analysis is beneficial for pearls set in close-set jewellery.

Scanning Electron Microscopy (SEM)

All samples are coated with a very thin layer of gold to prevent surface charging during electron bombardment while viewing the SEM images.

The surfaces of naturally-coloured cultured pearls (samples 1-5), studied at magnifications up to 2000 times (*Figure 8*), consist of layered, contoured, and flake-like patterns. Similar patterns were observed on dyed cultured pearls (samples 6-8), and they are the top view of crystalline layers of calcium carbonate which were deposited gradually over time. The layers consist of aragonite platelets separated by conchiolin (Wada, 1999; Landman *et al.*, 2001). In contrast, the surface morphology of the pearl imitations (samples 10 to 13) is very different as shown in *Figure 9*. Small cubic particles of regular size are randomly distributed over the whole surface. These particles could be polymeric cubes in dense suspension in a matrix layer to cause the iridescence effect which imitates a natural pearl. The difference in the SEM observations is quite significant and could be useful for differentiating cultured pearls from their imitations.

For EDXRF and SEM experiments, all samples are coated with a very thin layer (a few nanometres) of gold using a vapour deposition method normally at a temperature of about 80°C in the chamber. For the smooth surfaces of pearls, the gold layer can be easily removed by wiping the surfaces with a soft texwipe dampened with distilled water. No resulting scratches were detected using a 10x loupe. For FTIR work, additional sample preparation is needed to make flat circular pellets. This takes about ten minutes for each sample preparation. The collection of a FTIR spectrum for a sample would take about five minutes. In EDXRF and SEM methods where the sample is placed in an evacuated chamber, each energy spectrum run or image focusing would take a total time of about 15

minutes, including pumping down time. The gold-coating process for these two methods is relatively simple and would take about ten minutes. For EDXRF and SEM measurements the experimental time is greatly reduced when a batch of 5 samples can be mounted on the same holder and studied in a single process run. Normally EDXRF and SEM measurements can be done on a sample concurrently using the same system. Generally, a conservative estimate of the total time required for each sample using all three tests: FTIR, EDXRF, and SEM is less than one an hour.

Conclusion

Basic gemmological tests such as optical spectroscopy and ultraviolet fluorescence are not sufficiently accurate for distinguishing cultured from imitation pearls. However, comparing their FTIR absorption peaks, pearl imitations can be distinguished from cultured pearls. In the present FTIR investigation, samples of pearl imitations on the market were found to be constructed of material consistent with a polymer. Also, on the basis of their FTIR absorption peaks, the cultured pearls consist of aragonite rather than calcite. Although the FTIR technique is reliable, it was destructive as a small amount of the cultured pearl or pearl imitation material had to be scraped from the surface to make circular pellets. In contrast, the EDXRF method is non-destructive, and the present investigations of cultured pearls, imitation pearls and the respective beads showed that accurate identification and differentiation of cultured pearls from pearl imitation are possible by determining which elements are present. Although it is not possible to distinguish naturally-coloured cultured and dyed cultured pearls using the FTIR and EDXRF techniques, imitation pearls could be reliably identified. Furthermore, the bead in the imitation pearls was found to be glass while that in cultured pearls was calcium carbonate. SEM micrographs of the surfaces of cultured pearls and pearl imitations are

significantly different and therefore useful for identification purposes. Hence judicious use of FTIR, EDXRF, and SEM techniques can lead to reliable identification of imitation pearls and cultured pearls.

Acknowledgement

The authors are grateful for the financial support of the National Institute of Education through the research grant RP7/02 TTL.

References

- Baird, T., and Solomon, S.E., 1979. Calcite and aragonite in the eggshell of *Chelonia Mydas* L. *Journal of Experimental Marine Biology and Ecology*, **36**, 295-303
- Blake, D., 1990. Scanning electron microscopy. In: Dale L.Perry (Ed.), *Instrumental surface analysis of geologic materials*, VCH, New York, U.S.A., 11-43
- Brown, G., 2002. An update of Australian pearling and its pearls. *The Singaporean Gemologist*, **9**(1), 2-9
- Clark, C., 2000. *Tropical gemstones*. Periplus, Singapore, 46-51
- Hayashi, M., 1999. The present status of application of instrumental methods of gem identification - examples of identifications using EDS, X-radiography and FTIR. *The Journal of the Gemmological Society of Japan*, **20**(1-4), 99-106
- Kennedy, S., 2001. Notes from the laboratory. *The Journal of Gemmology*, **27**(8), 486-7
- Landman, N.H., Mikkelsen, P.M., Bieler, R., and Bronson, B., 2001. *Pearls, a natural history*. Harry N. Abrams, New York, U.S.A., 23-61
- Li L.P., 2001. Production and colour changing treatment of Chinese cultured pearl. *The Singaporean Gemologist*, **8**(1), 11-14
- Li L.P. and Chen Z.H., 2001. Cultured pearls and colour-changed cultured pearls: Raman Spectra. *The Journal of Gemmology*, **27**(8), 449-55
- Matlins, A.G., and Bonanno, A.C., 1997. *Gem identification made easy*. Gemstone Press, Woodstock, VT, U.S.A., 25-45
- Potts, P.J., 1993. Laboratory methods of analysis. In: C. Riddle (Ed.), *Analysis of geological materials*. Marcel Dekker, New York, U.S.A., 138-47
- Safar, A., and Sturman, N., 1998. Notes from the Gem and Pearl Testing Laboratory, Bahrain. *The Journal of Gemmology*, **26**(1), 17-23
- Shirai, S., 1981. *Pearls*. Marine Planning Co. Japan, 10-34
- Shirai, S., 1994. *Pearls and pearl oysters of the world*. Marine Planning Company. Japan, 610
- Smith, B., 1999. *Infrared spectral interpretation - a systematic approach*. CRC Press, London, 31-112, 171
- Socrates, G., 1994. *Infrared characteristic group frequencies: tables and charts*. John Wiley, New York, U.S.A., 80-121
- Wada, K., 1999. Formation and quality of pearls. *The Journal of the Gemmological Society of Japan*, **20**(1-4), 47-56

X-ray luminescence, a valuable test in pearl identification

Professor Dr H.A. Hänni, Dr L. Kiefert* and P. Giese

SSEF Swiss Gemmological Institute

e-mail: gemlab@ssef.ch

*Now at AGTA-GTC, New York, U.S.A.

Abstract: *The increasing similarity of structures encountered in natural pearls and beadless freshwater cultured pearls requires one or more additional criteria for their differentiation. The majority of natural pearls are from saltwater oysters; in contrast, most beadless cultured pearls come from freshwater mussels. For some time it has been known that freshwater pearls produce luminescence under X-rays, whereas pearls grown in saltwater do not. The reason is because freshwater nacre contains traces of manganese. By using a sensitive camera this visible luminescence can be recorded and displayed on a monitor. The beads (from freshwater nacre) in Japanese saltwater cultured pearls (Akoya) also react to the X-ray excitation and may shine through the cultured overgrowths that are relatively thin. The method is used as an additional test and is not an alternative for X-radiograph images.*

Keywords: *freshwater nacre, Mn in aragonite, pearl identification, X-ray luminescence*

Pearl identification

Natural and beaded cultured pearls

In testing pearls, natural and cultured pearls are usually differentiated using X-ray shadow graphs (Lorenz and Schmetzer, 1986). X-ray shadowgraphs provide the most meaningful images to enable identification. Drill hole investigation by endoscope is now a historic method as needles for this technique are no longer available. A modern successor to the endoscope has been produced in a few prototypes (Atalay, 1994) and works with a red laser light. The proof for a bead in a cultured pearl is most efficiently detected by good radiography. With small beads and thick overgrowths, however, an X-ray

shadowgraph will rarely show evidence of a bead. The Laue method is then a supplementary method when the presence of a nacre bead should be checked (Barnes, 1944). The method depends on interpreting the patterns obtained from unfiltered X-ray radiation directed on a bead consisting of well ordered layers of aragonite platelets (Barnes, 1944; Hänni, 1983). Six-spot patterns or four-spot patterns (Webster, 1994, p.547) may appear, depending on the direction of the ray with respect to the layers of an aragonite bead nucleus. Should the bead be of amorphous or unordered crystalline material, the

pattern obtained would have no definite point structure, e.g. it may have a blurred halo or ring. A recent bead material manufactured from the giant clam shell (*Tridacna*), produces haloes on lauegrams when the X-ray beam is parallel to the growth layers. Perpendicular to the growth layers, clear four point patterns are visible. In any case, direct radiography (X-ray shadow method) is the preferred method to distinguish natural pearls from cultured pearls with a bead, either on fine-grained film or by digital imaging.

The growth structures of natural pearls as seen on X-radiographs have been known for many years; they reflect the individual growth development of each pearl (Alexander, 1939; Hänni, 2002). Characteristically there is an approximately round central body (formed by conchiolin-rich columnar calcite) coated by a more or less thick overgrowth of nacre formed by minute scales of tabular aragonite in concentric array. The X-radiographs of the aragonite coating can show concentric or bow-shaped lines.

Most natural pearls (all oriental pearls) derive from marine oysters, and the majority of beadless cultured pearls form in freshwater mussels. When there is no indication of a bead, a first separation of the two types can thus usually be made on the basis of whether nacre is saltwater or freshwater. A number of authors have already reported that freshwater nacre has an elevated concentration of manganese compared to saltwater nacre (Komatsu, 1987; Gutmannsbauer, 1992, 1994). Mn-doped calcium carbonate, including aragonite, possesses a characteristic luminescence when excited with X-rays or cathode rays (Waychunas, 1998). Freshwater nacre shows a characteristic fluorescence in whitish yellow (Lorenz and Schmetzer, 1985). In a recent publication Hänni *et al.* (2004) have demonstrated the usefulness of Mn-related X-ray luminescence in pearl identification.

Beadless cultured pearls

In the past the identification of beadless cultured pearls was straightforward because their radiography showed clear indications of their origin. The distinctive features on the film consist of a curved fine line or tangle of

lines in the centre of the pearl, being the image of a complex central cavity, often empty or containing brown organic material. Note that the organic material is not the tissue transplant, as often reported. The tissue transplant grows into the pocket which is later the pearl sac, producing and containing the cultured pearl. However, these central features in older freshwater beadless cultured pearls are no longer as clear and large in the newer Chinese freshwater beadless cultured pearls. Smaller tissue parts are being transplanted and more years are allowed for the growth of the pearl. Because of the smaller graft the first pocket on whose surface the calcium carbonate is precipitated is also smaller. Any resulting cavity in the cultured pearl would be minute and would most probably be eliminated by the drilling process. Other growth features in the near-round to round Chinese freshwater cultured pearls may exist but are not always clearly visible in a random position of the pearl, although wavy growth lines or dividing lines have been shown by Scarratt *et al.* (2000). Beadless saltwater cultured pearls may show central cavities, too. Two cases may be discussed:

1. If the oyster has expelled the first bead, but the tissue graft still forms a pearl sac, a beadless cultured pearl can result. In the trade, beadless cultured saltwater pearls (South Sea and Tahiti) are often called 'Keshi'. There is no need and it is rather incorrect to call these products 'Keshi'. Originally Japanese Keshi cultured pearls were mantle pearls produced by accidental injury to the mantle of Akoya oysters. The term should definitely not be used for cultured pearls in gonad-grafted oysters.
2. If, after the first pearl crop, a second bead is inserted and the oyster expels it, the pearl sac, ready for further production, collapses, with nothing there to support it. Consequently, the shape of the second cultured pearl is very baroque, usually flattened. There is no need to call it 'Keshi' either, it is just a beadless cultured pearl. This kind of beadless Tahiti or South Sea cultured pearl is relatively simple to identify with an X-radiograph.



Figure 1: Working situation with X-ray apparatus, CCD camera and screen. A pearl necklace is ready in the X-ray chamber, the camera F-View II is visible. Photo H.A. Hänni © SSEF Swiss Gemmological Institute.

Investigation of the X-ray luminescence of nacre

For the observation of X-ray luminescence it could be sufficient to look at the objects in the dark when they are under X-ray excitation were it not for health and safety requirements. Since X-rays scatter and reflect off surfaces, it is absolutely necessary that the observer is protected from any of the rays which might reach the body. The excitation has thus to be made in a conventional X-ray cabinet, i.e. a conventional device for X-radiography with an observation window of lead glass. Safety is then guaranteed. The tungsten tube is operated at 95 kV and 4 mA. Instead of just looking at the effect, we propose here the use of a very sensitive digital camera system which records the luminescence pictures. The low intensity light emitted requires a special CCD camera and a computer programme (AnalySIS) which manages the recording. Preliminary experiments have proven the validity of the commercially available viewing system 'F-View II' by Soft

Imaging Systems (Figure 1). The camera is equipped with a Peltier element that cools the detector. This provides low noise and the signals produce excellent pictures. The software allows easy control of the system and picture management (Figure 2). Since the camera is very sensitive to light, only low light is

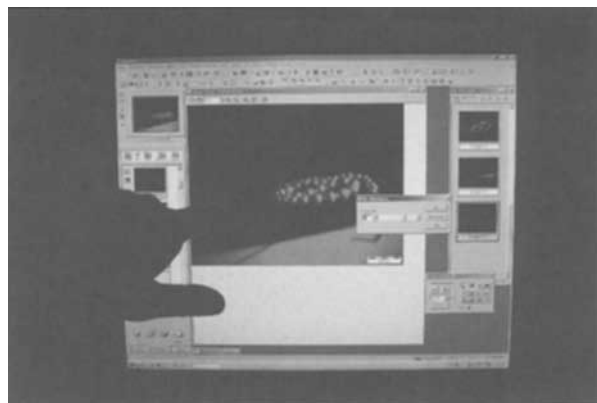


Figure 2: A pearl necklace, ready in the X-ray chamber, is pictured in room light and shown on the screen. The management and recording of images are done with a special programme. Photo H.A. Hänni © SSEF Swiss Gemmological Institute.



Figure 3: A strand of South Sea cultured pearls from Australia (right) and a strand of freshwater cultured pearls from China (left) in the weak room light supplied by a diode. Photo P. Giese © SSEF Swiss Gemmological Institute.



Figure 4: The same necklace as in Figure 3 under X-ray excitation. The South Sea cultured pearls (from saltwater) do not show any luminescence while the freshwater cultured show clear luminescence. Photo P. Giese © SSEF Swiss Gemmological Institute.

needed to provide the first reference picture, and a diode was chosen, already fixed in the sample room. A second picture of the pearls in the same position was then taken under X-rays. Figures 3 and 4 show a strand of Australian saltwater cultured pearls with thick overgrowths on the beads, next to a strand of beadless Chinese freshwater cultured pearls for comparison.

When Akoya cultured pearls are tested it becomes apparent that the bead which is made of shell grown in freshwater, also gives a luminescence reaction to the X-ray excitation. Depending on nacre thickness and the amount of organic material on each bead, different amounts of light may be registered (see Figures 5 and 6). The luminescence reaction may also be inhibited when pearls are dyed with dark colours or beaded cultured pearls have naturally pigmented overgrowths as e.g. from Tahiti or Mexico – although even in these examples, response can be variable.

No luminescence reaction appears with *Tridacna* (giant clam shell) beads, since this shell material grows in saltwater and does not contain the Mn which causes the luminescence.

Conclusions

X-rays cause weak luminescence in freshwater nacre or pearls. This effect is due to a weak concentration of manganese. Since nacre or pearls from saltwater are free of manganese, luminescence does not occur. The luminescence is only visible in the dark, either by the naked eye or with a sensitive CCD digital camera. This is an additional means of differentiation between freshwater and saltwater pearls and cultured pearls where X-ray features are not sufficient. Since Chinese freshwater cultured pearls are taking an increasing share of the market, possibilities of mixing them up with South Sea



Figure 5: An Akoya cultured pearl necklace (freshwater nacre beads with saltwater nacre overgrowth) in room light, ready in the X-ray apparatus for a luminescence picture. Photo P. Giese © SSEF Swiss Gemmological Institute.



Figure 6: The Akoya cultured pearl necklace shown in Figure 5 recorded under X-ray radiation. Depending on the thicknesses of the overgrowths, a different luminescence is visible in different pearls, indicating that Mn is present in the beads. Photo P. Giese © SSEF Swiss Gemmological Institute.

cultured pearls or with natural marine pearls are growing. Since pearl identification may be increasingly problematic, especially when only X-radiographs are considered, the observation of X-ray luminescence will be most useful for testing strands with a mixture of different types of pearls, and the attribution of pearls of a different type within a strand can be made with more confidence. The method is limited when nacre is rich in colouring pigment which generally suppresses the luminescence. This can occur with naturally coloured as well as with dyed pearls.

Acknowledgements

SSEF pearl research has been greatly supported by Golay (Lausanne). A variety of cultured pearls of all kinds have been donated to the SSEF pearl collection by Paspaley (Darwin), Pacific Perles (Papeete), Golay (Lausanne), Schöffel (Hong Kong) and Frieden (Thun). Preliminary experiments with the F-View II System were made possible by courtesy of Gloor Instruments (Uster, Switzerland) and F. Meier of this firm who installed and tuned the F-View System.

References

- Alexander, A.E., 1939. Pearls through artifice. *Scientific American*, April
- Atalay, H., 1994. Le 'Pearlscope'. *Revue de Gemmologie* **120**, 15-16
- Barnes, W.H., 1944. *Pearl identification – the diffraction of X-rays by pearls*. The Gemmological Laboratory, Mappin's Ltd., Montreal
- Gutmannsbauer, W., 1992. *Morphologische, strukturelle und chemische Untersuchungen an Perlmutter und Perlen einiger perlenbildende Muscheln*. Diplomarbeit, Min.-petr. Institut der Universität Basel, Switzerland
- Gutmannsbauer, W., 1994. Structural and chemical investigations on shells and pearls of nacre forming salt- and fresh-water bivalve molluscs. *J.Gemm.* **24**(4), 241-52
- Hänni, H.A., 1983. The influence of the internal structure of pearls on Lauegrams. *Journal of Gemmology*, **18**(5), 386-400
- Hänni, H.A., 2002. *Pearls: The formation of shell and pearls*. SSEF Tutorial CD Rom, SSEF Swiss Gemmological Institute, Basel, Switzerland
- Hänni, H.A., Kiefert, L., and Giese, P., 2004. Ein notwendiger Test in der Perlenuntersuchung. *Gemmologie. Z.Dt.Gemmol.Ges.*, **53**(1), 39-42
- Komatsu, H., 1987. *Introduction to pearl testing*. Zenkoku hōsekigaku kyōkai shuppanbu, Tokyo. 1-24 (in Japanese)
- Lorenz, I., and Schmetzer, K., 1985. Möglichkeiten und Grenzen der röntgenographischen Untersuchung von Perlen. *Z.Dt.Gemmol.Ges.* **34**, 57-68
- Lorenz, I., and Schmetzer, K., 1986. Possibilities and limitations in radiographic determination of pearls. *Journal of Gemmology*, **20**(2), 114-23
- Scarratt, K., Moses, T., and Akamatsu, S., 2000. Characteristics of nuclei in Chinese freshwater cultured pearls. *Gems & Gemology*, **36**(2), 98-109
- Waychunas, G.A., 1998. Luminescence, X-ray emission and new spectroscopies. In: *Spectroscopic methods in mineralogy and geology*. F.C. Hawthorne (Ed.). *Reviews in Mineralogy*, **18**. Mineralogical Society of America, Washington
- Webster, R., 1994. *Gems: their sources, descriptions and identification*. 5th edn. rev. P.G. Read. Butterworth-Heinemann Ltd., Oxford

NEW from Gem-A Instruments

C-Master Gauge

A digital scale that calculates the weight of loose and set gemstones, including diamond, ruby, sapphire, emerald and alexandrite.

- **Easy to use**
- **Easy to read**
- **Ideal for valuers**

Price £250.00
plus VAT, postage and packing



Gem-A Instruments

27 Greville Street (Saffron Hill entrance), London EC1N 8TN
t: +44 (0)20 7404 3334 f: +44 (0)20 7404 8843 e: shop@gem-a.info

A **new** course from Gem-A, run in conjunction with Dianet

ROUGH DIAMOND ASSESSMENT COURSE

Wednesday 26 to Friday 28 October 2005
at the Gem-A London headquarters

This new three-day intensive course will cover the value factors needed for the assessment of rough diamonds, including sizing, model/shape, colour and quality, and rough to polished yields. There will be a résumé of diamond localities, mining and cutting, as well as information on simulants and testing tools used to identify them.

Price: £675 (including VAT)

All participants will receive a Gem-A diamond kit bag containing basic equipment.

For further details visit the Gem-A website at www.gem-a.info or call Claire on 020 7404 3334



The variation of RI with rotation of a doubly refractive gemstone on the refractometer hemicylinder

Xinhua Song, Ruihua Wu and Weizheng Wu

Beijing DiDa Gem Testing Centre, China University of Geosciences, 29 Xue Yuan Lu, Beijing, 100083, P.R. China

Abstract: *The hemicylinder refractometer is used to determine the refractive index (RI) of faceted anisotropic gemstones as a function of crystal orientation. The technique is difficult due to large errors in measurement and uncertainty in the orientation of facets. The theoretical variation is investigated using analytical geometry to generate comprehensive parametric graphs of RI variation. These graphs are analysed systematically, providing methods with reference examples for determining the optic character of anisotropic gemstones.*

Keywords: *analytical geometry, double refraction, indicatrix section, optic orientation, refractive index variation*

Introduction

The refractive indices of a doubly refractive gemstone with $RI < 1.8$ can be determined by placing it in the centre of a refractometer hemicylinder with contact fluid ($RI > 1.8$) and recording the RI readings as it is rotated (see Hurlbut and Kammerling, 1991, 102, Fig. 7.26). The technique may be used on uniaxial and biaxial crystals regardless of optic sign. Readings are taken approximately every 15° or 30° as the stone is rotated on the hemicylinder through 180° . A graph of RI variation for such a gemstone may be obtained by plotting all sets of readings on a two-dimensional right-angled coordinate system, in which the vertical axis is the value of RI and the horizontal axis is the degree of rotating angle. Because of limits on the accu-

racy of measurement and difficulty in identifying the facet orientation of a gemstone, it is difficult to work out comprehensive and accurate graphs of RI variation for doubly refractive gemstones. This study, a theoretical model of the practical operational procedures, generates systematic graphs of RI variation using the analytical geometry method (Figures 3 and 4). By analysing these graphs, we can improve the study of the variation of RI with rotation of a gemstone on the refractometer hemicylinder. The following sections fulfil two purposes: they explain the actual technique of performing such measurements, and also show how the analytical geometry equations are solved in order to generate parametric graphs.

The selections of initial orientation

The definition of the initial orientation

The initial orientation is the spatial relation between the gemstone's indicatrix and the surface of the refractometer hemicylinder; it is the position of the first measurement of RI before any rotation.

In order to indicate the orientation of a gemstone's indicatrix, we construct a three-dimensional right-angled system with Ox, Oy and Oz coordinates as follows (Figure 1):

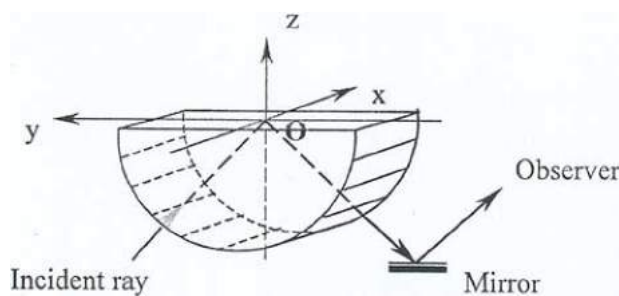


Figure 1: A schematic diagram to show the spatial relation of the coordinate system and the surface of the refractometer hemicylinder.

The coordinate plane xOy lies on the hemicylinder surface, and the following text relates to Figure 1. The origin O of the coordinates is located at the centre of the hemicylinder surface and represents the spot or position of total reflectance of the incident ray for angles

greater than the critical angle. The Ox -axis is perpendicular to the long side of the rectangular hemicylinder surface, and points to the right of the observer. The Oy -axis is parallel to the long side and points forward from the observer and to the left of the reader. The Oz -axis is vertical and points upward.

After the relationship between the $Oxyz$ coordinates and the refractometer hemicylinder has been established, the centre of the indicatrix of a gemstone placed on the refractometer can also be established to coincide with the origin of the $Oxyz$ coordinates. With this in place, the initial orientation for a uniaxial gemstone can be determined by two angular measures: one between the vibration direction of the extraordinary ray and the Oy -axis (Figure 2a), and the other between the plane $NeOy$ (containing the Ne -semiaxis of indicatrix and the Oy -axis), and the coordinate plane xOy . These measures are respectively expressed by the symbols $Ne^{\wedge}Oy$ and $NeOy^{\wedge}xOy$. The initial orientation for a biaxial gemstone is also determined by two angles. The first is between the vibration direction of the intermediate index (Nm) and the Oy -axis (Figure 2b), and the other is between the vibration direction of the greatest index (Ng) and the Oz -axis. These measures are respectively expressed by the symbols $Nm^{\wedge}Oy$ and $Ng^{\wedge}Oz$.

The selections of initial orientation

To illustrate the theory outlined in later sections, different initial orientations of a uniaxial gemstone have been selected and are

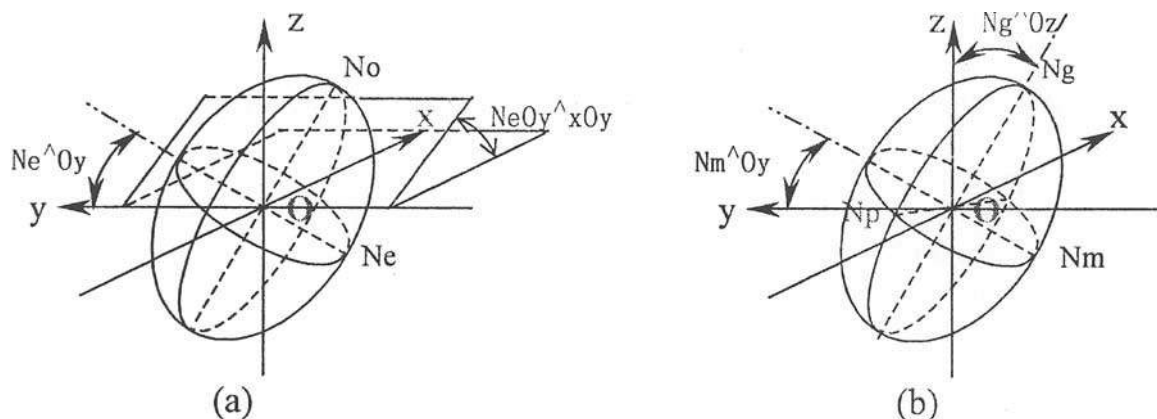


Figure 2: The relation of the indicatrix to the $Oxyz$ coordinates in the initial orientation ((a) represents a uniaxial and (b) a biaxial gemstone).

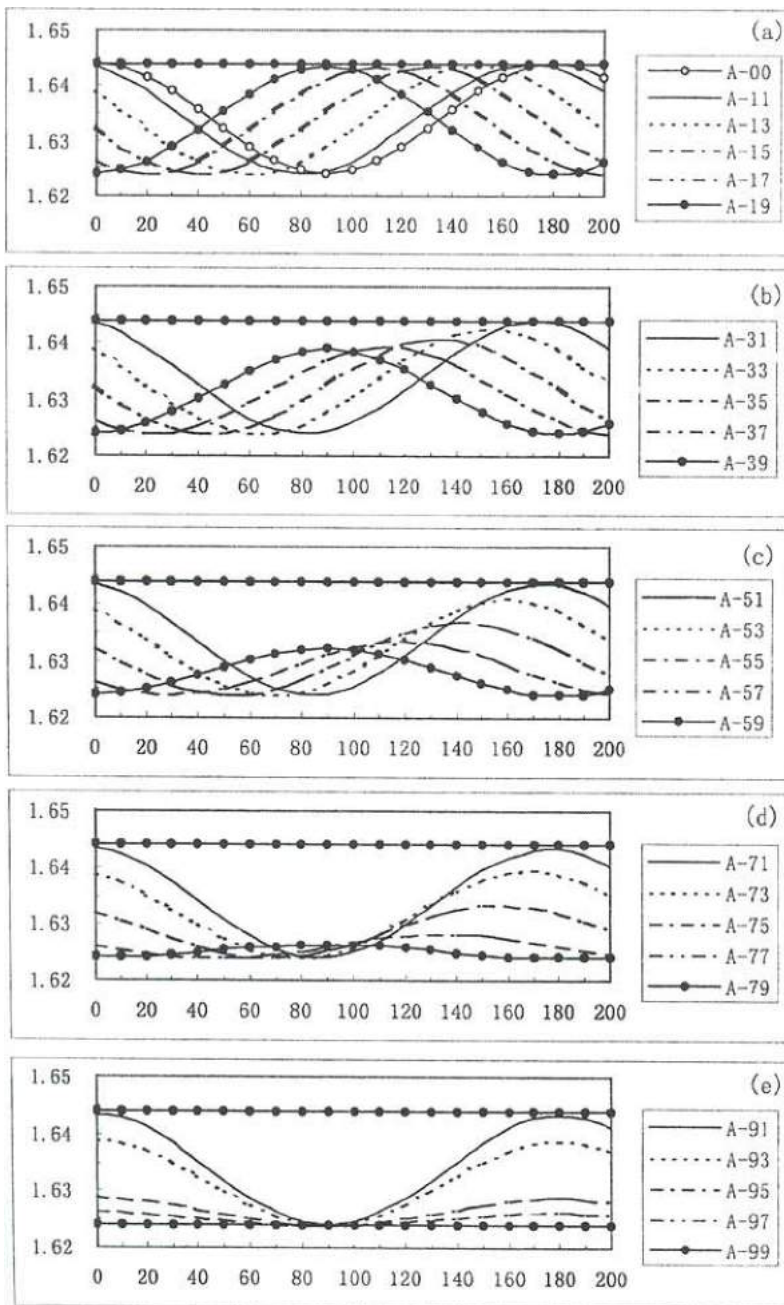
listed in Table I ; these relate to Figure 3. Similarly, Table II contains selections of initial orientation for biaxial gemstones and these relate to Figure 4.

On rotation on a refractometer, biaxial gemstones produce more complex graphs

than do uniaxial stones, so in this paper, more examples of different initial orientations of the former are listed and illustrated.

Figure 3: Graphs of RI variation of tourmaline as it is rotated on a refractometer hemicylinder. The vertical coordinate axis represents RI, and the horizontal axis represents the angle of rotation θ . Positions of initial orientation (A-00 etc.) are listed in Table I.

Table I: The selection of initial orientation for uniaxial gemstones.



Number	Ne°Oy	NeOy°xOy
A-00	00°	00°
A-11	10°	10°
A-13	30°	10°
A-15	50°	10°
A-17	70°	10°
A-19	90°	10°
A-31	10°	30°
A-33	30°	30°
A-35	50°	30°
A-37	70°	30°
A-39	90°	30°
A-51	10°	50°
A-53	30°	50°
A-55	50°	50°
A-57	70°	50°
A-59	90°	50°
A-71	10°	70°
A-73	30°	70°
A-75	50°	70°
A-77	70°	70°
A-79	90°	70°
A-91	10°	90°
A-93	30°	90°
A-95	50°	90°
A-97	70°	90°
A-99	90°	90°

Table II: The selection of initial orientation for biaxial gemstones.

Number	Nm°Oy	Ng°Oz									
B-00	00°	00°	B-25	50°	20°	B-50	00°	50°	B-75	50°	70°
B-01	10°	00°	B-26	60°	20°	B-51	10°	50°	B-76	60°	70°
B-02	20°	00°	B-27	70°	20°	B-52	20°	50°	B-77	70°	70°
B-03	30°	00°	B-28	80°	20°	B-53	30°	50°	B-78	80°	70°
B-04	40°	00°	B-29	90°	20°	B-54	40°	50°	B-79	90°	70°
B-05	50°	00°	B-30	00°	30°	B-55	50°	50°	B-80	00°	80°
B-06	60°	00°	B-31	10°	30°	B-56	60°	50°	B-81	10°	80°
B-07	70°	00°	B-32	20°	30°	B-57	70°	50°	B-82	20°	80°
B-08	80°	00°	B-33	30°	30°	B-58	80°	50°	B-83	30°	80°
B-09	90°	00°	B-34	40°	30°	B-59	90°	50°	B-84	40°	80°
B-10	00°	10°	B-35	50°	30°	B-60	00°	60°	B-85	50°	80°
B-11	10°	10°	B-36	60°	30°	B-61	10°	60°	B-86	60°	80°
B-12	20°	10°	B-37	70°	30°	B-62	20°	60°	B-87	70°	80°
B-13	30°	10°	B-38	80°	30°	B-63	30°	60°	B-88	80°	80°
B-14	40°	10°	B-39	90°	30°	B-64	40°	60°	B-89	90°	80°
B-15	50°	10°	B-40	00°	40°	B-65	50°	60°	B-90	00°	90°
B-16	60°	10°	B-41	10°	40°	B-66	60°	60°	B-91	10°	90°
B-17	70°	10°	B-42	20°	40°	B-67	70°	60°	B-92	20°	90°
B-18	80°	10°	B-43	30°	40°	B-68	80°	60°	B-93	30°	90°
B-19	90°	10°	B-44	40°	40°	B-69	90°	60°	B-94	40°	90°
B-20	00°	20°	B-45	50°	40°	B-70	00°	70°	B-95	50°	90°
B-21	10°	20°	B-46	60°	40°	B-71	10°	70°	B-96	60°	90°
B-22	20°	20°	B-47	70°	40°	B-72	20°	70°	B-97	70°	90°
B-23	30°	20°	B-48	80°	40°	B-73	30°	70°	B-98	80°	90°
B-24	40°	20°	B-49	90°	40°	B-74	40°	70°	B-99	90°	90°

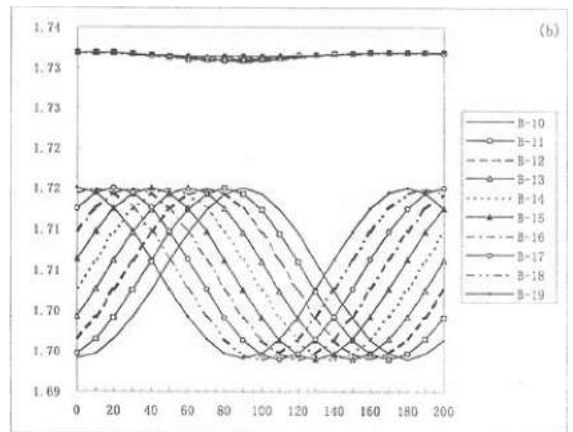
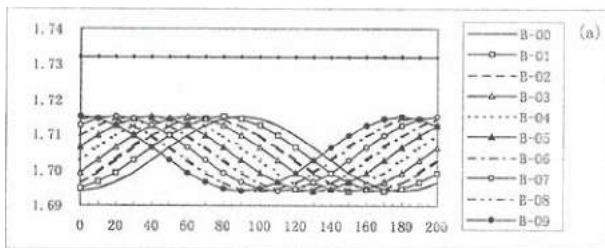
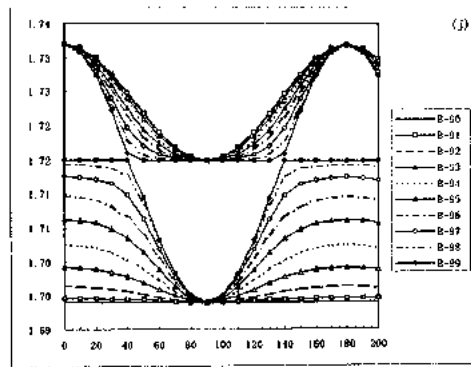
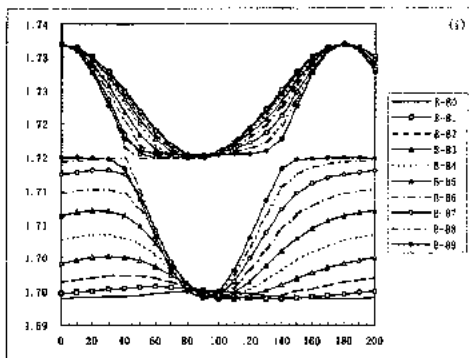
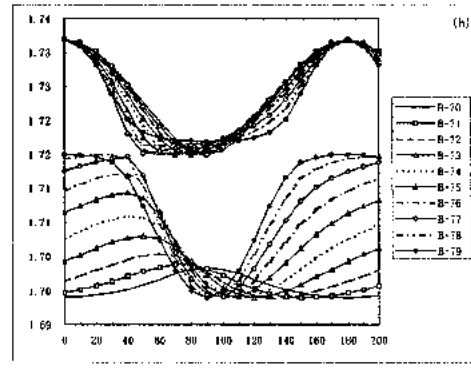
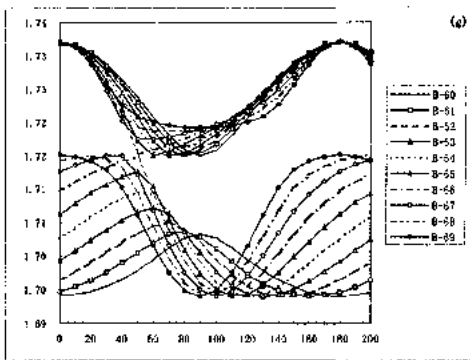
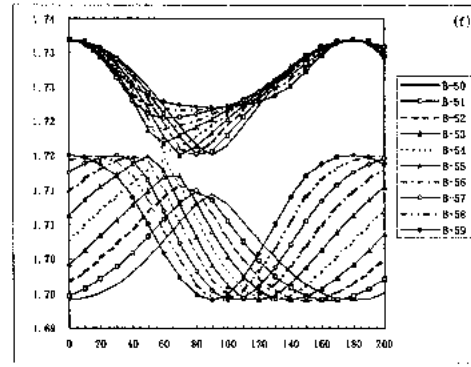
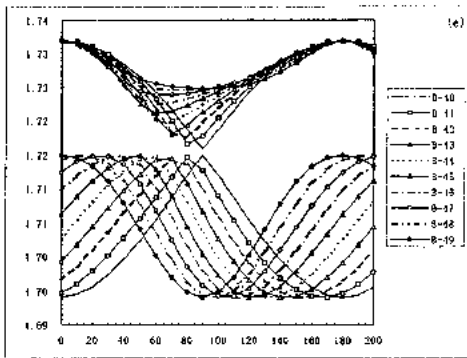
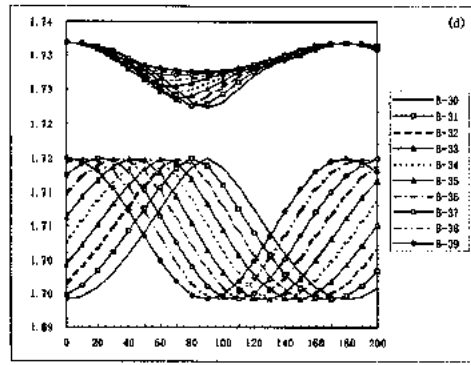
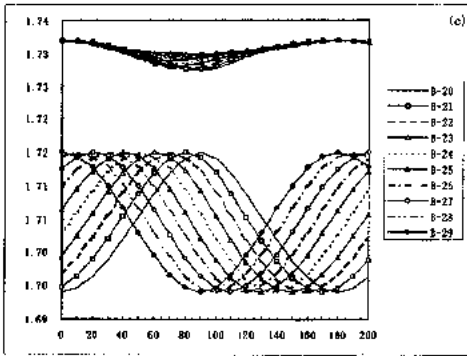


Figure 4: Graphs of RI variation of chrysolite as it is rotated on a refractometer hemicylinder. The vertical coordinate axis represents RI, and the horizontal axis represents the angle of rotation θ . Positions of initial orientation (B-00 etc.) are listed in Table II.



The variation of RI with rotation of a doubly refractive gemstone on the refractometer hemicylinder

Construction of the graphs of RI variation by rotation of the gemstone

Just as RI variation can be plotted from practical measurements after an initial orientation is given, the RI values can be calculated using analytical geometry, with the process repeated for increments of 10° rotation of the gemstone, from 0° up to 200° on the hemicylinder (for the mathematical details, see Appendix). The angle of rotation of the gemstone on the hemicylinder is represented by the symbol θ , which is the angle of rotation around the Oz-axis from the initial orientation to the orientation in which the stone is being tested. To complete the parametric graph of RI variation for an initial orientation, plot all sets of the refractive indices and angles on a two-dimensional right-angle coordinate system, with the abscissa being the angle of rotation θ and the ordinate, the RI value.

Parametric graphs of tourmaline's RI variation are given in Figure 3 as an example of a uniaxial crystal with negative optic sign. There are 26 parametric graphs corresponding with the initial orientations listed in Table I; 25 consist of five sets of five graphs representing five values of $\text{NeOy} \times \text{Oy} (\beta_0)$, and one exceptional case, the graph A-00 is plotted on Figure 3(a). For uniaxial crystals, the graph of RI variation for a positive crystal is the inverted image of that for a negative crystal in the same initial orientation, so this aspect of the investigation is complete.

Graphs of chrysolite's RI variation are listed in Figure 4 as examples of a biaxial crystal. These correspond with the 100 initial orientations listed in Table II and consist of 10 groups, each group of graphs having the same angle $\text{Ng} \wedge \text{Z} (\beta_0)$.

Discussion

Each graph obtained from a uniaxial negative crystal consists of two lines (see Figure 3): one is a straight line (i.e. the RI remains stationary) resulting from the ordinary ray and

the other usually is a waveform curve resulting from the extraordinary ray (denoted by Ne' , as opposed to Ne which is restricted to the one value furthest from No). They respectively represent the constancy of the RI No and the variation of Ne' as the stone is rotated on the hemicylinder. For the graphs of random initial orientations (i.e. the A-00 and A-99 graphs are excepted), the distance between the straight line No and the curve Ne' increases as the angle $\text{Ne} \wedge \text{Oy}$ increases, with the angle $\text{NeOy} \times \text{Oy}$ unchanged. Similarly, this distance increases as the angle $\text{NeOy} \times \text{Oy}$ increases, with the angle $\text{Ne} \wedge \text{Oy}$ unchanged. In a special initial orientation with the angles $\text{Ne} \wedge \text{Oy} = 90^\circ$ and $\text{NeOy} \times \text{Oy} = 90^\circ$ (i.e. the plane of vibration of Ne is vertical), both lines are straight in this graph (see A-99 in Figure 3(e)), and the higher and lower RIs respectively express the values No and Ne (the crystal is optically negative).

The graphs of a biaxial gemstone in initial orientations usually consist of two curves (see Figure 4). They respectively represent the variations of the RI Ng' and the RI Np' curves as the gemstone is rotated on the hemicylinder. For chrysolite, when the angle $\text{Ng} \wedge \text{Oz}$ is less than 40° ($\text{Ng} \wedge \text{Oz} = 0$ is excepted), the minimum of the curve Ng' rises as the angle $\text{Nm} \wedge \text{Oy}$ increases (angle $\text{Ng} \wedge \text{Oz}$ unchanged), and the minimum falls as the angle $\text{Ng} \wedge \text{Oz}$ increases (angle $\text{Nm} \wedge \text{Oy}$ unchanged). When the angle $\text{Ng} \wedge \text{Oz}$ is more than 40° , the relation between the distance of the two curves and the angle $\text{Nm} \wedge \text{Oy}$ or $\text{Ng} \wedge \text{Oz}$ is more complex than when the angle is less than 40° . Under special initial orientations, such as the angle $\text{Ng} \wedge \text{Oz} = 0^\circ$ and $\text{Nm} \wedge \text{Oy} = 0^\circ$ to 90° (i.e. the vibration plane of Ng is vertical), all parametric graphs have a straight line showing the refractive index Ng , and have similar curves (only their phase angles vary) showing the variations Np' for different angles $\text{Nm} \wedge \text{Oy}$ (see graphs B-00 to B-09 in Figure 4 (a)). Also in the special initial orientation $\text{Nm} \wedge \text{Oy} = 0^\circ$ and $\text{Ng} \wedge \text{Oz} = 90^\circ$ (i.e. the vibration plane Np is vertical), one line is straight showing the refractive index Np , the other is a curve showing the variation of Ng' (see B-90 in Figure 4 (j)). Again, in the case of

the angle $Nm^{\wedge}Oy=90^{\circ}$ and $Ng^{\wedge}Oz=90^{\circ}$ (i.e. the vibration plane of Nm is vertical), a straight line represents the refractive index Nm and the curve represents the variation of Ng' or Np' (see B-99 in Figure 4 (j)). A straight line on a plot for a biaxial gemstone can appear only with an initial orientation whereby one of the vibration planes of the three principal refractive indices is vertical.

Generally, the curve of RI variation of a doubly refractive gemstone is undulant with a period of 180° . In the RI variational graph of uniaxial gemstones, the curve Ne' looks like a sine wave. Both the ascending and descending segments have the same gradient and length. In other words, the waveform of the curve Ne' is symmetrical about the vertical line through the wave peak or wave trough. The principal refractive index Ne for uniaxial crystals is found from the highest points of the curve Ne' of optically positive crystals or from the lowest point of optically negative crystals. Unlike uniaxial crystals, the curves Ng' or Np' of a biaxial gemstone in random orientation are not symmetrical about any vertical line. The gradient and length of an ascending segment are different from those of the descending segment. This results from the inequality of the three principal axes in the biaxial indicatrix. The principal refractive indices, Ng and Np in biaxial crystals, are respectively found from the highest point of the curve Ng' and from the lowest point of the curve Np' .

The Nm value can be obtained only if one of the following three cases has occurred. Firstly the graph has been constructed using a special initial orientation (i.e. one of the vibration directions of the three principal indices is vertical). For instance, when the vibration of Ng is vertical, the value Nm is the maximum of the curve Np' (see B-00 to B-09 in Figure 4(a)). And when the vibration of Np is vertical, the value Nm is the minimum of the curve Ng' (B-90 in Figure 4(j)). When the vibration of Nm is vertical, the value Nm is expressed by the stationary RI in the graph (B-99 in Figure 4 (j)). Secondly the curves Ng' and Np' have a conjunct point. This point

indicates the value of Nm. For example, the RI variational graphs of chrysolite have this point in the initial orientation about $Nm^{\wedge}Oy = 60^{\circ}$ and $Ng^{\wedge}Oz = 60^{\circ}$ (B-66 in Figure 4 (g)). In the third case, the Nm is determined using two graphs: the maximum of the curve Np' from one graph should coincide with the minimum of the curve Ng' from another graph and indicate the value of Nm. Although it may be more difficult to obtain the value Nm than Ng or Np in practical measurement, the optic sign of a biaxial gemstone can be determined if the minimum of the curve Ng' is lower than the middle value between Ng and Np, or the maximum of the curve Np' is higher than the middle value (Read, 1990, p.98).

Conclusions

Parametric RI curves relative to rotations on a hemicylinder have been calculated for uniaxial and biaxial gemstones, and these have been used to illustrate the principles and problems associated with the practical technique of determining the refractive indices of gemstones. The curves can be used to guide smoothing of actual measurements, and improve procedures and accuracy of RI determinations. The complexities indicate how essential it is to try and orient at least one axis of the indicatrix parallel to the normal of the hemicylinder surface.

Acknowledgements

We thank Dr Barron Larry, Geological Survey of Australia, and Dr Joe Xie, Department of Mineral Resources of Australia, very much for their helpful suggestions and advice concerning the paper.

Appendix

The analytical geometry method used to produce graphs of RI variation

The definition of the basic orientation and the spherical surface equations of the indicatrix.
In this paper, the **basic orientation** is estab-

lished so that the vibration direction of the principal index N_e coincides with the Oy -axis of the $Oxyz$ coordinates for uniaxial crystals. The vibration directions of the principal indices N_p , N_m and N_g of biaxial crystals coincide respectively with the Ox -axis, Oy -axis and Oz -axis. The equations for the spherical surfaces of a uniaxial indicatrix (eq.1) and of a biaxial indicatrix (eq.2) respectively are:

$$x^2 / N_o^2 + y^2 / N_e^2 + z^2 / N_o^2 = 1 \quad (1)$$

$$x^2 / N_p^2 + y^2 / N_m^2 + z^2 / N_g^2 = 1 \quad (2)$$

The initial orientation and the spherical surface equation of the indicatrix

The definition of **initial orientation** is the same as that given in the text.

Initial orientations can be obtained from the basic orientation by the following means. First, rotate the gemstone's indicatrix clockwise by an angle θ_o on the coordinate plane xOy (i.e. round the Oz -axis). Then rotate the indicatrix clockwise by an angle β_o on the plane xOz (i.e. round the Oy -axis). For this case, the initial orientation of the gemstone is indicated by the pair of angles θ_o and β_o . This operation of clockwise rotation of the indicatrix is the same as the counter-clockwise rotations of the coordinates xOy and xOz in order by the angles θ_o and β_o . Note that the angle θ_o is the same as $N_e \hat{O}y$ for uniaxial and $N_m \hat{O}y$ for biaxial gemstones, whereas the angle β_o is same as $N_e \hat{O}y \hat{x}Oy$ for uniaxial and $N_g \hat{O}z$ for biaxial gemstones (see Table I and Table II).

The position of a general point P on the surface of a gemstone's indicatrix, is identified by three coordinates (x,y,z) in the basic orientation. The coordinates of the same point have been changed after the rotation of the indicatrix by θ_o and β_o (here $\theta_o \neq 0$ and $\beta_o \neq 0$). If the point P in the initial orientation θ_o and β_o is identified by the coordinates (x_i, y_i, z_i) , the following set of equations can express the relationship of the coordinates (x,y,z) to the coordinates (x_i, y_i, z_i) .

$$\begin{aligned} x &= x_i \cos \theta_o \cos \beta_o - y_i \sin \theta_o - z_i \cos \theta_o \sin \beta_o \\ y &= x_i \sin \theta_o \cos \beta_o + y_i \cos \theta_o - z_i \sin \theta_o \sin \beta_o \\ z &= x_i \sin \beta_o + z_i \cos \beta_o \end{aligned} \quad (3)$$

Substituting in equations (1) and (2), the spherical surface equation of the uniaxial indicatrix becomes equation (4), and for the biaxial indicatrix it becomes equation (5):

$$[(x_i \cos \theta_o \cos \beta_o - y_i \sin \theta_o - z_i \cos \theta_o \sin \beta_o)^2 + (x_i \sin \beta_o + z_i \cos \beta_o)^2] / N_o^2 + (x_i \sin \theta_o \cos \beta_o + y_i \cos \theta_o - z_i \sin \theta_o \sin \beta_o)^2 / N_e^2 = 1 \quad (4)$$

$$(x_i \cos \theta_o \cos \beta_o - y_i \sin \theta_o - z_i \cos \theta_o \sin \beta_o)^2 / N_p^2 + (x_i \sin \theta_o \cos \beta_o + y_i \cos \theta_o - z_i \sin \theta_o \sin \beta_o)^2 / N_m^2 + (x_i \sin \beta_o + z_i \cos \beta_o)^2 / N_g^2 = 1 \quad (5)$$

The elliptic equation of the indicatrix section on the xOz plane after rotation by an angle θ

Like the procedure used in practical measurement to generate RI values, after the initial orientation (θ_o, β_o) is given and the first RI values have been calculated, this procedure is continued as the gemstone's indicatrix is rotated in 10° increments on the xOy plane through to 200° .

As the indicatrix is rotated by an angle θ from the initial orientation (θ_o, β_o) , the coordinates of the point P also change. If the coordinates of the point P in this orientation are expressed by (x_r, y_r, z_r) , a set of three equations (Eq. (6)) can represent the relationship of (x, y, z) to (x_r, y_r, z_r) .

$$x = (x_r \cos \theta - y_r \sin \theta) \cos \theta_o \cos \beta_o - (x_r \sin \theta + y_r \cos \theta) \sin \theta_o - z_r \cos \theta_o \sin \beta_o$$

$$y = (x_r \cos \theta - y_r \sin \theta) \sin \theta_o \cos \beta_o + (x_r \sin \theta + y_r \cos \theta) \cos \theta_o - z_r \sin \theta_o \sin \beta_o$$

$$z = (x_r \cos \theta - y_r \sin \theta) \sin \beta_o + z_r \cos \beta_o \quad (6)$$

In terms of optic principles and the defined basic orientation, as a beam of light passes from the hemicylinder into a gemstone the ray is refracted away from the normal. When the angle of incidence is at the critical angle, the refracted ray moves in the direction opposite to that of the Oy -axis as it is in Figure 1 on the gemstone's surface, and its vibration direction is parallel to the coordinate plane xOz . This means that the gemstone's indicatrix section relative to this light lies on the plane xOz , and its elliptic equation can be obtained from the spherical surface

equation of the indicatrix by constraining $y_r = 0$. In this situation, the elliptic equation for the uniaxial indicatrix section is expressed as:

$$E_u z_r^2 + F_u x_r z_r + G_u x_r^2 = 1 \quad (7)$$

where:

$$E_u = [(\cos^2 \beta_o + \cos^2 \theta_o \sin^2 \beta_o) / No^2 + \sin^2 \theta_o \sin^2 \beta_o / Ne^2]$$

$$F_u = 2 \{(\cos \theta \sin \beta_o \cos \beta_o - (\cos \theta \cos \theta_o \cos \beta_o - \sin \theta \sin \theta_o) \cos \theta_o \sin \beta_o) / No^2 - (\cos \theta \sin \theta_o \cos \beta_o + \sin \theta \cos \theta_o) \sin \theta_o \sin \beta_o / Ne^2\}$$

$$G_u = [(\cos^2 \theta \sin^2 \beta_o + (\cos \theta \cos \theta_o \cos \beta_o - \sin \theta \sin \theta_o)^2) / No^2 + (\cos \theta \sin \theta_o \cos \beta_o + \sin \theta \cos \theta_o)^2 / Ne^2]$$

For the biaxial indicatrix, the elliptic equations are:

$$E_b z_r^2 + F_b x_r z_r + G_b x_r^2 = 1 \quad (8)$$

where:

$$E_b = [\cos^2 \beta_o / Ng^2 + \sin^2 \theta_o \sin^2 \beta_o / Nm^2 + \cos^2 \theta_o \sin^2 \beta_o / Np^2]$$

$$F_b = 2 [\cos \theta \sin \beta_o \cos \beta_o / Ng^2 - (\cos \theta \sin \theta_o \cos \beta_o + \sin \theta \cos \theta_o) \sin \theta_o \sin \beta_o / Nm^2 - (\cos \theta \cos \theta_o \cos \beta_o - \sin \theta \sin \theta_o) \cos \theta_o \sin \beta_o / Np^2]$$

$$G_b = [\cos^2 \theta \sin^2 \beta_o / Ng^2 + (\cos \theta \sin \theta_o \cos \beta_o + \sin \theta \cos \theta_o)^2 / Nm^2 + (\cos \theta \cos \theta_o \cos \beta_o - \sin \theta \sin \theta_o)^2 / Np^2]$$

Production of the graph of RI variation

Tourmaline is used as the example for a uniaxial gemstone, and the graph of its RI variation is produced as follows:

The initial orientation is given as $\theta_o = 30^\circ$, $\beta_o = 70^\circ$. After the stone is rotated by an angle $\theta = 50^\circ$, the coefficients E_u , F_u and G_u of equation (Eq. (7)) can be calculated. The result is $E_u = 0.37202$, $F_u = -0.00666$ and $G_u = 0.37548$, generating the ellipse:

$$0.37202z_r^2 - 0.00666x_r z_r + 0.37548x_r^2 = 1. \quad (9)$$

On this ellipse, an adequate number of points at regular intervals are chosen, expressed by p_k ($k = 1, 2, 3, \dots, n$). For each point p_k denoted by the coordinate pair (x_k, z_k) , the values of the x_k and z_k must be derived from equations (9), for example by picking k values of x , and calculating k values of z .

The distance from point p_k to the centre of the ellipse (i.e. the origin of the Oxyz coordinates) is a radius of the ellipse, it can be obtained by equation $Op_k = [(x_k^2 + z_k^2)^{1/2}]$.

Distances from every point on the ellipse to the centre are calculated and then the longest and the shortest radius can be found. The two radii equal the two refractive indices of the stone in the orientation $\theta_o = 30^\circ$, $\beta_o = 70^\circ$, $\theta = 50^\circ$. The sample calculations result respectively in $No = 1.6440$ and $Ne' = 1.6276$.

Still under the initial orientation of $\theta_o = 30^\circ$, $\beta_o = 70^\circ$, by exchanging the rotation angle θ

Table III: The RI variation of tourmaline with an initial orientation of $\theta_o = 30^\circ$, $\beta_o = 70^\circ$.

Angle θ	00°	10°	20°	30°	40°	50°	60°
No	1.6440	1.6440	1.6440	1.6440	1.6440	1.6440	1.6440
Ne'	1.6389	1.6375	1.6353	1.6327	1.6301	1.6276	1.6256
Angle θ	70°	80°	90°	100°	110°	120°	130°
No	1.6440	1.6440	1.6440	1.6440	1.6440	1.6440	1.6440
Ne'	1.6244	1.6240	1.6246	1.6260	1.6281	1.6307	1.6334
Angle θ	140°	150°	160°	170°	180°	190°	200°
No	1.6440	1.6440	1.6440	1.6440	1.6440	1.6440	1.6440
Ne'	1.6359	1.6379	1.6392	1.6395	1.6389	1.6375	1.6353

and repeating the preceding operations, another pair of refractive indices can be obtained. By this means, all 21 pairs of RI can be calculated using the angles $\theta = 0^\circ, 10^\circ, 20^\circ, 30^\circ \dots \dots 200^\circ$. The calculated data for the graph of RI variation of tourmaline under the initial orientation of $\theta_0 = 30^\circ, \beta_0 = 70^\circ$ are listed in *Table III*. The relevant graph is A-73 in *Figure 3(d)*.

In order to obtain other graphs with various initial orientations, start with various angle pairs θ_0 and β_0 (see *Table I*) and then calculate each longest and the shortest radius of the indicatrix section under every orientation θ, β_0 and angle θ . Using this procedure, all the graphs of RI variation of tourmaline can be determined.

For a biaxial gemstone, a similar procedure for calculating the graphs of RI variation can be carried out using equation (8).

References

- Hurlbut, Jr., C.S., and Kammerling, R.C., 1991. *Gemology*, 2nd Ed. Wiley, New York. 336 pp
Read P.G., 1990. *Gemmology*. Butterworth-Heinemann Ltd., Oxford. 326 pp

Use of the polarizing filter on the refractometer

B. Darko Sturman

Curator Emeritus, Royal Ontario Museum, Canada

Abstract: *Use of the refractometer is summarized and a new comprehensive method to obtain reliable refractive indices is described. A single table contains all possible combinations of RI data and should be kept with the gemmological refractometer for practical use by both beginners and expert gemmologists.*

Introduction

The refractometer is one of the most used instruments in gemmology. Unfortunately, very few gemmologists feel confident that they can properly interpret all of the data that can be observed. Most can accurately measure the range of refractive indices (RIs) but few can differentiate between uniaxial or biaxial (in special orientation) or determine the optic sign from observations on the shadow edges.

It is not because they were not willing to invest their time and effort. Interpretation of the observations on the refractometer is a part of many gemmology courses. The problem lies in the instructions for use of the refractometer – they are complex and are often difficult to understand. Many students learn just enough to pass an examination and later they do not apply the method fully in practice. In many practical identifications, determination of the range of the RIs is all that is needed. In some cases, however, proper interpretation of the observed data can save time and the cost of an additional test.

Previous methods

One of the best descriptions of the use of the refractometer is, also, one of the oldest.

At the beginning of the 20th century Herbert Smith developed a modern refractometer. An excellent description of the use of the polarizing filter is found in Smith (1972). This method requires a good understanding of optical mineralogy theory and use of the indicatrix. At Smith's time many gemmologists were also excellent optical mineralogists and could easily follow his instructions.

Later, in the second half of the 20th century, gemmologists became more and more involved in the detection of synthetic materials and various enhancement or alteration processes. The techniques used did not require such a sound understanding of optical mineralogy theory. Consequently, some attempts to simplify refractometer use have produced complex, confusing and sometimes simply wrong instructions.

Present practice

It is very difficult to evaluate the present teaching of refractometer use. Many schools or institutions have their own course manuals (notes) and do not rely exclusively on the text books. The level of instruction varies a great deal.

Table 1: Optical properties which can be determined on the refractometer.

	Isotropic	Anisotropic			
		Uniaxial		Biaxial	
Crystal system	amorphous and cubic	tetragonal and hexagonal		orthorhombic, monoclinic and triclinic	
RIs	N	N_o N_e		N_z N_y N_x	
Optic sign		Positive $N_e > N_o$	Negative $N_o > N_e$	Positive N_y closer to N_x	Negative N_y closer to N_z
Optical angle				$2V_z = 0 - 90^\circ$	$2V_x = 0 - 90^\circ$
Maximum birefringence		$N_e - N_o$	$N_o - N_e$	$N_z - N_x$	

NB: Other symbols used include:

Uniaxial gems = $N_o = \omega$, $N_e = \epsilon$; lower case n is also used.

Biaxial gems = $N_x = \alpha$, $N_y = \beta$, $N_z = \gamma$; $2V_z = 2V(+)$, $2V_x = 2V(-)$.

In fact, the only safe statement that can be made is that the use of the polarizing filter is a minor (and difficult) part of many courses and rarely used later. This should not be so. A new approach to the teaching of refractometer use is proposed whereby a student, a jeweller or an experienced gemmologist can become familiar with the new method in about an hour. This new graphical approach does not require an extensive background in optical mineralogy and very little needs to be memorized. All that is required for the practical use of the refractometer is presented in a single table.

With mastery of this procedure, a lot of time and effort can be saved, leaving more time for the ever increasing number of new methods needed for the identification of enhancements and alteration processes. Most of all, the confidence that they can use this basic instrument to its fullest, stays with gemmologists or jewellers for life.

New approach

The new approach comprises graphical presentation and step-by-step instructions in

a single table. Every new method combines old and new ideas and experiences. Here, diagrams similar to those in Hurlbut and Kammerling (1991) are used in order to describe six basic patterns. However, the vertical scale is reversed so that it corresponds to the image seen in the refractometer (the highest value is at the bottom) as is shown in the diagrams by Read (1999).

The new approach is characterized by the following features:

1. There is no recording of the rotation angles and corresponding RIs, or plotting of this information on diagrams.
2. All possible combinations of optical data and the orientation of the gem table are presented in six patterns and the interpretation of each pattern is described separately.
3. A single table describes step-by-step interpretation of the observed data. Nothing needs to be memorized. A table kept next to the refractometer is all that is needed (the table is downloadable from the Gem-A website at www.gem-a.info).
4. The use of an optic angle diagram for biaxial gemstones makes determination of the optic sign very simple.

Review of optical properties determined on a refractometer

All of the optical properties that can be determined on a gemmological refractometer are listed in *Table I*. The term 'gemstone' in this context includes minerals and synthetic materials.

Isotropic gemstones

Isotropic gemstones crystallize in the cubic system or are amorphous (e.g. opal, glass). They show the same refractive index (RI) regardless of the direction of light rays moving through them. This produces a single and constant shadow edge during the rotation of the gemstone on the refractometer (*Table II*, Pattern I).

Anisotropic gemstones

In general, a light ray entering an anisotropic gemstone is divided into two rays that:

1. move at different speeds and have different RIs (birefringence);
2. are polarized and have vibration directions perpendicular to each other;
3. may have different absorption – resulting in different colours for each ray (pleochroism);
4. may move in slightly different directions – resulting in the doubling of images.

It is important to remember that there are exceptions to the above and when, for example, the light moves in special directions (called optic axes), it continues as a single ray.

The rotation of an anisotropic gemstone on the refractometer can bring it into a position where the light rays are moving in the direction of an optic axis. In this case, a single shadow edge is observed as in isotropic gemstones. However, further rotation brings into view two shadow edges – representing RIs of the two rays. This allows for the easy distinction between anisotropic and isotropic gemstones.

Anisotropic gemstones can have either one or two optic axes and on this basis are divided into two groups: uniaxial and biaxial.

Anisotropic uniaxial gemstones have one

optic axis and crystallize in either the tetragonal or hexagonal crystal systems. One ray – called the ordinary ray – has a constant RI regardless of the direction of light through the gemstone and is designated N_o . During rotation of a uniaxial gemstone, one shadow edge remains constant, indicating the constant RI (N_o) of the ordinary ray.

In most orientations of a gem, the other shadow edge – representing the extraordinary ray – varies during the rotation. We refer to this shadow edge as variable and it is designated N_e . Uniaxial gemstones are characterized by two principal RIs N_o and N_e .

During the rotation, the variable shadow edge can show any RI - N_e' – between the two extremes of N_o and N_e . Patterns II, III and IV in *Table II* show the range of relationships between the shadow edges representing ordinary and extraordinary rays.

The RI of the ordinary ray (N_o) is read on the constant shadow edge. The RI of the extraordinary ray (N_e) is read on the variable shadow edge in the position where the constant and variable shadow edges are at maximum separation.

Two special cases (shown in patterns II and III) are more common than one might think, because many uniaxial gem crystals have prominent faces perpendicular or parallel to the optic axis. The table facet of a zircon is commonly cut perpendicular to the optic axis, while that of a tourmaline is commonly parallel – producing these special patterns II and III.

Anisotropic biaxial gemstones have two optic axes and crystallize in either the orthorhombic, monoclinic or triclinic crystal systems. They are defined by three principal RIs and three principal vibration directions, Z, Y and X. N_x is the smallest RI and is observed when light vibrates parallel to the principal vibration direction X, N_y is the intermediate RI for light vibrating parallel to the principal vibration direction Y, and N_z is the largest RI for light vibrating parallel to the principal vibration direction Z. It is important to note that N_y can be any value between N_z and N_x – generally it is not exactly halfway between the two.

RIs of the two rays formed in biaxial gemstones depend on the direction of light

through a gemstone. In general, when a biaxial gemstone is rotated on a refractometer, two variable shadow edges are observed (pattern VI). One ray has RI (N_x') that varies between N_x and N_y , and the other ray's index (N_z') varies between N_y and N_z . On rotation on the refractometer, the direction of light in the gemstone changes and so do the RIs (N_z' and N_x') of the two rays.

Special orientations of the optical elements and the gem table – when any of the principal vibration directions Z, Y and X is perpendicular to the gem table – are characterized by one constant and one variable shadow edge (patterns IV and V). As in uniaxial gemstones, these special orientations can be fairly common, because the principal vibration directions Z, Y and X are often perpendicular to the prominent faces chosen and fashioned as the table facet.

Determination of the optic sign

The optic sign depends on the relationship between the principal RIs (N_o/N_e and $N_z/N_y/N_x$). In order to avoid complex descriptions of the behaviour of the shadow edges during the rotation of a gemstone - in this method, the principal RIs are determined first and then two simple rules are used to identify the optic sign.

Uniaxial gemstones: The optic sign of an anisotropic uniaxial gemstone is

Positive if $N_o < N_e$

Negative if $N_o > N_e$

Biaxial gemstones: The optic sign of an anisotropic biaxial gemstone is

Positive if N_y is closer to N_x

Negative if N_y is closer to N_z

The optic sign and angle between the optic axes depends on the three principal RIs ($N_z/N_y/N_x$) and can be found using the Optic Angle Diagram in Figure 1. The use of the diagram is shown in the following example illustrated in Figure 2.

First, the three RIs of a gemstone were determined as:

$$N_z = 1.625$$

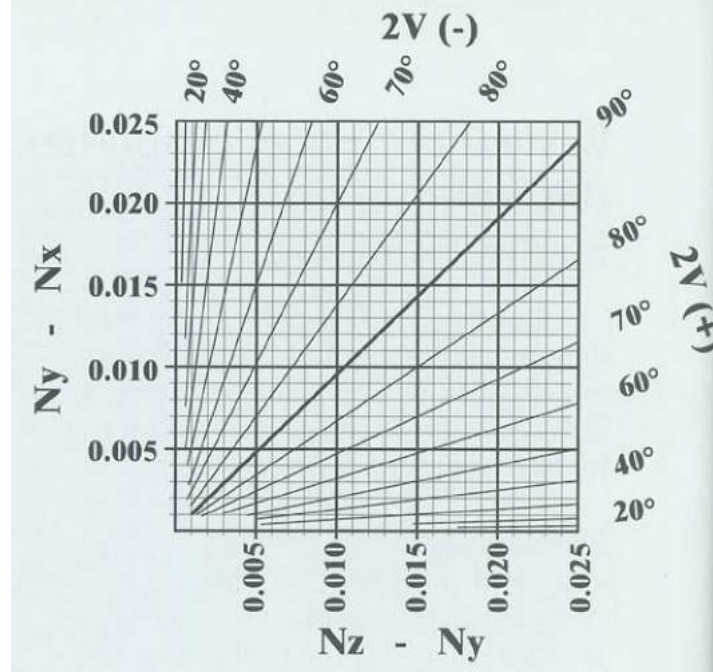


Figure 1: Diagram for determination of the optic sign and the optic angle of anisotropic biaxial gemstones.

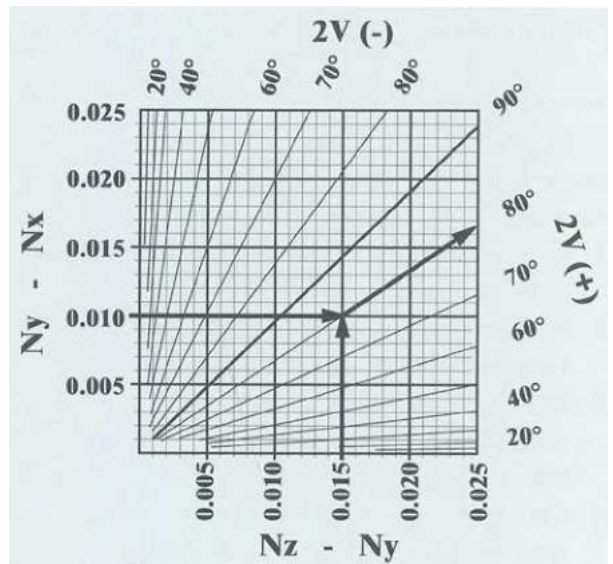


Figure 2: The optic angle diagram showing values plotted for $N_y - N_x$ and $N_z - N_y$ as discussed in the text.

$$N_y = 1.610$$

$$N_x = 1.600$$

Second, $N_z - N_y$ and $N_y - N_x$ were calculated as:

$$N_z - N_y = 0.015$$

$$N_y - N_x = 0.010$$

Third, these values were plotted on the Optic Angle Diagram and indicate that the gemstone is biaxial - positive with a 2V angle about 80°.

The Optic Angle Diagram can also be used to show how errors in the observed RIs can

have a significant bearing on determination of the optic sign.

The use of Table II

The determination of the optical properties of a gemstone on the refractometer is divided into several stages in this new approach. *Table II* summarizes the patterns obtainable from a refractometer, indicates which patterns yield further information with use of a polarizing filter, gives step-by-step instructions on how to obtain this information, and indicates the relevant orientation of the gem under measurement.

There are six possible pattern types, represented in six rows in *Table II*. The **Initial observation** column (column 2) charts the patterns of shadow edges obtainable if one rotates the gemstones through 180°. At this stage, the polarizing filter is not used.

For patterns I and II, the shadow edges are constant and the orientation of the gem when rotation is started is not significant, but for patterns III, IV and V, 0° on the pattern diagram indicates the point of maximum separation of the shadow edges. Pattern VI starts where the largest RI (N_z) is observed.

Patterns I, III and V yield the maximum optical information obtainable from the refractometer but patterns II, IV or VI, require detailed observations.

Detailed observation is done with the polarizing filter set into one of the two positions (north-south or east-west). The gemstone is first rotated to the position indicated by a red dot in *Table II* and the polarizing filter is set on the eye-piece. Identification is then based on the disappearance of a particular shadow edge.

A polarizing filter is supplied with most modern refractometers. Its vibration direction is indicated by a dot. If this dot is erased, a very simple procedure can be used to accurately determine the filter's vibration direction. A quartz crystal (with enough faces to indicate the crystallographic axis c) is set in the horizontal position on the refractometer table. The crystal is rotated in the position where the c -axis is perpendicular to the long

axis of the refractometer. Two shadow edges are observed. The one with the RI of 1.544 represents the ordinary ray with its vibration direction being north-south. The polarizing filter is set on the eye-piece and rotated until this shadow edge ($N = 1.544$) disappears. The vibration direction of the polarizing filter is now exactly east-west (parallel to the refractometer table) and this direction should be marked on the polarizing filter. This test can be done with any uniaxial crystal where the c -axis and the shadow edge representing the ordinary ray can be identified.

Isotropic gemstones produce *pattern I* and this is characterized by a single shadow edge that stays constant during rotation. The rotation test is very important because, in particular positions, anisotropic gemstones can also show a single shadow edge (see patterns III and V).

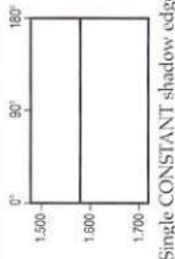
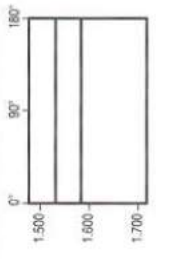
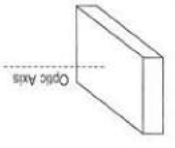
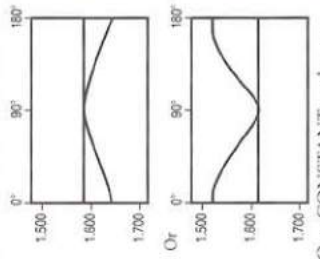
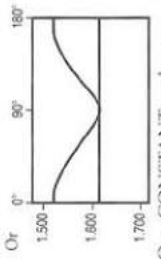
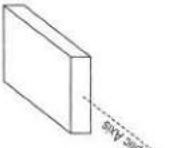
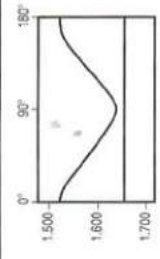
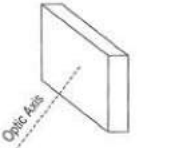
Pattern II is a special case of a uniaxial gemstone where the optic axis is perpendicular to the gem table. The two shadow edges representing ordinary and extraordinary rays stay constant during rotation of the gem. The polarizing filter is used to identify the ordinary and extraordinary ray shadow edges in *Table II*.

Pattern III is the other special case where the optic axis of a uniaxial gemstone is parallel to the gem table. It is characterized by the variable shadow edge touching the constant shadow edge at one position during the rotation. The polarizing filter is not needed for determination of the optic sign. Read N_o on the constant shadow edge and read N_e on the variable shadow edge in the position where the two shadow edges are at maximum separation.

Pattern IV can be generated by both uniaxial and biaxial gemstones. In both cases we observe one constant shadow edge and one variable shadow edge which do not touch at any position of the gem during rotation.

The polarizing filter is used to determine whether the gemstone producing this pattern is uniaxial or biaxial. With the filter set in the north-south position on the eye-piece, if the constant shadow edge disappears the stone is

The use of the polarizing filter on the refractometer

PATTERN NUMBER	INITIAL OBSERVATION	POLARIZING FILTER	DETAILED OBSERVATION	ORIENTATION AND OPTICAL PROPERTIES	RESULTS
I	 <p>Single CONSTANT shadow edge</p>	Not used	<p>Detailed Observation not needed.</p> <p>Make sure that the SINGLE Shadow edge stays CONSTANT during the rotation of the gemstone.</p>	<p>Isotropic</p>	Record N
II	 <p>Two CONSTANT and PARALLEL shadow edges</p>	<p>Set in the North - South position</p> 	<p>1. Observation can be made in any position during the rotation of a gemstone.</p> <p>2. Insert the polarizing filter. (Shadow edge of the ordinary ray (N_o) disappears.)</p> <p>3. Read N_e on the shadow edge that stays visible.</p> <p>4. Remove the polarizing filter. Read N_o on the shadow edge that is now visible.</p>	<p>Uniaxial</p> <p>Optic axis is perpendicular to the gem table</p> 	<p>Record N_e, N_o</p> <p>Determine the optic sign</p> <p>Calculate the maximum birefringence</p>
III	 <p>Or</p>  <p>One CONSTANT and one VARIABLE shadow edge TOUCHING</p>	Not used	<p>Detailed Observation not needed.</p> <p>1. Read N_o on the constant shadow edge.</p> <p>2. Read N_e on the variable shadow edge when two shadow edges are separated the most. (as shown by the green dots).</p>	<p>Uniaxial</p> <p>Optic axis is parallel to the gem table</p> 	
IV	 <p>Or</p> 	<p>Set in the North - South position</p> 	<p>1. Rotate gemstone in the position indicated by the red dot (where shadow edges are the closest).</p> <p>2. Insert the polarizing filter</p> <p>CONSTANT shadow edge DISAPPEARS</p> <p>Observe which shadow edge disappears.</p>	<p>Uniaxial</p> <p>Random orientation</p> 	

The use of the polarizing filter on the refractometer

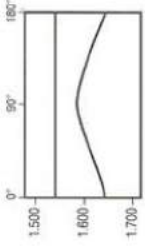
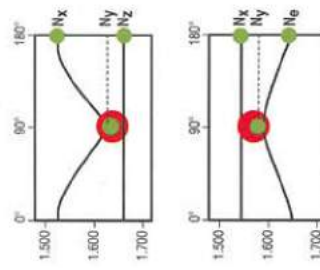
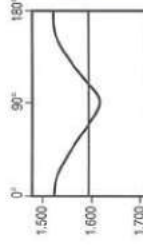
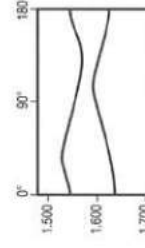
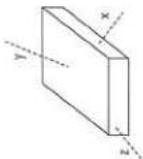
<p>IV</p>	 <p>One CONSTANT and one VARIABLE shadow edge NOT TOUCHING</p>	<p>Observe which shadow edge disappears.</p> <p>Identify gemstone as uniaxial or biaxial.</p> <p>3. Remove the polarizing filter. Read principal refractive indices in positions shown by green dots.</p>	 <p>Biaxial Z perpendicular to the gem table</p> <p>Biaxial X perpendicular to the gem table</p>	<p>Biaxial Z perpendicular to the gem table</p> <p>Biaxial X perpendicular to the gem table</p>	<p>Record N_z, N_y and N_x</p> <p>Calculate the maximum birefringence</p>
<p>V</p>	 <p>One CONSTANT and one VARIABLE shadow edge INTERSECTING</p>	<p>Not used</p>	<p>Detailed Observation not needed.</p> <p>Read N_z, N_y and N_x as indicated by green dots</p>	<p>Biaxial Y perpendicular to the gem table</p>	<p>Use 2V diagram to determine the</p> <ol style="list-style-type: none"> 1. optic sign 2. optic angle (2V)
<p>VI</p>	 <p>Two VARIABLE shadow edges NOT TOUCHING</p>	<p>Set in the East - West position</p> 	<p>N_z AND N_x ARE DETERMINED AS THE LARGEST AND THE SMALLEST REFRACTIVE INDEX OBSERVED DURING THE ROTATION.</p> <p>N_y CAN BE READ EITHER ON THE UPPER OR ON THE LOWER SHADOW EDGE</p> <p>Each shadow edge must be observed separately to determine N_y</p> <p>Rotate gemstone in the position A indicated by the red dot. Insert the polarizing filter in the East-West position. If the shadow edge containing N_x disappears - read N_y and N_z on the other shadow edge.</p> <p>If the shadow edge containing N_x does not disappear, test the other shadow edge.</p> <p>Rotate gemstone in the position B indicated by the red dot. Insert the polarizing filter in the East-West position. If the shadow edge containing N_z disappears - read N_y and N_x on the other shadow edge.</p>	<p>Biaxial Random Orientation</p> 	<p>Record N_z, N_y and N_x</p> <p>Calculate the maximum birefringence</p>

Table II: Patterns of shadow edges and use of polarizing filter to determine the optical properties of gems. (The Table may be downloaded from the Gem-A website at www.gem-a.info.)

uniaxial; if the variable shadow edge disappears it is biaxial.

Uniaxial in random orientation - where the optic axis is inclined at an angle to the gem table which is not 0° or 90° . The gemstone is rotated to the position of maximum separation of the two shadow edges and N_e is determined (with polarizing filter removed). N_o is read on the constant shadow edge.

Biaxial in special orientations - where the principal vibration directions X or Z are perpendicular to the gem table. N_y is read on the variable shadow edge when the two shadow edges are as close as possible. If the two shadow edges are almost touching it may be difficult to read N_y accurately, so the polarizing filter should be placed over the eyepiece and rotated until the constant shadow edge disappears; this should make it easier to measure N_y . N_z and N_x are read in the position where the constant and variable shadow edges are at maximum separation (with polarizing filter removed).

Pattern V represents the third special case of the biaxial gemstone - where the principal vibration direction Y is perpendicular to the gem table. The polarizing filter is not used. N_y is read on the constant shadow edge and N_z and N_x on the variable shadow edge in the positions where the two shadow edges are at maximum separation.

Pattern VI is the general case of a biaxial gemstone - where none of the principal vibration directions X, Y or Z is perpendicular to the gem table. It is characterized by two variable shadow edges. N_y is read on only one of them, and the polarizing filter must be used to identify which shadow edge contains N_y .

Each shadow edge must be observed in the separate position indicated in *Table II*. For the shadow edge showing N_x this is a position with the highest RI reading. For the shadow edge showing N_z this is the position with the lowest RI reading. To obtain the value of N_y and determine the optic sign of the gemstone, place the polarizing filter on the eyepiece in the east-west orientation and follow the procedure in *Table II*.

Sometimes bringing the gemstone to the

required maximum or minimum position may be difficult if the shadow edge moves little during the rotation (shows almost the same RI). In such cases a rotation of the polarizing filter $10\text{-}15^\circ$ off the proper position may help. If not, possible readings of N_y from both the N_x and N_z shadow edges must be considered in assessing which is the best value to use when attempting to identify the stone.

Conclusions

The refractometer is one of the most used gemmological tools. Its use including observation with the polarizing filter is a part of many courses and study programmes. However, many instructions concerning the filter are descriptive with very few drawings, making them complex and sometimes confusing for students. The new approach enables one to learn the use of the polarizing filter on the refractometer in a fraction of the time needed previously. This leaves more time for the study of the new techniques and methods used in identification of alteration or enhancement processes.

Any jeweller or gemmologist can become familiar with the use of the polarizing filter in about one hour. After that, *Table II* kept next to the refractometer will give them the confidence that they can properly interpret any observation made on the refractometer.

A set of standards representing the six patterns can easily be prepared. These could be combined with a set of drawings on CD showing vibration directions and RIs during the rotation.

Acknowledgement

I wish to thank my colleague Malcolm Beck for the critical reading of the manuscript.

References

- Hurlbut Jr, C.S., and Kammerling, R., 1991. *Gemology*. John Wiley & Sons Inc., New York
- Read, P.G., 1999. *Gemmology*. 2nd Edn. Butterworth Heinemann, Oxford
- Smith, G.F.H., 1972. *Gemstones*. Chapman and Hall, London

Note: *Table II* may be downloaded From the Gem-A website at www.gem-a.info

Letter to the editor

Computational science

I would like to draw the attention of the gemmological community to a very significant article: Computational Science Demands a New Paradigm. *Physics Today*, 58(1), 35-41, Jan. 2005, by D.E. Post and L.G. Votta (both prominent computation experts).

There have been a number of studies reported in the gemmological literature on the computation of the effect of cut on the appearance of diamonds. I do not give references since these are well known and I wish to indicate neither approval nor criticism, either directly or indirectly, of any of these. However, I had thought that with my background in technical and computational matters I would be able to evaluate the 'models' used in such reports, yet a perusal of the cited article (dealing predominantly with physics and engineering) convinces me that only the original workers can both verify and validate such calculations.

In the words of the cited article:
 "... much computational science is still troublingly immature ... Verification and validation ... are crucial ... If a code is unverified, any agreement between its results and experimental data is likely to be fortuitous ... experiments [to validate a code] ... can often be relatively simple and inexpensive."

Any such computation involves a 'model' or 'code' (i.e. the specific computational instructions), including the assump-

tions made (here the nature of the illumination used, importance of body vs edge colours, which factors to include, which to ignore, etc.), and the range of parameters used (e.g. the angular range of the illumination, amount of obscuration by the head, the range of cutting angles, etc.).

I cannot repeat the details of this lengthy article, but the essential points made are these: To produce valid results, any approach must have all the steps used in the computation verified, i.e. demonstrated that there are no errors (typically about seven faults per 1000 lines of Fortran, according to the article), and then validated, that is shown to give the appropriate results. This last should be done not by confirming known results (see the above quotation), but by predicting new results and then showing agreement with actual experimental reality, i.e. observations.

The important point is also made that predictions should be limited only to the ranges of parameters over which results have been verified, since it has often happened that computations will give incorrect results outside of these ranges.

I apologize for not giving more details (which would be excessively lengthy and at least partially outside my sphere of competence), but I believe that anyone interested in this field needs to acquaint themselves with these rather complex concepts.

Kurt Nassau
Lebanon, NJ 08833
U.S.A.

Abstracts

Diamonds

[About signs of mechanical and chemical effects upon diamond crystals from the Urals deposits.]

V.N. ANFILOGOV

(iminchf@ilmeny.ac.ru),
Proceedings of the Russian Mineralogical Society, **133**(3), 2004, 105-8 (Russian with English abstract).

The complex morphology of diamond crystals is reviewed from the point of view of its application to location of their primary source.

Dislocations on the surface of the crystals cannot be explained by mechanical distortion; they appear during growth due to internal defects. The occurrence in the Urals placer deposits of rounded diamonds cannot be explained by rolling in surf conditions. It is suggested that the primary source of diamonds in the Urals is in kimberlites near the placer deposits. The predominance of rounded dodecahedra among the Urals diamonds may be related to the composition of the host rocks intruded by the kimberlites.

R.A.H.

In the pink: Argyle's diamond gift to Australia.

A. BEVAN AND P. DOWNES,
Australian Gemmologist, **22**(4), 2004, 150-5, 4 illus.

The Argyle AK1 diamond mine in the East Kimberley region of Western Australia produces around 30 million carats of diamonds per year. Although this represents about a quarter of the world's current total production, only about 5% of the diamonds recovered from the AK1 pipe are of gem quality, with a further 70% classified as near-gem. These diamonds range in colour from white (colourless) through champagne and cognac (yellow to brown) to the rare pink stones, the latter

comprising less than 0.1% of the total diamond extraction in Australia. In a gift to the nation, Argyle Diamonds have donated several hundred pink diamonds (including four pink octahedrons) to the mineralogical collection of the Western Australian Museum, Perth. For comparison, the collection also includes two colourless diamonds and two champagne coloured diamonds. Part of the sponsorship agreement between Argyle Diamonds and the Museum is that the stones be placed on permanent display and that other institutions throughout Australia may apply to the Museum to borrow material for temporary exhibition.

P.G.R.

Characterisation of carbonado used as a gem.

K. DECORTE, Y. KERREMANS, B. NOUWEN AND J. VAN ROYEN,
Gemmologie. Z.Dt.Gemmol.Ges., **53**(1), 2004, 5-22 16 photographs, 2 tables, 5 diagrams, bibl.

Carbonado is a polycrystalline diamond composed of a large number of very small diamond crystal grains, randomly orientated. The pores between these crystals can be filled with different minerals – therefore carbonado cannot be considered pure diamond. It is never transparent and usually black. It often has a low SG around 3.52. Twenty-one rough carbonados were modelled and partially polished for use as gem material using laser processing techniques. Density, composition, colour and some aspects of morphology were studied. Morphological analysis differentiated between two categories of carbonado; the first consists of only one dominant grain size, while the second comprised larger diamond crystals embedded in a fine grained diamond matrix. Sr, Pb, Fe and Y were found in most samples. Optical luminescence spectra showed diamond lattice defects mainly due to radiation. The studied stones contain significant concentrations of isolated nitrogen atoms.

E.S.

The modern De Beers and the significant changes to the diamond pipeline over the past decade - A literature review.

J. MORRIS, *Australian Gemmologist*, **22**(3), 2004, 112-24, 11 illus.

This paper covers the long history of De Beers who once controlled 90% of the world's rough diamond supply and was able to regulate the quantity of diamonds on the market at any one time. Comparison is made between the original diamond 'pipeline', the new 'supplier of choice' model and the possible final shape of the latter model. An abridged version of the restructured 2002 De Beers ownership 'family tree' is also included. Competition with companies such as BHP Billiton's Aurias Diamonds in Canada, and Rio Tinto's diamonds in Australia is also discussed as are Conflict diamonds and the Kimberley Process.

P.G.R.

Diamonds in Russia – A literature review.

F. PAYETTE, *Australian Gemmologist*, **22**(3), 2004, 99-111, 10 illus. 6 tables.

This paper was presented by the author as the research part of the Australian Gemmological Association's Diploma of Diamond Technology course. It covers the geology of occurrence, the history of discoveries, the exploration and recovery techniques, the type of goods, and their marketing in Russia. Among the illustrations are views of five of the principal Russian diamond mines and a selection of typical Yakutian rough diamonds. A list of famous Russian diamonds is included.

P.G.R.

Diamonds: time capsule from the Siberian mantle.

L.A. TAYLOR AND M. ANAND,
Chemie der Erde: Geochemistry, **64**(1), 2004, 1-74.

In this invited review, the authors report their systematic studies on diamondiferous eclogite xenoliths from

Siberia. The steps in investigating these are: (1) high-resolution computed X-ray tomography of the xenoliths to give 3D images that relate the minerals of the xenolith to their diamonds, (2) detailed dissection of the entire xenolith to reveal the diamonds inside followed by characterization of the setting of the diamonds within their enclosing minerals, and (3) extraction of diamonds from the xenolith to facilitate further investigation of the diamonds and their inclusions. In this last step, it is important to record carefully the nature and relative positions of the inclusions in the diamonds to maximize the number of inclusions that can be exposed simultaneously on one polished surface. In this modus operandi, CL imaging together with FTIR aggregation and C/N isotopic analyses are performed on polished diamond surfaces to reveal their internal growth zones and the spatial relationship of the mineral inclusions to these zones. Such multiple lines of evidence obtained in this way indicate the ultimate crustal origin for the majority of mantle eclogites. Similar pieces of evidence, particularly from $\delta^{13}\text{C}$ in P-type diamonds and $\delta^{18}\text{O}$ in peridotitic garnets lead to the suggestion that at least some of the mantle peridotites, including diamondiferous ones, as well as inclusions in P-type diamonds, may have a crustal protolith as well. R.A.H.

X-ray fingerprinting routine for cut diamonds.

R. DIEHL AND N. HERRES, *Gems & Gemology*, 40(1), 2004, 40-57.

X-ray topography is a non-destructive technique that permits the visualization of internal defects in the crystal lattice of a gemstone, especially diamond, which is highly transparent to X-rays. This technique yields a unique 'fingerprint' that is not altered by gem cutting or by treatments such as irradiation and annealing. Using the table facet as a point of reference, the sample is crystallographically oriented in a unique but reproducible way in front of the X-ray source so that only one topograph is necessary for fingerprinting. Should the diamond be recovered after loss or theft, even after recutting or exposure to some forms of treatment, another topograph generated with the same routine could be used to confirm its identity unequivocally. R.A.H.

Diamants bruns: classification et origine de la couleur.

T. HAINSWANG, *Revue de Gemmologie*, 150, 2004, 13-17.

The origin of the brown colour in diamond is examined with a question-and-answer dialogue. M.O'D.

A foundation for grading the overall cut quality of round brilliant diamonds.

M.L. JOHNSON, B. GREEN, T. BLODGETT, K. CINO, R.H. GEURTS, A.M. GILBERTSON, T.S. HEMPHILL, J.M. KING, L. KORNYLAK, I.M. REINITZ AND J.E. SHIGLEY, *Gems & Gemology*, 40(3), 2004, 202-28.

Observations by the authors and detailed discussions with diamond manufacturers, dealers, retailers and potential customers confirmed that, in addition to brightness and fire, additional factors contribute to the appearance of a cut diamond, and that factors in addition to face-up appearance are important in assessing the quality of a diamond's cut. With the trade interaction as a starting point, the authors (1) tested the brightness and fire metrics to find the best fit with human observations, (2) identified and quantified factors in addition to brightness and fire that contribute to face-up appearance, (3) developed a standard viewing environment that mimics common trade environments, (4) created the basis for a comprehensive diamond cut grading system and (5) began development of reference software to predict the overall cut grade of a particular diamond. The GIA cut grading system described here includes the components of brightness, fire, scintillation, polish and symmetry, as well as weight and durability concerns, into a single overall grade for cut quality for standard round brilliants. Photographic examples of five categories are displayed in a double-page fold out. R.A.H.

Lab notes.

T. MOSES, I. REINITZ, S.F. MCCLURE AND M.L. JOHNSON (EDS), *Gems & Gemology*, 40(3), 2004, 240-51.

Notes are included on the Cullinan blue diamond necklace containing several rare type IIb blue diamonds, a 11.60 ct diamond crystal with strong blue colour due to laboratory irradiation, a natural grey to blue diamond owing its colour to a scattering of light from clouds of pin-point inclusions (the Tyndall effect) and cuprian tourmalines from Mozambique exhibiting a colour change from purple in fluorescent light to grey-bluish green in incandescent light. R.A.H.

Raman spectroscopy of diamond and doped diamond.

S. PRAWER (s.prawer@unimelb.edu.au) AND R.J. NEMANICH, *Philosophical Transactions of the*

Royal Society, Section A, 362(1824), 2004, 2537-65.

Raman spectroscopy (RS) is an essential non-destructive technique in research on diamonds and chemical vapour-deposited diamond films. Thus the typical Raman spectrum excited by a visible laser (1000 to 2000 cm^{-1} region) contains information on the phase purity and crystalline perfection of the diamond sample, while surface-enhanced RS shows new and unexpected structures on diamond surfaces, and the Raman spectrum can be used to map stress and strain in crystallites on the μm scale, remotely monitor the surface T of diamond and to monitor defects, annealing and electrical doping. The latest developments in Raman techniques are reviewed, and applications of RS in diamond science are described, including the measurement of phase purity and crystalline perfection, phonon confinement effects for finite crystal domains, non-contact measurement of T , annealing and defects, and doping with, e.g. boron, S, P or Li. The Raman spectrum is sensitive to the interaction of dopants with the electronic continuum, and it is the carrier concentration rather than the dopant concentration to which the RS is most sensitive. R.A.H.

Gems and Minerals



Elemental analysis of Australian amorphous banded opals by laser-ablation ICP-MS. L.D. BROWN (Leslie.Brown@uts.edu.au), A.S. RAY AND P.S. THOMAS, *Neues Jahrbuch für Mineralogie, Monatshefte*, 9, 2004, 411-24.

Several banded Australian opal-AG samples were found to contain darker-coloured black or grey bands adjacent to lighter-coloured white or clear bands. A study of the distribution of trace elements between these bands showed that darker-coloured bands contained significantly higher contents of transition elements (Ti, Co, V, Ni, C, Zn and Y) and REE (La, Ce) than lighter-coloured bands. A solution depletion model, involving the charge neutralization of silica colloids by highly charged transition metal cations, is proposed to explain these results. Irrespective of the origin of the opal, the distribution of the trace elements for the white, translucent and play-of-colour opal bands was shown to be similar, consistent with the proposed model. R.A.H.

Sapphire in basalt fake.

T. COLDHAM, *Australian Gemmologist*, **22(4)**, 2004, 171, 1 illus.

While visiting the basaltic sapphire fields of Shandong, China, over a decade ago, the author picked up a piece of basalt containing a corundum xenocryst. Unfortunately his Chinese host then confiscated the find. However, in 2004 a similar specimen was seen by the author in Tucson and was purchased by him for US\$80.00. The following day about ten similar specimens were on sale at US\$10.00 each. Using a penknife and loupe soon revealed a line of black gritty glue around the sapphire crystals proving these cheaper samples to be fakes. A further inspection of the purchased US\$80.00 specimen proved this also was a fake although more cleverly concealed than the cheaper versions!

P.G.R.

The Kasumigaura pearl™.

B. DILLENBURGER, *Australian Gemmologist*, **22(4)**, 2004, 156-61, 7 illus.

The Kasumigaura pearl™ is a natural coloured bead-nucleated slightly off-round freshwater pearl that is cultivated in and around Japan's second largest lake, Lake Kasumigaura. Historically the Japanese culture of freshwater pearls can be traced back to the thirteenth century, although the culture of commercial quantities of pearls first began in the late nineteenth century in Lake Biwa, Japan's largest lake. However, the increasing level of pollution in Lake Biwa led to a rapid decline in the production of the freshwater Biwa pearl. The paper describes how the Biwa pearl culture was eventually relocated to Lake Kasumigaura and refined by years of research using hybrids of Japanese and Chinese freshwater mussels. Details are included on the identification characteristics of these relatively rare and expensive cultured pearls.

P.G.R.

Aplicações de microscopia eletrônica de varredura (MEV) e sistema de energia dispersiva (EDS) no estudo de Gemas: exemplos brasileiros.

L. DA C. DUARTE (laurenduarte@bol.com.br), P.L. JUCHEM, G.M. PULTZ, T.M.M. BRUM, N. CHODOR, A. LICCARDO, A.C. FISCHER AND R.B. ACAUAN, *Pesquisas (1st Geociências, Univ. Fed. De Rio Grande do Sul, Brazil)*, **30(2)**, 2003, 3-15.

SEM and EDS results in a study of Brazilian gemstones are presented. Emerald from Campos Verdes, in the State of Goiás, contains inclusions of talc, dolomite, chromite, pyrite, magnetite, etc.; sylvite crystals were identified by SEM/EDS. These salt inclusions suggest the percolation of K-bearing fluids during crystallization. These Campos Verdes emeralds are richer in Cr³⁺ in the outer green zones than in the inner colourless zones, i.e. Cr³⁺ acts as a chromophore. Amethyst from Rio Grande do Sul State contains needle-like inclusions of goethite (rather than cacoenite and rutile, as suggested by others). Pyrofusite and hollandite were identified in agate and quartz geodes. In corundum from Barra Velha (Santa Caterina) application of SEM/EDS showed that the silk effect is due to inclusions of diasporite. The asterism in this corundum is ascribed to empty needle-like channels, rather than to rutile. In corundum from various localities in Minas Gerais, rounded inclusions of zircon are common: others have sillimanite and/or kyanite inclusions, suggesting a metamorphic origin.

R.A.H.

A recent observation of corundum-spinel-sapphire assemblage at Kaltota in Balagoda region, Sri Lanka, and its significance as a cabochoning material.

M.D.P.L. FRANCIS AND H. MATSUEDA, *Gemmologie. Z.Dt.Gemmol.Ges.*, **53(1)**, 2004, 43-52, 2 maps, 3 diagrams, bibl.

Most of the gems found in Sri Lanka are alluvial. The Balagoda region houses all types of in situ corundum deposits. This paper describes one such in situ deposit and how the material could be used in cabochon production. As the corundum is embedded in weathered soft rock, sometimes well exposed, it can be easily mined. Sapphirine is also found in this region but is rare.

E.S.

Relationship between nanostructure and optical absorption in fibrous pink opals from Mexico and Peru.

E. FRITSCH (Fritsch@cnr-imm.fr), E. GAILLOU, M. OSTROUMOV, B. RONDEAU, B. DEVOUARD AND A. BARREAU, *European Journal of Mineralogy*, **16(5)**, 2004, 743-52.

Translucent pink opals from Mexico (Mapimi and Michoacan states) and Peru (Acari area, near Arequipa) are

opal-CT, containing 10-40 % palygorskite, as demonstrated by XRD, IR and specific gravity measurements. They have an unusual nanostructure, with bunches of fibres 20-30 nm in minimum diameter, related to the fibrous nature of the palygorskite crystals, as seen by electron microscopy. A complex absorption centred at about 500 nm is the cause of the pink colour. It is suggested that the absorption is due to quinone fossil products associated with the phyllosilicate fibres. The Raman spectrum of monoclinic palygorskite is deduced from that of its mixture with opal. The opal-CT - palygorskite - quinone association is a geological marker for a specific environment, presumably a fossil lake environment in a volcanic region.

R.A.H.

Pezzottaite - a new mineral.

H.A. HÄNNI AND M.S. KRZEMNICKI, *Gemmologie. Z.Dt.Gemmol.Ges.*, **53(1)**, 2004, 3-4, 1 photo, 1 diagram.

The caesium-rich morganites described in *Gemmologie. Z.Dt.Gemmol.Ges.*, **52**, 2003 have been identified as a new mineral by the International Mineralogical Association (IMA) in Sept. 2003. The new name is pezzottaite. The material comes from Afghanistan and Madagascar and is closely related to pink beryl.

E.S.

A necessary test in pearl identification.

H.A. HÄNNI, *Gemmologie. Z.Dt.Gemmol.Ges.*, **53(1)**, 2004, 39-42, 4 photographs, bibl.

Because their structures are very similar, an additional test is required to distinguish between natural and non-nucleated freshwater cultured pearls. The majority of natural pearls come from saltwater oysters, while most beadless cultured pearls are grown in freshwater mussels. Freshwater pearls produce luminescence under X-rays, because their nacre contains more magnesium. This visible luminescence can be recorded by a sensitive camera. Beads from freshwater nacre in Japanese saltwater pearls also react on X-ray excitation and show through the usually thin layers. This method offers an additional test for the detection of freshwater pearls and is not an alternative for X-ray shadow pictures.

E.S.

Origine du jade jadeite.

G.E. HARLOW, *Revue de gemmology*, **150**, 2004, 7-11.

General survey of jadeite with a question-and-answer dialogue.

M.O'D.

On the distinction between natural and artificially coloured chalcedony/agate.

U. HENN, *Gemmologie*.

Z. Dt. Gemmol. Ges., 53, 2003, 23-32, 14 photographs, 3 tables, 2 diagrams, bibl.

Natural chalcedony is found in a wide spectrum of colours, but it can easily be dyed because of its porosity. This technique has been known for 2000 years and the traditional methods developed during the nineteenth century need not be specifically declared. However, recent guide lines of nomenclature include the declaration of all treatment techniques and therefore methods of distinguishing between natural and artificially coloured chalcedony/agates must be used, whether by microscope or spectroscope. E.S.

Rhodochrosite-Vorkommen in Peru.

J. HYRSL AND Z. ROSALES,

Mineralien Welt, 16(1), 2005, 54-61.

Rhodochrosite is described from Peruvian locations of Pachapaqui, Raura, Hauron, Milpo, Atacocha and Manuelita. Local geology and mineralization is discussed. M.O'D.

Neue Fluorite aus Namibias Nordwesten.

S. JAHN, *Mineralien Welt*, 16(1), 2005, 50-3.

Pale pink and green transparent to translucent fluorite is described from a site about 25 km north-west of Uis (Otjonomewa), Namibia. M.O'D.

An interesting Australian abalone pearl.

S.M.B. KELLY AND G. BROWN,

Australian Gemmologist, 21(12), 2003, Geoff Tombs Memorial Issue (Part 2), 498-501, 8 illus., 2 maps.

A large crescent-shaped abalone pearl was recovered from a black lip or rubra abalone that was fished from the waters off Clay Head in northern New South Wales. Details are included of this rare pearl's gemmological characteristics. P.G.R.

Cultured pearls from the Gulf of California, Mexico.

L. KIEFERT, D. MCLAURIN MORENO, E. ARIZMENDI, H.A. HÄNNI AND S. ELEN, *Gems & Gemology*, 40(1), 2004, 26-38.

An overview is given of the history of natural and cultured pearls from Mexico and describes the production of commercial quantities of mabe as well as bead-nucleated full-round cultured pearls from the indigenous pearl oyster *Pteria sterna*. These cultured pearls have a brown or grey to dark grey body colour, with various interference colours caused by the stacking of platy aragonite crystals and organic matter. They show a red fluorescence to long-wave UV radiation. R.A.H.

A new deposit of gem quality colour-change diaspore from Mông Hsu, Myanmar.

U.HLA KYI AND KYAW KHAING WIN, *Australian Gemmologist*, 22(4), 2004, 169-70, 5 illus., 2 tables.

Gem quality strongly pleochroic diaspore crystals displaying a distinct colour change were first found during the authors' field trip to the Mông Hsu gem field in the Shan State, Myanmar, during November 2003. The 20 crystals collected by the authors ranged in colour from pale green to pale purple and purplish-red. Tabulated results and illustrations show the pleochroic and colour change effects under varying conditions of illumination and crystallographic orientation. P.G.R.

Gem News International.

B.M. LAURS (Ed.), *Gems & Gemology*, 40(2), 2004, 170-81.

Items mentioned include a large (6.2 cm tall) transparent crystal of yellow scapolite from northern Mozambique, specimens from the Cryo-Genic mine near Warren Springs, California, including beryl, pink tourmaline and metallic grey inclusions of päakköonite in quartz, some cleverly assembled imitations of tanzanite in matrix and a natural tanzanite crystal (4.0 × 2.2 × 1.4 cm) associated with calcite, diopside and graphite. R.A.H.

Gem News International.

B.M. LAURS (Ed.) (blairs@gia.edu), *Gems & Gemology*, 40(3), 2004, 252-69.

Items noted include an untreated type Ib diamond exhibiting green transmission luminescence and H2 absorption, gem amphiboles (richterite from Afghanistan, vivid green pargasite [coloured by V] from Pakistan and yellowish-brown pargasite and colourless edenite from Myanmar), a green gem beryl (more than 1 kg in weight) from Luumäki in Finland, cuttable rhodonite from Brazil, a range of orange-red spessartines from

Afghanistan, green to blue gem tourmalines from Congo and dyed cultured pearls fading on exposure to heat in a parked car. R.A.H.

Gemstones in Vietnam.

P.V. LONG, G. GIULIANI, V. GARNIER AND D. OHNENSTETTER, *Australian Gemmologist*, 22(4), 2004, 162-8, 12 illus.

Vietnamese research in geology indicated a high potential for the recovery of gemstones in both north and south Vietnam. In the late 1980s, placer deposits of ruby were uncovered by farmers during routine agricultural activities. Following this major discovery of high quality ruby in the Luc Yen and Yen Bai areas of northern Vietnam, gemstone sources were found in many other locations and culminated in 1988 with the setting up by the government of Vinagemco, a state-owned company for the investigation, mining, processing and trading of gem materials in Vietnam. This paper provides an overview of gemstone localities in Vietnam with special reference to ruby and sapphire. P.G.R.

Red grossular from the Sierra de Cruces, Coahuila, Mexico.

V.W. LUETH AND R. JONES, *Mineralogical record*, 36(6), 2003, 73-95.

Pink to red crystals of grossular were first discovered in 1974 in the area of Lake Jaco, Coahuila, Mexico where well-formed dodecahedral specimens were found in association with good quality crystals of mustard-yellow vesuvianite. Details of the occurrence and geology are given, with short descriptions of other minerals found in the area. There is a sketch map and a short list of references. M.O'D.

Gem News International.

B.M. LAURS (Ed.), *Gems & Gemology*, 40(1), 2004, 66-86.

Items include an update on demantoid and cat's-eye demantoid from Iran, pink to pink-orange spinel from a new locality in Tanzania, fine crystals (to 1.5 cm) of tsavorite and green grossular from Merelani, Tanzania, and commercially produced highly saturated green-yellow diamonds that appear greener in daylight than in incandescent light. R.A.H.

Amethyst from Four Peaks, Arizona.

J. LOWELL AND J.I. KOIVULA, *Gems & Gemology*, 40(3), 2004, 230-8.

For more than a century, the Four

Peaks mine in Maricopa County, Arizona, has produced gem-quality amethyst from crystal-lined or crystal-filled cavities in fractures in a brecciated quartzite. Crystals from this deposit exhibit a range of purple colours, uneven colour zoning and variable transparency, presenting challenges for obtaining a steady supply of material suitable for faceting. The faceted material may display fluid inclusions, tiny reddish-brown flakes of hematite, growth zoning and Brazil-law twinning, all of which provide visual clues for the distinction of Four Peaks amethyst from synthetic material. Recovery of amethyst at this locality continues on a limited basis. R.A.H.

Diamond Geezer.

J. MCCALL, *Geoscientist*, **14**(3), 2004, 10-11.

Short review of the history of diamond recovery in India. M.O'D.

Lab Notes.

T.M. MOSES, I. REINITZ, S.F. MCCLURE AND M.L. JOHNSON (EDS), *Gems & Gemology*, **40**(1), 2004, 58-65.

Notes are given on a natural faint pink 20.24 ct type IIa diamond with numerous green radiation stains, two yellow synthetic diamonds (the metallic inclusions in one of which caused it to be attracted to a magnet), a 78.35 ct green herderite, and four translucent purple beads of spurrite. R.A.H.

Lab Notes.

T.M. MOSES, I. REINITZ, S.F. MCCLURE AND M.L. JOHNSON (EDS), *Gems & Gemology*, **40**(2), 2004, 162-9.

Notes are included on cat's-eye demantoid garnet, a high refractive index (> 1.81) glass sold as peridot, a synthetic 8.85 ct sapphire with an unusual yellowish-green body colour resembling emerald, and a natural 8.88 ct orange-red spinel containing M-shaped etch tubes. R.A.H.

Gem treatment disclosures and U.S. law.

T.W. OVERTON, *Gems & Gemology*, **40**(2), 2004, 106-27.

In recent years, the obligation to disclose fully all gem treatments has changed in the U.S.A. from a mere ethical responsibility to a legal one. The U.S. Federal Trade Commission guides for the gem and jewellery trade now require the disclosure of any treatment of a gem material that substantially affects its value. In addition, all state

deceptive practice regulations in the U.S. require that vendors do not mislead customers as to the treatment status of gems they sell. Vendors should also be aware that insufficient disclosure can subject them to substantial civil liability for fraud by non-disclosure. Several case studies are outlined and suggestions for avoiding legal problems are made. R.A.H.

Alabandin (MnS) a new inclusion mineral in colourless chrysoberyl from Sri Lanka.

J. PONAHL, F. BRANDSTAETTER AND T.T. TRAN, *Gemmologie. Z.Dt.Gemmol.Ges.*, **53**, 2004, 33-7, 6 photographs, 2 tables, 1 graph, bibl.

A relatively large alabandite inclusion of about 670 μ was found in a rough colourless chrysoberyl from Sri Lanka. The method of examination is described. E.S.

Chemical composition and mineralogical properties of a pink tourmaline from pegmatites around Rajgarh, Ajmer District, Rajasthan, India.

L.A.K. RAO, S.R. ALI AND P. SINGH, *Australian Gemmologist*, **22**(4), 2004, 146-9, 1 illus., 1 map, 3 tables.

Pink tourmaline (rubellite) was extracted from a pegmatite body 1.5 km south of the village of Rajgarh in Ajmer District. Details are given of the mineral's gemmological properties and chemical constituents. The chemical data reveal that the Rajgarh tourmaline is characterized by unusually high concentrations of boron, manganese and ferric iron. P.G.R.

Opals from Slovakia ('Hungarian' opals): a re-assessment of the conditions of formation.

B. RONDEAU (brondeau@mnhn.fr), E. FRITSCH, M. GUIRAUD AND C. RENAC, *European Journal of Mineralogy*, **16**(5), 2004, 789-99.

Slovakian opals found in an andesitic host-rock in the Dubnik area, near Košice (part of Hungary until the end of World War I) are believed to have formed by water circulation during a tectonic event. Their physical properties were investigated by XRD, Raman spectra (main peak at 437 cm^{-1}) and scanning electron microscope (large silica spheres 125-270 nm in diameter).

Surprisingly, these are properties of opals usually found in sedimentary deposits rather than those found in opals of volcanic rocks. Some preliminary results of a study of their oxygen isotopes indicate a high $\delta^{18}\text{O}$ for Slovakian and Australian opals (31 ‰), consistent with temperatures of formation less than 45°C; in contrast, Mexican opal-CT shows a lower $\delta^{18}\text{O}$ of 13 ‰ consistent with formation at a higher temperature, possibly as high as 190°C. R.A.H.

The origin of the color of pearls in iridescence from nano-composite structures of the nacre.

M.R. SNOW (snow.mike@saugov.sa.gov.au), A. PING, P. SELE, D. LOSIC AND J. SHAPTER, *American Mineralogist*, **89**(10), 2004, 1353-8.

The variety of body colours shown by South Sea pearls is in part due to a newly recognized structure of the nacre, the edge-band structure, which gives rise to interference colours characteristic of the width. With the pearl oyster, *Pinctada maxima*, the colours include a range of silver tones, creams, yellow and gold in various degrees of colour saturation. The authors have established that the primary body colour of *Pmaxima* pearls arises from the interference of light within the binding regions of the aragonite tiles. The tile faces terminate in a fissured nano-composite structure with an organic matrix within the margin of the aragonite tiles. This edge-band structure gives rise to an optical film formed of organic matrix in aragonite. TEM images show that the edge-band structure increases in width from 74 nm in a silver pearl to 80 nm in a cream pearl, and to 90 nm in a gold pearl. These are first-order Newton's colours which, when mixed with the specular reflection of the nacre and modified by any pigmentation present, give the body colour of the pearl. The more common non-metallic whiter pearls can be accounted for by disorder of this structure leading to unsaturation of the colour. R.A.H.

TPR, EPR and UV-Vis studies of Ni(II) speciation in chryso-prase.

Z. SOJKA, S. WITKOWSKI, W. ZABINSKI, K. DYREK AND E. BISINSKA, *Neues Jahrbuch für Mineralogie, Monatshefte*, 2004(1), 2004, 11-25.

TPR (temperature programmed reduction), epr (electron paramagnetic resonance) together with UV-visible

methods were used to study the status of nickel ions in chrysoprase from three localities (Szylary, Lower Silesia, Poland [apple-green with Ni 1.71 wt.%], Marlborough Creek, Australia [emerald-green with Ni 0.98 wt.%] and an unknown African locality [dark-green with Ni 4.38 wt.%]). The speciation of Ni into 2:1 highly dispersed phyllosilicates (similar to Ni-talc and Ni-lizardite) and extra-framework species grafted onto the surface of chalcedony was demonstrated. Both kinds of Ni exhibit a distorted octahedral coordination giving rise to a broad e.p.r. spectrum with $g=2.17$ and three characteristic d-d bands that can be parameterised with $10Dq = 8897 \text{ cm}^{-1}$ and $B = 953 \text{ cm}^{-1}$. Dedydration of the samples influences significantly the coordination sphere of the extra-framework Ni ions, indicating that water molecules are directly involved as supplementary ligands.

R.A.H.

Spectroscopic and related evidence on the colouring and constitution of New Zealand jade.

C.J. WILKINS, W.C. TENNANT, B.E. WILLIAMSON AND C.A. MCCAMMON, *American Mineralogist*, **88**(8-9), 2003, 1336-44.

IR, optical absorption spectroscopy and Mössbauer spectroscopy were used to investigate the colour of jade [nephrite] from the South Island of New Zealand. Mössbauer spectra gave the distribution of Fe^{2+} and Fe^{3+} at the cation sites and also show how the $\text{Fe}^{3+}/\text{Fe}^{2+}$ ratio increases due to oxidative weathering. The development of the attractive flecking in gem-quality jade is due to agglomerations of colloiddally dispersed magnetite or chromite that can also lead to the formation of black spots. Darker samples are generally high in total iron, although not all lightly coloured samples are low in iron. Weathering in the climatic conditions may give either a brown, hydrated iron oxide or a whitish outer rind if the acidity is high enough to remove the oxide; in either case the nephrite matrix is unaltered. Two quite rare variations were found and ascribed to (1) incomplete nephrite formation in samples developed in association with an unusual ultramafic protolithology and (2) the formation of chromian margarite giving rise to a bluish green (pseudo) jade. EPMA results are given.

R.A.H.

Instruments and Techniques

LIBS: A spark of inspiration in gemmological analytical instrumentation.

T. THEMELIS, *Australian Gemmologist*, **22**(4), 2004, 138-45, 9 illus., 1 table.

LIBS (laser induced breakdown spectroscopy) or LASS (laser ablation spark spectroscopy) is a form of optical emission spectroscopy used primarily for qualitative analysis of elemental compositions. This paper describes a preliminary study of the use of LIBS for the detection of elements in gemstones. The technique provides a method of detecting the low concentrations of Be, Li, B and other elements used in some heat treatments of corundum and which are not detectable by other more conventional analytical instruments. More than 70 natural specimens of chrysoberyl, beryl, corundum heat-treated with beryllium, corundum heated with flux and beryllium, and corundum heat-treated with lithium were tested using the LIBS method. In this preliminary evaluation Be, Li and B were detected but had an error tolerance of around 20%. Although further development of this new method is expected to reduce the error tolerance, the author suggests that the slightly destructive LIBS technique may limit its use to rough specimens.

P.G.R.

Synthetics and Simulants

The 3543 cm^{-1} infrared absorption band I natural and synthetic amethyst and its value in identification.

V.S. BALITSKY (balvad@iem.ac.ru), D.V. BALITSKY, G.V. BONDARENKO AND O.V. BALITSKAYA, *Gems & Gemology*, **40**(2), 2004, 146-61.

The proper use and limitations of IR spectroscopy for identifying natural vs. synthetic amethyst of various types have been studied, focusing on the 3800-3000 cm^{-1} region. The presence of absorption bands at approximately 3680, 3664 and 3630 cm^{-1} unambiguously proves a synthetic origin, but only for samples grown in near-neutral NH_4F solutions. Conversely, there are no unambiguous diagnostic features in the IR spectra of the more commercially significant synthetic amethyst grown in alkaline K_2CO_3 solutions. Nevertheless,

previous investigators have found potential diagnostic value in absorption bands at ~ 3595 and 3543 cm^{-1} . The 3595 cm^{-1} band is found in the spectra of synthetic amethyst, it also is frequently absent from those of natural amethyst. The 3543 cm^{-1} band is found in most synthetic amethysts grown in alkaline solutions but this band also is sometimes present in natural amethyst, so it provides only tentative evidence of synthetic origin. The unambiguous identification of natural vs. synthetic amethyst must be based on a combined examination of the IR spectra, internal growth structures (including twinning) and inclusions.

R.A.H.

Diamond simulants

– A literature review.

P. CARTWRIGHT, *Australian Gemmologist*, **22**(3), 2004, 125-31, 3 illus., 1 table.

The review contains a brief history of the manufacture of diamond simulants. This is followed by lists of the properties of diamond simulants. An indication of how these simulants can be distinguished from diamond is covered under the headings 'The unique properties of diamond' and 'The separation of diamond'. This is followed by a table of diamond simulant properties (which, for completeness, would have benefited from the inclusion of the several colourless natural diamond simulants). A footnote warns of the existence of a new diamond simulant – synthetic moissanite coated with a thin film of synthetic (CVD) diamond. P.G.R.

Identification of synthetic diamond grown using chemical vapour deposition (CVD).

P.M. MARTINEAU, S.C. LAWSON, A.J. TAYLOR, S.J. QUINN, D.J. EVANS AND M.J. CROWDER, *Gems & Gemology*, **40**(1), 2004, 2-25.

Studies carried out at the DTC Research Centre in Berkshire have shown that single-crystal CVD synthetic diamond is clearly distinguishable from natural diamond. The history of the development of the CVD process, the different kinds of CVD synthetic diamond and the properties that differentiate them from natural diamond are outlined. Absorption, photoluminescence and cathodoluminescence spectra of CVD synthetic diamonds show a range of different impurity-related features not seen in natural diamond. Photoluminescence imaging is also useful in identifying CVD synthetic diamond, and X-ray topography may give supportive evidence.

R.A.H.

Lab-grown colored diamonds from Chatham Created Gems.

J.E. SHIGLEY, S.F. MCCLURE, C.M. BREEDING, A.H.-T. SHEN AND S.M. MUHLMEISTER, *Gems & Gemology*, 40(2), 2004, 128-45.

Synthetic yellow, blue, green and pink diamonds from a new source are now being sold by Chatham Created Gems of San Francisco. Some of this new material displays hues and weaker saturations that more closely resemble natural diamonds than most of the synthetic diamonds recently encountered, which typically had very intense colours. These as-grown and treated type I and type II synthetic diamonds, produced by a high-pressure/high-temperature process, have many distinc-

tive visual and spectroscopic features that serve to distinguish them from natural diamonds. These features include geometric patterns of colour zoning and luminescence, metallic inclusions, and bands seen in the visible and photoluminescence spectra; examples are illustrated. R.A.H.

[About mechanism of the fibrous structure appearing in cubic diamond crystals.]

V. M. SONIN, D. G. BAGRYANTSEV, A.I. CHEPUROV AND J.-M. DEREPPE, *Proceedings of the Russian Mineralogical Society*, 132(2), 2003, 95-8 (Russian with English abstract).

The growth of diamond crystals at high P in the Fe-Ni-C system was studied in terms of a T decrease of $\sim 1-2^\circ/\text{sec}$. A phenomenon has been detected of octahedral crystals re-facing via the transformation of numerous tiny cubic sub-individuals on their faces. Data show that this is possibly the formation mechanism of natural cubic diamond crystals with a fibrous structure. This is based on the growth of cubic sub-individuals parallel to one another in the $\{111\}$ direction with the formation of subparallel fibres. Because of this phenomenon, sectors of cubic growth become enlarged while the octahedral growth sectors are declining; the main cause of this change in the growth mechanism is the sharp increase of supersaturation in the crystallization media provided by the falling T . R.A.H.

Abstractors

R.A. Howie

R.A.H.

M. O'Donoghue

M.O'D.

P.G. Read

P.G.R.

E. Stern

E.S.

Book Reviews

Achat + Jaspis.

Various authors, 2004.

Kuratorium der Stiftung

Deutsches Edelsteinmuseum,

Idar-Oberstein, Germany.

Edition des Deutschen

Edelsteinmuseums. Bd 7. pp 88,

illus. in colour. Map in colour

loosely inserted. Hardcover

ISBN 3 932515 42 0. €19.00.

The contributing authors of this beautiful tour d'horizon of the agate and jasper world are Professor Dr Hermann Bank, Rudolf Dröschel and Rainer Hoffmann-Rothe. Each opening from pages 49 to 88 shows magnificent examples of sliced and polished specimens with dimensions given. The standard of photography is the highest I have seen, certainly for this material. The location is given for each specimen depicted - all are from the Idar-Oberstein region.

Preceding the illustrated section are notes, some with English summaries, on some of the notable localities whose history is summarized. The map, not being bound in, can be used in a variety of circumstances. M.O'D.

Rio Grande do Sul, Brasilien.

Landschaften - Menschen -

Edle Steine.

R. BALZER, 2003. Reinhard

Balzer [Eichendorfstrasse 7, D-

35039], Marburg, Germany. pp

234, illus. in colour. Hardcover

ISBN 3 88293 136 1. DM 58.00.

Just over half the book is devoted to a survey of the gemstones found in the Brazilian state of Rio Grande do Sul, their mining and fashioning. The remainder deals with folk-lore, agriculture and history. Most of the items described and illustrated are varieties of quartz and the link between Rio Grande do Sul and Idar-Oberstein is discussed. Both text and presentation are unusual (square format) and attractive. The photographs are excellent, in particular

those of agate, and there is a useful bibliography. M.O'D.

Mana Pounamu.

New Zealand jade

R.J. BECK and M. MASON, 2002.

Reed Books, Auckland, New Zealand. pp 180, illus. in colour.

Softcover ISBN 0 7900 0863 7.

NZ\$29.00.

An attractive and authoritative book describing the many varieties of nephrite found and worked in New Zealand. The senior author, a gemmologist, also has experience of jade carving and this topic is covered in some detail in the second part of the book. Early chapters describe New Zealand nephrite locations, the material recovered from them and the uses to which fashioned jade has been put by the Maoris. Colour photographs occupy a central section and the artefacts selected for reproduction are both beautiful and well presented. Diagrams and black-and-white photographs in the text show details of occurrences and fashioning. The type chosen lends itself to easy reading and the double spacing and the graceful font selected are pleasing to the eye.

An extensive bibliography includes many local sources which will not appear elsewhere and there are numerous references in the text to nephrite locations in other countries. This is an excellent study at a very low price. Most jade literature is in languages other than English and this book is especially welcome on this account. M.O'D.

Seeing the light.

R.H. CARTIER, 2004. [The author: no place of publication given]

pp 324. Softcover ISBN 0

9735316 1 4. No price given.

The title will ensure that the book may be ordered by a large number of readers with (religious) evangelical tastes but this is an original book and, yes, the subtitle (Understanding optics without the mathematics) does intro-

duce the text more or less accurately, though mathematics of a kind is necessarily implicit throughout and finally throws off its cloak in the Appendices.

By 'optics' the author means 'optics as applied to gem testing' and he very thoroughly explores virtually all the optical phenomena that the gemmologist is likely to come across. He succeeds quite well though a word-by-word examination of the text would be necessary to pinpoint heresy if it exists. Several observations I chose at random were accurately described in some cases linked to related ones with which the gemmologist may not be so familiar; I found this stimulating and useful. There could perhaps be more diagrams but if this is a self-published book the selection and obtaining of text illustrations would easily take up a great deal of time and expense. This is a book that can be consulted at random; the style is easy and the typescript good to read.

A minor criticism is the absence of a place of publication and a price, though the book can no doubt be ordered through its ISBN. The serious student will find much of interest and, yes, I have read (some of) it in bed. M.O'D.

Edle Steine vom Dach der Welt.

Various authors, 2003. Christian Weise Verlag, Munich,

Germany. pp 96, illus. in colour.

Softcover ISBN 3 921 65662 1

[ISSN 0945 8492] *extraLapis* no

14. €28.40.

As beautifully illustrated and as well written as the other numbers in this excellent series [now appearing in English], the present number describes the gem minerals of Afghanistan and Pakistan (the title can be translated as Gemstones from the roof of the world). As always the different sections follow one another without a break and an extensive bibliography concludes the survey. As this reviewer is familiar with some at least of the gem mines of Pakistan it was interesting to read that pargasite of appropriate colour is being

called 'Hunza emerald' and that the list of Pakistan gem species has grown to include fine green transparent zoisite and fine orange scheelite. M.O'D.

Minerales de Bolivia.

O. KEMPF, S. TAWACKOLI and W.H. PAAR, 2003. The authors (Casilla 1283), La Paz, Bolivia. pp xix, 121, xvi, illus. in colour. Softcover ISBN 99905 0 417 2. €48.00.

A useful account in chemical order of the mineral species found in Bolivia, with small but adequate illustrations. Several species of more or less gem quality are included; tourmaline and the transparent quartzes; ametrine (given the alternative name bolivianite but not illustrated) and phosphophyllite (a very fine specimen illustrated) are among them. Several previous studies of Bolivian minerals by Ahlfeld have been published and they are listed, with other useful books, in the 38-item bibliography. There is a useful glossary. Perhaps the binding will need care over years of heavy reading. While the standard of photography and reproduction is moderate, the book is none the less welcome. M.O'D.

Fleischer's glossary of mineral species (9th edn).

J.A. MANDARINO and M.E. BACK, 2004. The Mineralogical Record, Tucson, U.S.A. pp xiv, 309. Softcover, ring-back, US\$26.00.

The previous edition, published in 1999, contained 183 pages and the present edition 309. This represents a considerable increase in descriptions since the present edition now lacks the section on mineral groups, which took up 41 pages last time. Around 250 new species have appeared in the major journals and deletions (of discredited species) have been few.

The mineral groups section, revised, will appear in a future issue of *The Mineralogical Record*. Where species are group members their membership is indicated in their entry here, together with the now customary citations to *American Mineralogist* and other journals: a list of those consulted runs to six pages. As usual, each description gives composition, crystal system, main occurrence, series and group membership where relevant. The ring-back binding has served me well with constant use over the previous editions.

This text is essential for the collector as well as the professional mineralogist and its very low price gives little reason for neglect. M.O'D.

Diamond handbook; how to look at diamonds and avoid rip-offs.

R. NEWMAN, 2005. International Jewelry Publications, Los Angeles, U.S.A. pp 186, illustrated in black-and-white. Softcover ISBN 0 929975 36 7. US\$ 18.95.

Yet again it is left to Renée Newman to provide the gem world with a guide which manages to give the trade reader virtually all the essential information needed to buy and sell diamonds: even if there were no HPHT treated diamonds or synthetic diamonds the problems of the ages have not gone away and are just as pressing as they ever were. The book is an advance of the same author's *Diamond ring buying guide* (6th edn, 2002).

The text covers everything the buyer needs to know, with useful comments on lighting and first-class black and white images that show up features better than those in colour. At all relevant points the author gives an up-to-date list of references.

I found several sections particularly interesting; no other text in current circulation discusses re-cutting and its possible effects and the author's discussion of the new topic of branded diamonds conveniently brings together a number of examples of particular cuts peculiar to different firms. I was pleased to see that the Old Mine cut is regaining popularity and that some diamonds have been re-cut in that style from their original cut (probably those giving spread rather than maximum dispersion).

Brief and useful notes describe the present position of synthetic gem diamond and treated diamond. Rip-offs are soberly described and sensation avoided. This is a must for anyone buying, testing or valuing a polished diamond and for students in many fields. I greatly welcome it. M.O'D.

China.

B. OTTENS, 2004. Christian Weise Verlag, Munich, Germany. pp 195, illustrated in colour. Softcover ISBN 3 921656 64 8 ISSN 0945-8492. *ExtraLapis* 26/27. €35.60.

This double issue of the elegant and informative series *ExtraLapis* is one of the first recent attempts to survey the more spectacular minerals (including gemstones) so far discovered in China. As always all of the openings show at least two fine photographs and there is a 38-item bibliography of European-language works only but including maps. Naturally we hope for the now

customary English translation to appear before long.

Though a section on gem materials begins on page 138, previous sections also include gem and ornamental species. Beryl, amethyst, tourmaline, turquoise, peridot, diamond, corundum and diopside, together with remarks on jadeite and nephrite come in the gemstones section though sphalerite and fluorite, described elsewhere, might very well have found a place here. Some locations are given in a table arranged in (romanized) alphabetical order of location but I should imagine that not all species described are included. Chinese characters for some species are also given in a table. Gemmologists and mineral collectors should subscribe to this series and, maybe, to the main journal, *Lapis*. M.O'D.

Faszination Turmalin.

P. RUSTEMEYER, 2003. Spektrum Akademischer Verlag, Heidelberg, Germany. pp x, 309, illus. in colour. Hardcover. ISBN 3 8274 1424 5. €99.95.

The book is certainly designed to catch the eye and tourmaline serves this purpose admirably. This is the second book on tourmaline to have come from Germany in the past few years and though it is not on the same physical scale as Benesch (1990), one of the largest books on a single gemstone, the general conception is similar. Photographs in colour appear on the recto of every page and are faced either with text, diagrams or additional photographs. The reader is left in no doubt that tourmaline can often be sectioned to give beautiful and intriguing patterns.

Readers should be advised that this is not a study of fashioned stones but only of crystals, their symmetry and some of their inclusions as displayed by tourmaline. In this context this is a beautiful book. There is a useful bibliography and an index. M.O'D.

Crystals, growth, morphology and perfection.

I. SUNAGAWA, 2005. Cambridge University Press, Cambridge. pp xii, 295. Hardcover ISBN 0 521 84189 5. £55.00.

Compared with the late nineteenth and early twentieth centuries, the output of books on this type of crystallographic survey has declined. This may be due to either to the attainment of near-perfect methods of structural investigation or to the assumed establishment of required crystallographic data resources making another review superfluous. This being said, the reader is recommended to be within reach of

Professor Sunagawa's *Handbook of crystal growth* (1995) and *Morphology of crystals* (1988). The present text has been translated from the original Japanese.

However, here is an entirely up-to-date treatment of the crystalline state with many references to current investigative methods, well printed and illustrated and with chapter references rather than a bibliography. Professor Sunagawa is known for his interest in gemstones: gem- and ornamental-quality mineral crystals are frequently cited and illustrated.

The text begins with a statement of the fundamental concepts of the crystalline state. Some history of work carried out as far back as the seventeenth century is given before the establishment of the terms form and habit is reviewed. Succeeding chapters deal with growth, heat and mass transfer, spirals, twinning and etching. By chapter 10 the author has chosen four examples of mineral crystals to be examined in detail, rock crystal and agate, pyrite and calcite.

Following an intervening examination of crystal growth in pegmatites Sunagawa returns to individual species, with hematite, phlogopite and the development of the trapiche effect in emerald and ruby. Final chapters discuss the formation of muscovite by regional metamorphism, crystal growth in living bodies and crystals formed through excretion processes. Appendixes illustrate Miller indices, Bravais lattices and the seven crystal systems.

This is an excellent overview of the crystalline state and can be recommended to all students of mineralogy and to gemmologists who wish to pursue the subject beyond the artificial limits of the diploma curriculum.

M.O'D.

Suomen Gemmologinen Seurary.

Gemmologia/Jalokivet, Helsinki, 1991. pp 114, illustrated in colour. Softcover ISSN 1458-4646. Price on application.

Notes on gem species, including organic and synthetic materials with notes of methods of testing, assembled apparently from an unidentified serial but very well produced and attractively illustrated.

M.O'D.

Tourmaline: a gemstone spectrum.

Lapis International LLC, East Hampton, Conn., USA, 2002. pp 106, illus. in colour. Softcover ISBN 0 971 5371 2 7.

extraLapis English 3. Price on application.

Published independently from but in collaboration with the journal *Lapis*, the *extraLapis* series translated into English has at the time of writing covered emeralds (issue 2) and calcite (4). The texts are literal translations of the German versions [reviewed in the *Journal passim*] and the illustrations are equally excellent.

M.O'D.

Lapin korukivet.

R. VARTIAINEN, 2001. [The author] Tampere. pp 80, illustrated in colour. Hardcover ISBN 952 91 3410 X. Price on application to risto.vartiainen@pp.inet.fi

Attractive and well prepared survey of the gem and ornamental minerals of Finland whose comparatively large area (for a European country) has produced a number of fine specimens whose locations are selectively given both in the text and on maps occupying pp 77-80.

A useful bibliography introduces many Finnish papers and monographs rather than the same old titles served to readers by many small guides. Probably since publication, diamond has been found in eastern Finland.

M.O'D.

Minerals, their constitution and origin.

H-R. WENK, AND A. BULAKH. 2004. Cambridge University Press, Cambridge. pp xxii, 646 illustrated in colour. Softcover ISBN 0 521 52958 1. £35.00.

It is some years since a comprehensive introduction to minerals at the undergraduate to graduate level was published and the present text is welcome for this reason and for its coverage of the geological processes which produce minerals. Chapters in the first section cover the chemical elements, crystal structures and morphology and crystal growth. In the second section comes the physical investigation of minerals, the third and fourth sections dealing with mineral varieties and the mineral-forming process and with the formation of mineral groups.

Section five deals with applied mineralogy, including a chapter on gemstones. Several appendices deal with cleavage, hardness and other basic phenomena. Each chapter includes 'test your knowledge': students are asked for the causes of colour of emeralds, rubies and sapphires, along with other reasonable questions.

Colour photographs, forming a section near the centre of the book, are

of good quality and include a number of gem and ornamental materials. While each chapter has its own list of references, additional items can be found in the seven-page bibliography. Readers need not stop with the gemstone chapter - later ones are equally valuable. At the price this text is worth buying.

M.O'D.

Magic of minerals and rocks.

D.J. WIERSMA, 2004. Springer, Berlin, Germany. pp 160, illus. in colour. Hardcover ISBN 3 540 21053 9. £25.00.

Large format well-produced book in which full-page photographs illustrate features of rocks and minerals considered aesthetically pleasing by the compiler-photographer. There is a very short introductory text and individual sections (which include gems, crystal, geode, texture, deformation among others) also have short lead-ins. The gem section includes mostly agates but the pictures are very fine. This reasonably-priced book would make an ideal present.

M.O'D.

Proceedings of the Gemmological Association and Gem Testing Laboratory of Great Britain and Notices

Presentation of Awards

The Presentation of Awards gained in the 2004 examinations was held at Goldsmiths' Hall in the City of London on Monday 1 November. Alan Jobbins, President of the Association, presided and welcomed those present, particularly those from as far away as Canada, China, India, Indonesia, Japan, Myanmar and the U.S.A., as well as the Netherlands and Ireland.

The President introduced Ian Mercer, Gem-A's Director of Education, who presented the awards and gave the address (see below). A vote of thanks to Ian Mercer was given by Professor Alan Collins, Chairman of the Council of the Association.

A reception attended by over 200 members, students and their guests, was held following the ceremony.

Ian Mercer's address

As Gem-A Director of Education, I am very glad to have this opportunity to talk to our Diploma graduates and prize winners here tonight. I would like to review just one or two of the many and various reasons for taking on this study. You and I both are pleased and relieved that you have been so successful. So, why might you have needed to put yourself through all this hard work? First, I think back to why I did the same, getting on for forty years ago now. It was because of our new President, Alan Jobbins, that I got into gemmology; and eventually that led to me being here, talking to you. I was starting out in a geological career and Alan was the curator of gems and minerals in the Geological Survey and Museum; he was also the Education Officer for the Survey and



Gem-A President Alan Jobbins (right) welcomes students to the Presentation and introduces Gem-A Director of Education, Ian Mercer, at the Presentation of Awards ceremony. Photo: Lewis Photos Ltd.

I went to him to seek advice to help me further into the world of minerals. He advised me that there were no pure mineralogy courses, but how about taking a gemmology course. I said, 'what's gemmology?', and that was the start of my everlasting learning curve in gems and ornamental materials. Actually, I sat my exams in this very Hall, with the sun streaming through those stained-glass windows introducing all sorts of selective absorption effects to my practical observations. But much more importantly, why and how did formal gem education get started first in Britain almost 100 years ago? This is relevant to why you needed to get your training right now.

At the start of the 20th century the British jewellery trade requested a gem training response to some serious changes in the gem trade. For example, Professor Verneuil was

First Hirsh Foundation Award goes to graduate from China



Guilin Institute of Technology student Jiang Huijing led the world in gemmology examination success this year. Jiang, of Zhuhai City in Guangdong province, China, was awarded the new Hirsh Award and the Anderson Medal for her top marks in the Foundation Certificate examination in January 2004 and also the Anderson-Bank Prize for highest marks for a non-trade candidate in the June Diploma examination. Jiang Huijing, who travelled to London for the presentation of her awards, is pictured left receiving her Diploma from Ian Mercer, Gem-A's Director of Education. "Among more than 1000 exam candidates in over 50 centres world wide," said Ian, "Jiang has demonstrated her ability to achieve the real-life aims of our courses. I wish her every success."

Photo: Lewis Photos Ltd.

creating challenges when his synthetic ruby was rapidly becoming commercial through 1904 to 1908. The world's first trade diploma course and exam for the Diploma in Gemmology were developed from that time, and the course notes were first produced 92 years ago (we have updated them since, by the way!). The world's first home-study gem course started in 1921 and was later taken up by a man called R. M. Shipley who took his exam in London in 1929. He returned to the U.S.A. and started up the GIA using his hard-won knowledge – so you can see that our Diploma comes in pretty handy for some purposes. By 1925, cultured pearls had become commercially successful enough to prompt the trade into starting up the world's first gem testing laboratory, headed for many years by the great Basil Anderson, who also became chief examiner for the FGA Diploma. Anderson occasionally lectured after retirement in 1966: I was lucky enough to receive occasional tuition from both Anderson and Robert Webster in 1968. The Association and the Gem Testing Lab, long in close cooperation, joined forces officially as one organization in 1990 and, together, now run under the

trade name 'Gem-A', as you know. And that was the year that I started working for the Association, although I had been a home-study tutor for some years.

Now let us think about a basic educational aspect and its relationship with the jewellery trade: what I call '*Observation and real-life gemmology*'. Gem education with qualification really got started with those changes and scares in the trade nearly 100 years ago. Now there are changes and scares by the shovel-full in the gem industry. Really, these should be seen as challenges. They lead to opportunity. I believe the gem and jewellery industry is set to change more drastically than ever. Consequently, there must be continual development in gem and diamond education and exam requirements. In practice, in real-life, there can be a dilemma between (i) the need for fast, observation-based decision-making in buying gems and gem-set jewellery, and (ii) the need for a second opinion, or an appraisal or lab report. Let us recognize the fact that a great number of our purchases are relatively quick decisions relying on our eyes alone. The decision to spend time and money on further information is based greatly on

Christie's Prize for Gemmology



Anu Manchanda of Bearwood, West Midlands, receiving the Christie's Prize for the best jewellery trade candidate of the year in the Gemmology Diploma examinations. Photo: Lewis Photos Ltd.

your experience. But without knowledge, and without good observation practice based on that knowledge, experience is pretty well degraded or even rather useless for safe trading or buying. 'Real-life', therefore, also involves knowing when and why you might need to get a further opinion or lab help. This has to be based on thorough training, so that you know the limits, both yours and those intrinsic to the gem itself. The problem is usually one of making time to build that practical foundation – time to take a course of training and then time to carry on learning through reading, conferences and seminars, short courses and the gathering of experience based on your training.

So what is the relevance of gem education in the jewellery industry? There is a difference between the *breadth* of learning and the *depth* of learning in any subject. In a practical subject like gemmology, the depth of detail can be great. However, most of the trade generally needs less depth than is contained in Webster's big textbook, for instance. Yet there are instances where trade knowledge needs to be deep enough to understand the great detail in what lies behind a problem such as gem origins: what are the criteria, why is it prone to differing interpretations, and what is really meant by the term 'Kashmir' when applied to a sapphire, for instance? These are questions which depend upon a deeper knowledge but they are essentially trade questions. It is true to say that the depth of information in the two Gem-A Diploma courses is tailored to the requirements of those in the trade who need to become *practically confident*. That is a key point. How *broad* an approach to gems does the jewellery trade need? For instance, the Gem-A Diplomas are broad in concept. This means that the training covers a wide spectrum of subjects including rough materials, crystallinity, great attention to the use of the eye in observation for a real-life approach both in gemmology and gem diamond studies, as well as a thorough understanding of testing techniques. Why? Because all of these aspects are required for the different areas of trade activity – retail jewellery, lapidary, diamond manufacture, jewellery design, mining and extraction, grading and valuation, antiques trading and auctioneering, to name just a few.

Now, as part of my experience and fascination with the subject, I would like to consider the relevance of the word '*real*' when applied to gems. As many of you might remember, even so long after your exam, synthetic sapphire is chemically the same as natural sapphire. Therefore, it is *real* sapphire, although it is produced artificially rather than naturally. So, why might most of the jewellery-buying public not think of synthetic sapphire as '*real*'? This word '*real*' is not generally useful for gem materials because it means different things in different contexts.

However, the jewellery-buying public could be helped to become more aware of the interesting possibilities and varieties in natural, imitation, synthetic and treated gem materials, so that they may start to decide for themselves the relative values, fitness for use or fascination, of these various gem materials in jewellery and ornaments. Gem-A's educational activities are directed towards the consumer as well as the gem and jewellery industry. About half of our students are not in the gem-related trades, although a proportion of these eventually join the trade. Education can then be provided by the trade itself in the form of informed advice, and that advice can be based on a sufficiently deep and practical knowledge provided by our courses, which in turn helps both the customer and the trade itself. For example, we know why a one-carat natural sapphire containing several healed fractures and other inclusions may be considered to be more valuable than a relatively clean one-carat synthetic sapphire of the same colour. Some customers would consider the more cloudy natural sapphire to be the more desirable object than the synthetic, whereas others may go for the perfection of the synthetic sapphire knowing that it is a man-made product. It is, after all, 'real' sapphire, isn't it? So which really is more valuable? Is it a trade decision, a consumer decision or an educator's decision? In this instance maybe you could vote for the public. They make the final decision, after all. But how could you possibly advise or inform the consumer if you have little or no knowledge of gemmology?

So there is another key point: transfer that awareness to the buying public, with a confident use of gemmological expertise, backed by sufficiently wide-based training, to a great enough depth, and based on realistic observation techniques, and you can increase business. Synthetic, treated or imitation gems can then be allowed to sell themselves, and they can be used to sell-on to the untreated natural gems in jewellery: the so-called 'real thing'. That is my message in this fast-changing gem world, and it is these changes that will make more opportunity, so long as the good training and observational awareness are

The Deeks Diamond Prize



Emma McMillan of Dalkeith, Mid Lothian, receiving the Deeks Diamond Prize for the best candidate of the year in the Gem Diamond examinations. Photo: Lewis Photos Ltd.

there to begin with, and so long as the consumer is enabled to be well aware. If you are the consumer then, with your training, you have already armed yourself with a good amount of personal consumer protection. Please continue to use this with full observational practice, please continue to use your eyes, your hand-lens and proper lighting, using every opportunity to notice what your training has enabled you to notice. And, after telling you all that, I advise you when buying not to believe anything written on the packet or anything anyone tells you (not even me) until you have looked for yourself and come to your own conclusion.

In order to produce that opportunity for you to gain the Association's Diplomas in all

our centres around the world, we have in the Gem-A education office a team of just a few very able people. I gladly take this opportunity to give them my personal and everlasting thanks, not least to Brenda Hunt, Lucy Dean and Hayley Smith for these three have worked to run the course and examination administration by sheer dedication and attention to detail. Lorne Stather is my development team, researcher and manager, for all the course materials and exams. I am not forgetting our Board of Examiners who are central to the existence of Gem-A; working in close cooperation with the education office, they are a group of experts who are dedicated and truly have your interests at heart. Please also remember that Gem-A exists as a membership association and that we vitally depend upon your continued support as qualified gemmologists by maintaining your membership, so that you can retain those coveted letters after your name, FGA or DGA.

Congratulations, all of you FGAs and DGAs!

Members' Meetings

Annual General Meeting

The 2004 Annual General Meeting was held on 14 September at 27 Greville Street, London EC1N 8TN (see report below). The AGM was followed by an illustrated talk entitled 'The rubies of Malawi: hidden gems of Africa' by David Hargreaves.

Gem-A Conference 2004

The Gem-A Annual Conference was held on Sunday 31 October at Kempton Park Racecourse, Sunbury-on-Thames, Middlesex. Keynote speaker was Tom Chatham of Chatham Created Gems Inc.

Conference events included a private viewing of the Crown Jewels with Crown Jeweller David Thomas, a champagne reception at antique dealers Wartski with a talk by Geoffrey Munn, and a visit to the Museum of London where groups had the opportunity to handle and examine items from the Cheapside Hoard of Elizabethan and

Jacobean gems and jewellery.

A full report of the Conference was published in the December 2004 issue of *Gem & Jewellery News*.

Exhibition tour

A tour of the exhibition 'Hungary's Heritage: Princely treasures from the Esterházy Collection' at Somerset House was held on 10 November.

Gem Discovery Club Specialist evenings

On the first Tuesday of each month Club members have the opportunity to examine items from the collections of gem and mineral specialists. The November guest was Tom Chatham, keynote speaker at the Gem-A Conference, who brought along samples of synthetic diamond. Marcus McCallum provided a selection of items from his personal collection in December, Roy Huddleston with a collection of doublets in February, Alan Jobbins was the March specialist with gems and crystals from over half a century of collecting and Marcia Lanyon brought along a collection of beads for the April Club evening. Reports of the specialist evenings are given in *Gems & Jewellery*.

The Gem Discovery Club meets every Tuesday from 6:00 to 8:00 p.m. at the Gem-A headquarters in Greville Street. For further details contact Mary Burland on 020 7404 3334, email mary.burland@gem-a.info.

Midlands Branch

Regular branch meetings were held at the Earth Sciences Building, University of Birmingham, Edgbaston. On 29 October Alan Jobbins gave a talk entitled 'Gems of the seven continents', on 28 January Dr Jeff Harris spoke on 'Diamonds from crust to core', on 25 February 'European jewellery from Elizabeth I to Elizabeth Taylor' was the subject of John Benjamin's talk and on 1 April David Callaghan gave a talk entitled 'Gems by candlelight'. The annual Bring and Buy and Team Quiz event was held at the Earth Sciences Building on 26 November.

Continued on p. 368

Gem-A Awards

Gem-A examinations were held worldwide in January 2005. In the Examinations in Gemmology, 125 candidates sat the Diploma Examination of whom 65 qualified including one with Distinction and eight with Merit, and 154 sat for the Foundation Examination, of whom 108 qualified. In the Gem Diamond Examination 90 candidates sat of whom 46 qualified, including five with Distinction and six with Merit. The names of the successful candidates are listed below:

EXAMINATIONS IN GEMMOLOGY

Gemmology Diploma

Qualified with Distinction

Smithie, Sheila Barron, Boston, Mass., U.S.A.

Qualified with Merit

Berden, Angela C.M., Balham, London

Braham, Adrian D., Reigate, Surrey

Huck, Perry, Stanford-in-the-Vale,
Oxfordshire

Leadbeater, Craig, Dulwich, London

Liu Rongjun, Yujishan, Wuhan, Hubei,
P.R. China

Pinckernelle, Kathia, London

Shwe Li, Yangon, Myanmar

Wagner, Olivier, Hammersmith, London

Qualified

Alcock, Kate, Byford, Hereford and
Worcester

Alliston, Erika, Hammersmith, London

Bae Hyo Jun, Daegu, Korea

Chaiyawat, Yuanchan, Bangkok, Thailand

Chan Wai Fong, Hong Kong

Chen Manli, Guangzhou, P.R. China

Cheng Wai Ping, New Territories, Hong
Kong

Cheung Yiu Hung, Kowloon, Hong Kong

Chiu Shu-Fen, Taipei, Taiwan, R.O. China

Chung Yim Ling, Mandy, Kowloon,
Hong Kong

Clement, Jenny, London

Ding Hua Yu, Toronto, Ontario, Canada

Eun Ok Joo, Gyunggi-Do, Korea

Fleming, John James, Kelso, Roxburghshire

Gemmill, Tanya Charlotte, London

Ho Hay Mo, John, Yangon, Myanmar

Jung Hae Sook, Gyungbuk, Korea

Kilby Hunt, Judith, London

Klimek, Karina Sophia, Truro, Cornwall

Lam Shun Kwong, New Territories,
Hong Kong

Li Fangwei, Wuhan, Hubei, P.R. China

Li Man, Wuhan, Hubei, P.R. China

Liang Liming, Guilin, Guangxi, P.R. China

Lin Shu-Zhen, Taipei, Taiwan, R.O. China

Liu Haimei, Guilin, Guangxi, P.R. China

Liu Xianyu, Guilin, Guangxi, P.R. China

Ma Yaw Lan Hsiung, Ruth, Hong Kong

Mai Zhi Qiang, Zhongshan, Guangzhou,
P.R. China

Maranhao, Priscilla Petra, London

Naw Htar Phyu, Yangon, Myanmar

Pan Han, Guilin, Guangxi, P.R. China

Phisuthikul, Piyamaporn, Bangkok, Thailand

Ren Chunhua, Wuhan, Hubei, P.R. China

Rowley, Elaine, London

Ruan Qingfeng, Guilin, Guangxi, P.R. China

Scragg, Claire Patricia, Great Missenden,
Buckinghamshire

Skaraas, Sonia C., London

Sue-a-Quan, Dona Marie, Yangon,
Myanmar

Taylor, Richard E., Carlsbad, California,
U.S.A.

Thomson, Alison, Ealing, London

Tripathi, Pooja, Jaipur, Rajasthan, India

Tsiknakis, Avgerinos, Athens, Greece

Vasant Gala, Rahul, Plaistow, London

Veitch, Tara MacNeil, Greenwich, London

Webb, Stephen Charles, Nelson,
New Zealand

Wreford, David, London

Xie Shanshan, Guilin, Guangxi, P.R. China

Yaddanapudi, Pratima, Dagenham, Essex

Yang Hanyuan, Guilin, Guangxi, P.R. China

Yang Hao, Wuhan, Hubei, P.R. China

Yang Ping, Guilin, Guangxi, P.R. China

Ying Weigui, Wuhan, Hubei, P.R. China

Gem-A Awards

You Hongwen, Wuhan, Hubei, P.R. China
 Yu Binxing, Wuhan, Hubei, P.R. China
 Zhong, Lihong, Zhongshan, Guangzhou,
 P.R. China
 Zhu Jia, Shanghai, P.R. China

Gemmology Foundation Certificate

Qualified

Axelson, Louise, Helsinborg, Sweden
 Badrov, Irena, London
 Bae Hyo Jun, Daegu, Korea,
 Bang, Moo Geun, Daegu, Korea
 Basnayake, Charmi K., Kandy, Sri Lanka
 Bendikssen, Bjorn, Lannavaara, Sweden
 Bickerstaff, Alastair, Newport, Shropshire
 Brand, Juliette, Geneva, Switzerland
 Buteyko, Tamara, London
 Cai Hui Hua, Shanghai, P.R. China
 Chan Mei Fong, Frances, Kowloon,
 Hong Kong
 Chan Suk Wah, Shirley, Kowloon,
 Hong Kong
 Chang Chi Wei, Taichung, Taiwan, R.O.
 China
 Chang Chin Feng, Taichung, Taiwan, R.O.
 China
 Cheng Chui Shan, Kowloon, Hong Kong
 Cheng Qi, Shanghai, P.R. China
 Cheung Ching Chung, Hong Kong
 Cheung Pui Ying, Kowloon, Hong Kong
 Chiu Fong Ting, Hong Kong
 Chong Joon Yau, Singapore
 Darell, Rikard, Lannavaara, Sweden
 Dunn, William A., Los Angeles, California,
 U.S.A.
 Fletcher, Robin, Reading, Berkshire
 Fossurier, Anne, Montreal, Quebec, Canada
 Fung Wing Yee, Hong Kong
 Geng Yan, Shanghai, P.R. China
 Gordon, Richard, Woodford Green, Essex
 Harn Boh-Sheng, Taipei, Taiwan, R.O. China
 Hattersley, Mark, Northwood, Middlesex
 Hay Man Than Htaik, Yangon, Myanmar
 Ho Siu Ming, Hong Kong
 Hong Xiao Bin, Shanghai, P.R. China
 Hsu Chia Jung, Taichung, Taiwan, R.O.
 China

Hwang Il Sik, Geoje, Korea
 Ip Lai Kwan, New Territories, Hong Kong
 Jang Wei-Jen, Taipei, Taiwan, R.O. China
 Jensen, Annalisa, Esher, Surrey
 Jiang Jie, Guilin, Guangxi, P.R. China
 Johansson, Maria, Hoganas, Sweden
 Jung Hae Sook, Gyungbuk, Korea
 Kalayar Pyi Wai Shan, Yangon, Myanmar
 Kau Yuk Ming, Eddie, Tuen Mun,
 Hong Kong
 Kent, Paul Allen, Aarwangen, Switzerland
 Khin Zar Thwe, Yangon, Myanmar
 Kim Ji Won, Seoul, Korea
 Kim Su Young, Gyungbuk, Korea
 Kim Su Hyun, Dalseo-Gu, Korea
 Latham, Elizabeth, Wallingford, Oxfordshire
 Lau Ka Yan, Kowloon, Hong Kong
 Lau Moon Lan, Stanley, Hong Kong
 Lee Su Jin, Gwangju, Korea
 Lee Wai Yee, New Territories, Hong Kong
 Leung Kim Ping, Vicky, New Territories,
 Hong Kong
 Li Na, Guilin, Guangxi, P.R. China
 Lin Cen, Shanghai, P.R. China
 Lin Jie, Guilin, Guangxi, P.R. China
 Low San, Chatham, Kent
 Lu Yi, Guilin, Guangxi, P.R. China
 Lundgren, Tobias, Stockholm, Sweden
 Lv Feng, Shanghai, P.R. China
 Lyons, Melinda, Holywell, Clwyd
 Ma Jun, Shanghai, P.R. China
 Maass, Nora V.S., London
 Mak Kim You Keung, New Territories,
 Hong Kong
 Mao Yuanjiong, Guilin, Guangxi, P.R. China
 Me Kyaw Khine, May, Yangon, Myanmar
 Moe Seint Seint Lin, Yangon, Myanmar
 Ong Chin Siang, Gary, Singapore
 Osman, Abdirahman Adam, Cardiff, S.
 Glamorgan
 Ottman, David Andrew, Carmichael,
 California, U.S.A.
 Overton, Thomas William, Carlsbad,
 California, U.S.A.
 Park Jae Young, Busan, Korea
 Peng Conghui, Guilin, Guangxi, P.R. China
 Perez, Christina, Citrus Heights, California,

Gem-A Awards

U.S.A.

Po Pui Chun, Tuen Mun, Hong Kong
 Potter, Madeline, Ingrave, Brentwood, Essex
 Prince, Ronald Fisher, Richmond, Surrey
 Rentsch, Jean-Marc, Zurich, Switzerland
 Riley, Deborah Mary, Discovery Bay,
 Hong Kong
 Ringhiser, Barbara G., Lake Worth, Florida,
 U.S.A.
 Shah, Nilay, Hatfield, Hertfordshire
 Shen Mengxi, Guilin, Guangxi, P.R. China
 Shin Chan Sik, Ulsan, Korea
 Siu Pui Ka, Kowloon, Hong Kong
 Song Ji Sun, Daegu, Korea
 Soubiraa, Guillaume, London
 Stewart, Sharon, Abbots Langley,
 Hertfordshire
 Su Yi Win, Yangon, Myanmar
 Susawee, Namrawee, Bangkok,
 Thailand
 Tam Tung Lee, Toni, New Territories,
 Hong Kong
 Tessari, Claudio, Ora, Italy
 Thawornmongkolkij, Monruedee, Bangkok,
 Thailand
 Traill, Lillian, Ladbroke Grove, London
 Tyler, Clare J., Den Bosch, The Netherlands
 Wacyk, Carri Tara, Antibes, France
 Wadhwa, Pritam, Harrow, Middlesex
 Wells, John, Bickerstaffe, Lancashire
 Wong Yi Tat, Eddy, Kowloon, Hong Kong
 Wong Lai Mun, Phyllis, New Territories,
 Hong Kong
 Wong Ching Man, Ruby, New Territories,
 Hong Kong
 Wong Wai Ming, New Territories,
 Hong Kong
 Wright, Nathaniel Thomas, Peoria, Illinois,
 U.S.A.
 Yeun, Dae Huem, Gyunggi-do, Korea
 Yeung Ka Yee, Anthea, Kowloon,
 Hong Kong
 Yeung, Angela, North Point, Hong Kong
 Yip Siu Ling, New Territories, Hong Kong
 Yuen-Ng Wai Kwan, Chrisdy, Hong Kong
 Zhang Yonghua, Guilin, Guangxi, P.R.
 China

GEM DIAMOND EXAMINATION

Qualified with Distinction

Ko Cheuk Wah, Kowloon, Hong Kong
 Leadbeater, Craig, Dulwich, London
 Lindwall, Torbjorn, Lannavaara, Sweden
 Wong Tung Wing, Kowloon, Hong Kong
 Wong Yuen Leung, Kowloon, Hong Kong

Qualified with Merit

Berden, Angela C.M., Balham, London
 Chawla, Jaspreet Kaur, London
 Ho Sze Man, Helen, New Territories,
 Hong Kong
 Kuo Yan Ki, Yannis, North Point,
 Hong Kong
 Ng Wing Kwan, New Territories,
 Hong Kong
 Terry, Dennis, Petts Wood, Kent

Qualified

Assouad, Carole Nathalie, Edgbaston,
 Birmingham, West Midlands
 Chan Chi Wai, Hong Kong
 Chan Kaman, Carmen, Hong Kong
 Chan Siu Ping, Kowloon, Hong Kong
 Chang Cheng Hsien, Taipei, Taiwan, R.O.
 China,
 Chong Chanthasone, Kowloon, Hong Kong
 Chuang Chang Chen, Taipei, Taiwan, R.O.
 China
 Deprez, Guillaume, London
 Fong Tik Kwan, Kowloon, Hong Kong
 Haralabopoulos, Irene Rania, Athens,
 Greece
 Ho Cham Wa, Kowloon, Hong Kong
 Huddy, William Rupert Hugh, Holcombe,
 Somerset
 Hui Ngai Yin, Kowloon, Hong Kong
 Ip Tan Ching, Kowloon, Hong Kong
 Kashaka, Jean-Claude M., Surbiton, Surrey
 Katembwe, J. Christian, Rainham, Kent
 Kiilu, Kyalo, Mayfield, East Sussex
 Kuo Chi-Cheng, Taipei, Taiwan, R.O. China
 Leung Kam Ping, Hong Kong
 Liao Dan, Wuhan, Hubei, P.R. China
 Lin Shu-Zhen, Taipei, Taiwan, R.O. China

Gem-A Awards

Lo Sunny, Kowloon, Hong Kong
 Lu, Lu, Morden, Surrey
 Mahmood, Zahid, Aston, Birmingham,
 West Midlands
 Morgan, Jacqueline, Chalfont St. Peter,
 Buckinghamshire
 Rudomino-Dusiacki, Patrick, London
 Towers, Jill C., St Heliers, Auckland,
 New Zealand
 Wan Ching Man, Kowloon, Hong Kong
 Wenham, Diana L., North Harrow,
 Middlesex
 Wong Tai-Wai, Kowloon, Hong Kong
 Wong Yan Yan, Amy, Kowloon Bay,
 Hong Kong
 Wong Pui Ying, Helena, Tsuen Wan,
 Hong Kong
 Wreford, David, London
 Yin Zhen, Beijing, P.R. China
 Zhang Yun Tao, Beijing, P. R. China

EXAMINATIONS IN GEMMOLOGY

The following candidates qualified in the June 2004 examinations but their results were not released in time for publication in the October 2004 issue of *The Journal*:

Gemmology Diploma

Qualified with Merit

Lin Bing, Toronto, Ontario, Canada

Qualified

Hellenbrand, Yosef Joe, Thornhill, Ontario,
 Canada

Hogan, Anne, North Vancouver, British
 Columbia, Canada

Sheikh, Afia, Scarborough, Ontario, Canada

Thurner, John Robert, Burlington, Ontario,
 Canada

Continued from p. 364

On 4 December at Barnt Green branch members enjoyed the 52nd Anniversary Dinner.

A one-day branch conference was held on 13 March at Barnt Green with the theme 'Man-made diamonds and their identification'. A report of the conference will appear in the June issue of *Gems & Jewellery*.

North West Branch

On 17 November at Church House, Liverpool, the Branch AGM was held when Deanna Brady, Ray Rimmer and Eileen Franks were re-elected Chairman, Secretary and Treasurer respectively. The AGM was followed by a social evening. This was the last branch event at the Church House venue; future meetings will be held at YHA Liverpool International, 25 Tabley Street, Liverpool 1.

Scottish Branch

A programme of talks was held at the British Geological Survey, Murchison House, West Mains Road, Edinburgh: on 16 November Brian Jackson spoke on the 'Gemstones of Pakistan', on 18 January Liz Goring was the speaker on the subject 'Suffragette jewellery', Dr Jeff Harris followed on 22 February with a talk entitled 'Diamonds – a research perspective' and Alan Hodgkinson on 15 March on 'Tucson and all that's new'.

Annual General Meeting

The 2004 Annual General Meeting of Gem-A was held on 14 September at 27 Greville Street, London EC1N 8TN. Lawrence Hudson chaired the meeting and welcomed those present. The Annual Report and Accounts were approved.

The Council had nominated E. Alan Jobbins for the office of President for the term 2004-2006 and the nomination was carried. Alan Jobbins thanked the outgoing President, Professor Alan Collins, for his support of the Association during his four years in the office of President.

Terry Davidson and Michael O'Donoghue were re-elected and Sheila Burgoyne, Professor Alan Collins, Sally Everitt, Alan Jobbins and Peter Wates elected to the Council.

Ian Thomson retired in rotation from the Council and was not seeking re-election.

Dr Tony Allnutt and Brian Jackson were re-elected to serve on the Members' Audit Committee. As Sheila Burgoyne, Sally Everitt and Peter Wates had been elected to the Council, they were no longer eligible to serve on the Members' Audit Committee, and therefore had retired from that Committee. Hazlems Fenton were re-appointed auditors.

Membership

Between 1 November 2004 and 31 March 2005 the Council approved the election to membership of the following:

Fellowship and Diamond Membership (FGA DGA)

Hanlon, Adrienne K., Ingol, Preston, Lancashire, 2001/2004

Manolia, Evgenia, Zografou, Greece, 2004/2004

Marsh, Claire, Stourbridge, West Midlands, 2004/2003

Wong Mei Wai, May, Kowloon, Hong Kong, 1995/1996

Fellowship (FGA)

Blanksma, Eelco, Arnhem, The Netherlands, 2004

Drijver, Joyce Marie-Louise, Utrecht, The Netherlands, 2004

Duan, Tiju, Beijing, P.R. China, 2002

Gaskin, Clare K., London, 2004

Gerber, Doris Christine, Zurich, Switzerland, 2004

Donations

The Council is most grateful to the following for their donations. Donation levels are Circle of Benefactors (£5000 and above), Diamond (£1000 to £4999), Ruby (£500 to £999), Emerald (£250 to £499), Sapphire (£100 to £249) and Pearl (£25 to £99).

The following join those donors listed in previous issues of *The Journal*:

Emerald Donation

Terry Davidson, FGA, London

Sapphire Donations

Eisuke Ashida FGA, Kyoto City, Kyoto, Japan

Torbjorn Lindwall FGA, Lannavaara, Sweden

Paul R. Milton, Liverpool, Merseyside

Robert L. Rosenblatt, FGA, Salt Lake City, Utah, U.S.A.

Pearl Donations

Burton A. Burnstein, Los Angeles, California, U.S.A.

Dennis Durham, Kingston upon Hull, East Yorkshire

Siu-Kam Fan FGA DGA, Kowloon, Hong Kong

Gwyn Green FGA DGA, Barnt Green, Hereford and Worcester

Bede Johnson, Lewes, East Sussex

Ernest R. Mindry FGA, Chesham, Buckinghamshire

Moe Moe Shwe FGA, Singapore

Sara Naudi FGA, London

Gabriella Parkes DGA, London

Elaine Rowley, London

Iamze Salukvadze FGA DGA, Dubai, United Arab Emirates

David John Sayer FGA DGA, Wells, Somerset

Sunny K. Tsui FGA, Melbourne, Victoria, Australia

Nancy Warshow FGA DGA, Nairobi, Kenya

Glady Yan Wah Lau FGA, Hong Kong

Zeng Chun Guang BSc MSc FGA, Singapore

Gifts

The Council is most grateful to the following for their gifts for research and teaching purposes:

Tom Chatham, San Francisco, California, U.S.A., for four Chatham Created diamonds (yellow, pink, blue and colourless).

Roland N. Clarkson FGA DGA RJ Dip FRNS, Chessington, Surrey, for a Rayner Diamond Tester.

Peter R Dwyer-Hickey FGA DGA, South Croydon, Surrey, for eight cut diamonds.

Gwyn Green FGA DGA, Barnt Green, Hereford and Worcester, for an assortment of fashioned gemstones.

Brendan Haddock FGA DGA, Edinburgh, for three beryl crystals from Scotland.

Melanie A Medniuk FGA DGA, Witham, Essex, for two spodumene beads.

Jonathan Mehdi, London, for a quartz crystal with internal clusters of dark star-shaped inclusions (hollandite) from Madagascar.

Renée Newman GG, International Jewelry Publications, Los Angeles, California, U.S.A., for two books, the *Diamond Handbook* and the *Diamond Buying Guide*.

One Plus One Gems, Sheffield, South Yorkshire, for a pyrope/almandine garnet

crystal, a sample of rock crystal with 'oily' inclusions (donated as 'Herkimer diamond'), and three faceted specimens, a spodumene (29.87 ct), a citrine (8.11 ct) and a zircon (14.85 ct).

Bob Springall, Woodside Park, London, for a large selection of cut and rough natural and synthetic gemstones as well as two table-top display cases, a Chelsea colour filter, a spectroscope, a calcite dichroscope with stand, a Chromoscope and a Jewellers' Eye reflectance meter.

Ian Thomson FGA, Thomson Gems, London, for two octagonal cut samples of green YAG, an Inamori synthetic alexandrite and an Inamori synthetic emerald.

Eric Van Valkenburg, High Pressure Diamond Optics Inc., Tucson, Arizona, U.S.A., for two carbon vapour deposition wafers (CVD).

Margot Willing FGAA DipDT, Claremont, Western Australia, for a piece of chrome chalcedony 'chloro-opalite' (Newman, W.A.), a piece of iron ore (Pilbara, W.A.), and an oval cabochon of 'tiger iron' (Ord Range, W.A.).

Gray, Mathew Neil, Lismore,
New South Wales, Australia, 2004

Hemlin, Colette, Anjou, Quebec, Canada,
2004

Hogan, Anne P., N. Vancouver, British
Columbia, Canada, 2004

Kuo, Chi-Cheng, Taipei, Taiwan, R.O.China,
2003

Leung Pui Fong, Helen, Hong Kong, 1984

Lovelock, Justina Elizabeth, London, 2004

Lyons, Annabel Helen, London, 2004

Pai, Vishnunarayan, Ernakulam, India, 2004

Peeters-Van Namen, Irene Françoise,
Warmond, The Netherlands, 2004

Pumpang, Sureeporn, Bangkok, Thailand,
2004

Ravaoarimalala, Voahanginirina F.,
Antanimora, Madagascar, 2004

Scott, John R.J., Vancouver, British Columbia,
Canada, 2004

Sheikh, Afia, Scarborough, Ontario, Canada,
2003

Singh, Amrinder Pal, Dehli, India, 2004

Stanyer, Natasha, Lewes, East Sussex, 2004

Diamond Membership (DGA)

Chan, Wing Tung, New Territories,
Hong Kong, 2004

Chang Wing Chi, Vivian, Kowloon,
Hong Kong, 2004

Giannakakis, Vasilios, Athens, Greece, 2002

Humphrey, Brian, Fulham, London, 2002

Jelinska, Emma, London, 2004

Johnson, Lisa Anne, Stourbridge,
West Midlands, 2004

Kiamos, George, Athens, Greece,
2004

Macrae, Margaret, Isle of Lewis, Scotland,
2002

Pennington, Maria Theresa, Norwich,
Norfolk, 2004
Riley, Deborah Mary, Lantay, Hong Kong,
2004
Sim, Ooi Kok, London, 2004
Southam, Karen Lesley, Oldbury,
West Midlands, 2004
Watling, David Robert Stuart, Sidcup, Kent,
2004
Wells, John, Ormskirk, Lancashire, 2004
Yeung Wing Chuen, Benny, New Territories,
Hong Kong, 2004
Yiu, Ka Wah, Kowloon, Hong Kong, 2004

Associate Membership

Al-Othaim, Ahmed, London
Anjum, Nabeel, Dublin, Ireland
Bello, Mohammed Ibrahim, London
Bonewitz, Ronald Louis, Rogate, Petersfield,
Hampshire
Bowers, Sally, Fulham, London
Bryce, Amy, Beatrix, Axminster, Devon
Burford, Murray, Victoria, British Columbia,
Canada
Chalfen, Brian, London
Cho Cho Kyaw, Yangon, Myanmar
Coppin, Daisy, Corsham, Wiltshire
Danjo, Keiji, Kofu City, Yamanashi Pref.,
Japan
De Syllas, Charlotte, London
Draysey, Jennifer, Bromley, Kent
Finn, Marion, London
Franzese, John C., Seattle, Washington, U.S.A
Fuller, Caitlin Victoria, Camps du Moulin,
Guernsey, Channel Islands
Gill, Jazz, Barnes, London,
Gits, Hugo, Knokke, Belgium
Gogna, Sanjeev, Dist Una., India
Goslee, Jennifer, London
Goto, Satoshi, Uji City, Kyoto, Japan
Green, Anthony, London
Hassaan, Fouad, London
Hirokawa, Natsuki, Chuo-City, Kobe City,
Japan
Hussain, Sajjad, Rawalpindi, Pakistan
Hyogo, Yuka, Saitama City, Saitama Pref.,
Japan
John, Huw A., Edinburgh, Scotland
Khan, Baz, Bolton, Greater Manchester
Kidachi, Masanobu, Sagamihara City,
Kanagawa Pref., Japan
Kim Yoonjin, Jenny, London

Komvokis, Vasilis, Budapest, Hungary
Lindström, Christina, Spanga, Sweden
McLintic, Lesley Anne, Swanage, Dorset
Mason, Raymond H. Jr., Scottsdale, Arizona,
U.S.A.
Matoba, Akiko, Nara City, Nara Pref., Japan
Maule, Peter William, Eastleigh, Hampshire
Minowa, Yumiko, Mitaka City, Tokyo, Japan
Miyazaki, Satoshi, Toyonaka City, Osaka,
Japan
O'Connor, Anne Mette, Hellerup, Denmark
Okuyama, Muneyuki, Kofu City, Yamanashi
Pref., Japan
Omotedani, Hiroki, Matsudo City, Chiba
Pref., Japan
Palmares, Richard, Sale, Cheshire
Pelletier, Lise, Montréal, Quebec, Canada
Rahn, Adelle, Pewsham, Chippenham,
Wiltshire
Penson, Teresa, Whitehill, Hampshire
Price, David, Colchester, Essex
Ravi Prakash, Bharathi, Chennai, India
Siahaan, Paula C., London
Tani, Saeko, Takaishi City, Osaka, Japan
Taylor, Martin, Ipswich, Suffolk
Taylor, Vivien, Burnham, Buckinghamshire
Thomasson, Valerie Elizabeth, Marsworth,
Hertfordshire
Tsiknakis, Avgerinos, Athens, Greece
Underwood, Anthony D., Sumner, Texas,
U.S.A.
Villepigue, Debórah A., Manhasset, New
York, U.S.A.
Webster, Eric T., West Chiltington, West
Sussex
Wijesekara, Chandana J., Chiba City, Chiba
Pref., Japan
Wilding, Mark, St Helens, Merseyside

Laboratory Membership

Michael Gardner Antiques, New Bond Street,
London W1
Hirsh London, Hatton Garden, London,
EC1N 8AH
J. W. Weldon, Clarendon Street, Dublin 2,
Ireland

Transfers

Transfer from Associate Membership
to Fellowship (FGA)
Inoue, Koichi, Osaka, Japan

Obituary

Huang Fengming 1965-2004

Huang Fengming studied and achieved her masters degree in the Department of Economic Geology in the China University of Geosciences in Wuhan and became an Associate Professor in the Gemmological Institute of China (CUG) within the university, working with the CUG for six years and teaching gemmology. The CUG was established through the work of Professor Chen Zhonghui as the first Gem-A Allied Teaching Centre in mainland China. Huang was a close academic associate of Professor Chen and she became an invaluable assistant with the detailed work for Gem-A and particularly for its crucial translation work under Professor Chen's exacting guidance. Huang, who had published two papers for *The Journal of Gemmology*, was studying for her gemmology doctorate when, after a protracted illness, she sadly died at the time of the International Gemmological Conference in September. She is remembered as a hard-working, respected and friendly colleague who is sadly missed.

Li Liping

A.H.G. Armstrong FGA (D.1951), Bridge of Allan, Stirling, died recently.

The Revd S. B. Nikon Cooper FGA DGA (D.1965), Walpole St Peter, Cambridgeshire, died on 11 October 2004. Nikon was a Gem-A correspondence course tutor for a record 35 years, retiring from the position in 2002. He was one of a team of three tutors with Keith Mitchell and Vera Hinton when he was appointed in 1967.

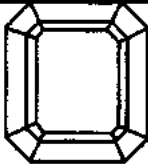
Walter Crombie FGA (D.1948), St Johns Wood, London, died on 23 October 2004.

Professor Dr Edward J. Gübelin FGA (D.1946 with Distinction), Lucerne, Switzerland, died on 15 March 2005. A tribute to Professor Gübelin is given on p. 257.

Neville Seymour Haile FGA (D.1972), Oxford, died in June 2004.

J. van Loo FGA (D.1951 with Distinction), Ra Epse, The Netherlands, died recently.

Pearls Coral Amber Bead Necklaces Carvings Cameos Mineral Specimens

The World  of Gemstones

Ruppenthal (U.K.) Limited

Gemstones of every kind, cultured pearls, coral, amber,
bead necklaces, hardstone carvings, objets d'art and
18ct gold gemstone jewellery.

We offer a first-class lapidary service.

By appointment only
1a Wickham Court Road, West Wickham, Kent BR4 9LN
Tel: 020-8777 4443, Fax: 020-8777 2321, Mobile: 07831 843287
e-mail: roger@ruppenthal.co.uk, Website: www.ruppenthal.co.uk

Modern 18ct Gem-set Jewellery

Opal Precious Topaz Ruby Star Ruby Sapphire Star Sapphire Tourmaline

Gemstones Aquamarine Alexandrite Amethyst Emerald Jade Lapis-Lazuli

**MODERN
MICRO-ANALYTICAL
TECHNIQUES
FOR GEMMOLOGISTS**

A 3-Day Course on
Laser Raman Spectroscopy & Imaging
To be held at Kingston University, Surrey
In collaboration with
The Gemmological Association of Great Britain

Gain a basic understanding of Raman Spectroscopy and its application to gem testing. Be introduced to other non-destructive methods of micro-analysis and micro-imaging.

Course fee: £375

Participants should have a relevant qualification (e.g. BSc or FGA) and an interest in gemmology or applied mineralogy (*max. 20 participants*).

Details and booking form from:
Dr S Bignold,
School of Earth Sciences & Geography,
Kingston University, Surrey KT1 2EE
+44 (0)20 8547 8850 – s.bignold@kingston.ac.uk

PL spectrum courtesy of DTC

**MODERN
MICRO-ANALYTICAL
TECHNIQUES
FOR GEMMOLOGISTS**

A 3-Day Course on
Laser Raman Spectroscopy & Imaging
To be held at Kingston University, Surrey
In collaboration with
The Gemmological Association of Great Britain

Gain a basic understanding of Raman Spectroscopy and its application to gem testing. Be introduced to other non-destructive methods of micro-analysis and micro-imaging.

Course fee: £375

Participants should have a relevant qualification (e.g. BSc or FGA) and an interest in gemmology or applied mineralogy (*max. 20 participants*).

Details and booking form from:
Dr S Bignold,
School of Earth Sciences & Geography,
Kingston University, Surrey KT1 2EE
+44 (0)20 8547 8850 – s.bignold@kingston.ac.uk

PL spectrum courtesy of DTC

Choosing
the right
insurance
is critical.

Pick carefully.



The insurance broker to the jewellery trade.

London 10/12 Ely Place, London EC1N 6RY
Tel 020 7405 0009 Fax 020 7404 4629
web www.thmarch.co.uk email insurance@thmarch.co.uk

Additional offices in:

Birmingham 10A Vyse Street, Hockley B18 6LT
Tel 0121 236 9433 Fax 0121 233 4901

Glasgow Empire House, 131 West Nile Street G1 2RX
Tel 0141 332 2848 Fax 0141 332 5370

Manchester 1st Floor, Paragon House, Seymour Grove M16 0LN
Tel 0161 877 5271 Fax 0161 877 5288

Plymouth Hare Park House, Yelverton Business Park, Yelverton PL20 7LS

Tel 01822 855555 Fax 01822 855566

Sevenoaks Sackville House, 55 Buckhurst Avenue, Kent TN13 1LZ
Tel 01732 462886 Fax 01732 462911

Ireland PO Box 5, Greystones, Co Wicklow

Tel 00 353 1 201 6851 Fax 00 353 1 201 6851

Authorised and regulated by the Financial Services Authority.

**Museums,
Educational Establishments,
Collectors & Students**

I have what is probably the largest range of genuinely rare stones in the UK, from Analcime to Wulfenite. Also rare and modern synthetics, and inexpensive crystals and stones for students. Computerised lists available with even more detail. Please send 12 1st class stamps refundable on first order (overseas free).

Two special offers for students:
New Teach/Buy service and free stones on an order.

Nola French
t/a A.J. French FGA
7 Orchard Lane, Evercreech
Somerset BA4 6PA
Telephone: 01749 830673
Email: french@frencht.freemove.co.uk
www.ajfrenchfga.co.uk

MEGA-LOUPE

Dark Field Illumination

at your fingertips

Features optimal lighting and a 3-position lens for fast and efficient inclusion detection on loose or mounted stones



2 MODELS

Both with the same high quality fully corrected 10X triplet lens

LUMI-LOUPE 15mm lens \$90
MEGA-LOUPE 21mm lens \$115

ADD: \$20 for shipping outside the continental USA
\$8 for shipping inside the continental USA

www.nebulamfg.com
email: info@nebulamfg.com

P.O. Box 3356, Redwood City, CA 94064, U.S.A.
Tel 650-369-5966 Fax 650-363-5911

ROCK 'n' gem SHOWS

Exhibitors displaying & selling a huge range of minerals, fossils, crystals & jewellery

ALEXANDRA PALACE

Wood Green, London

14 - 15 MAY

NEWCASTLE RACECOURSE

High Gosforth Park, Tyne & Wear

11 - 12 JUNE

KEMPTON PARK RACECOURSE

Staines Road East, (A308), Sunbury, West London

18 - 19 JUNE

MARGAM PARK

Neath, Port Talbot (Jct. 38 of M4)

6 - 7 AUGUST

NEWTON ABBOT RACECOURSE

Newton Abbot, Devon

3 - 4 SEPTEMBER

NEWARK SHOWGROUND

Winthorpe, Newark, Notts, (Off A46)

10 - 11 SEPTEMBER

BATH & WEST SHOWGROUND

Shepton Mallett, Somerset

17 - 18 SEPTEMBER

HATFIELD HOUSE

Hatfield, Herts (Jct. 4 of A1M)

1 - 2 OCTOBER

KEMPTON PARK RACECOURSE

Staines Road East, (A308) Sunbury, West London

29 - 30 OCTOBER

All shows open 10am - 5pm (Trade & Public)
Kempton Park only: Sat 10am - 6pm, Sun 10am - 5pm

Admission:

Alexandra Palace: Adults £3.75, Seniors £3.00

Kempton Park: Adults £3.50, Seniors £2.75

All other shows: Adults £2.60, Seniors £2.00

Children (8-16 yrs) £1.25 at all shows.

For further information please contact:

HD Fairs Ltd 01628 621697

Email: info@rockngem.co.uk www.rockngem.co.uk

Forthcoming Events

- 12 May** **London:** Castellani exhibition and lecture. A group visit to the exhibition 'Castellani and Italian Archaeological Jewellery' preceded by lecture 'Alessandro Castellani and his search for the secret of granulation' by Jack Ogden.
- 18 May** **North West Branch:** Mineralization of fossils. Wendy Simkiss
- 15 June** **North West Branch:** 1960 and all that. David Callaghan
- 15 June** **North East Branch:** The Chinese pearl revolution with John Carter
- 18 June** **Midlands Branch:** Summer Supper Party
- 12 July** **Gem Discovery Club Specialist evening:** Branko Deljanin
- 21 September** **North West Branch:** Some you win, some you lose! Stephen Whittaker
- 30 September** **Midlands Branch:** Cultured pearls - evaluation workshop. Michael Houghton
- 19 October** **North West Branch:** Gems of life. Maggie Campbell Pedersen
- 26 to 28 October** **London:** Three-day Rough Diamond Assessment Course
- 28 October** **Midlands Branch:** Identification of gem materials using a microscope. Gwyn Green
- 31 October** **Presentation of Awards**

contact details

When using e-mail, please give Gem-A as the subject:

- London:** Mary Burland on 020 7404 3334; e-mail mary.burland@gem-a.info
- Midlands Branch:** Gwyn Green on 0121 445 5359; e-mail gwyn.green@usa.net
- North East Branch:** Neil Rose on 0113 2070702; e-mail gema.northeast@gemro.com
- North West Branch:** Deanna Brady 0151 648 4266
- Scottish Branch:** Catriona McInnes on 0131 667 2199; e-mail scotgem@blueyonder.co.uk
- South East Branch:** Colin Winter on 01372 360290; e-mail info@ga-seb.org
- South West Branch:** Richard Slater on 01635 553572; e-mail rslater@dnfa.com

Gem-A Website

For up-to-the-minute information on Gem-A events visit our website on www.gem-a.info

Guide to the preparation of typescripts for publication in *The Journal of Gemmology*

The Editor is glad to consider original articles shedding new light on subjects of gemmological interest for publication in *The Journal*. Articles are not normally accepted which have already been published elsewhere in English, and an article is accepted only on the understanding that (1) full information as to any previous publication (whether in English or another language) has been given, (2) it is not under consideration for publication elsewhere and (3) it will not be published elsewhere without the consent of the Editor.

Typescripts Two copies of all papers should be submitted on A4 paper (or USA equivalent) to the Editor. Typescripts should be double spaced with margins of at least 25 mm. They should be set out in the manner of recent issues of *The Journal* and in conformity with the information set out below. Papers may be of any length, but long papers of more than 10 000 words (unless capable of division into parts or of exceptional importance) are unlikely to be acceptable, whereas a short paper of 400-500 words may achieve early publication.

The abstract, references, notes, captions and tables should be typed double-spaced on separate sheets.

Title page The title should be as brief as is consistent with clear indication of the content of the paper. It should be followed by the names (with initials) of the authors and by their addresses.

Abstract A short abstract of 50-100 words is required.

Key Words Up to six key words indicating the subject matter of the article should be supplied.

Headings In all headings only the first letter and proper names are capitalized.

A This is a first level heading

B *This is a second level heading*

First and second level headings are in bold and are ranged left on a separate line.

Third level headings are in italics and are indented within the first line of text.

Illustrations High resolution digital files, for both colour and black-and-white images, at 300 dpi TIFF or JPEG, and at an optimum size, can be submitted on CD or by email. Vector files (EPS) should, if possible, include fonts. Match proofs are essential when submitting digital files as they represent the colour balance approved by the author(s).

Transparencies, photographs and high quality printouts can also be submitted. It is recommended that authors retain copies of all illustrations because of the risk of loss or damage either during the printing process or in transit.

Diagrams must be of a professional quality and prepared in dense black ink on a good quality surface. Original illustrations will not be returned unless specifically requested.

All illustrations (maps, diagrams and pictures) are numbered consecutively with Arabic numerals and labelled Figure 1, Figure 2, etc. All illustrations are referred to as 'Figures'.

Tables Must be typed double spaced, using few horizontal rules and no vertical rules. They are numbered consecutively with Roman numerals (Table IV, etc.). Titles should be concise, but as independently informative as possible. The approximate position of the Table in the text should be marked in the margin of the typescript.

Notes and References Authors may choose one of two systems:

(1) The Harvard system in which authors' names (no initials) and dates (and specific pages, only in the case of quotations) are given in the main body of the text, (e.g. Collins, 2001, 341). References are listed alphabetically at the end of the paper under the heading References.

(2) The system in which superscript numbers are inserted in the text (e.g. ... to which Collins refers.³) and referred to in numerical order at the end of the paper under the heading Notes. Informational notes must be restricted to the minimum; usually the material can be incorporated in the text. If absolutely necessary both systems may be used.

References in both systems should be set out as follows, with *double spacing* for all lines.

Papers Collins, A.T., 2001. The colour of diamond and how it may be changed. *J.Gemm.*, 27(6), 341-59

Books Balfour, I., 2000. *Famous diamonds*. 4th edn. Christie's, London. p. 200

Abbreviations for titles of periodicals are those sanctioned by the *World List of scientific periodicals* 4th edn. The place of publication should always be given when books are referred to.



Contents

Professor Dr Edward Joseph Gübelin A tribute by E. Alan Jobbins	257	Stereoscopic effect in asterism and chatoyancy H. Killingback	312
HPHT treatment of different classes of type I brown diamonds T. Hainschwang, A. Katrusha and H. Vollstaedt	261	Identification of an imitation of pearl by FTIR, EDXRF and SEM T.L. Tan, T.S. Tay, S.K. Khairoman and Y.C. Low	316
Describing diamond beauty – assessing the optical performance of a diamond M.D. Cowing	274	X-ray luminescence, a valuable test in pearl identification H.A. Hänni, L. Kiefert and P. Giese	325
Gem-quality musgravite from Sri Lanka K. Schmetzer, L. Kiefert, H.-J. Bernhardt and M. Burford	281	The variation of RI with rotation of a doubly refractive gemstone on the refractometer hemicylinder Xinhua Song, Ruihua Wu and Weizheng Wu	331
Iron- and zinc-rich gem-quality taaffeites from Sri Lanka K. Schmetzer, L. Kiefert, H.-J. Bernhardt, M. Burford and D.P. Gunasekara	290	Use of the polarizing filter on the refractometer B.D. Sturman	341
Note on nephrite jade from Val Faller, Switzerland D. Nichol and H. Giess	299	Letter to the Editor	349
Nephrite jade from Mastabia in Val Malenco, Italy D. Nichol and H. Giess	305	Abstracts	350
		Book Reviews	357
		Proceedings of the Gemmological Association and Gem Testing Laboratory of Great Britain and Notices	360

Cover Picture: In honour of Professor Dr Edward J Gübelin – 1913-2005

Reflecting an adventurous life, this 10 mm spray of acicular tourmaline crystals protogenetically embellished with microcrystals of quartz rests for eternity encased in rock crystal, a true symbol of beauty in nature. Sample personally collected in 1987 by Edward J Gübelin and John I. Koivula at the Golconda Mine in Minas Gerais, Brazil, during a field excursion at the XXI International Gemmological Conference. Polarized light with compensator. Photomicrograph by John I. Koivula, courtesy of microWorld of Gems. (See tribute to Professor Dr Edward Gübelin, p.257)